

國立交通大學

電子工程學系 電子研究所碩士班

碩士論文

新穎材料 DyMn_2O_5 在電阻式記憶體上的機制研究與應用

**The Researching Mechanism and Application of the Novel
Material DyMn_2O_5 (DMO) in Resistive Random Access
Memory**

研究生：黃偉立

指導教授：施敏 院士

張鼎張 博士

中華民國一〇〇年七月

新穎材料 DyMn_2O_5 在電阻式記憶體上的機制研究與應用

The Researching Mechanism and Application of The Novel Material
 DyMn_2O_5 (DMO) in Resistive Random Access Memory

研究生：黃偉立

Student : Wei-Li Huang

指導教授：施敏 院士

Advisor : Prof. S. M. Sze

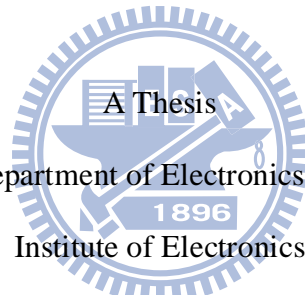
張鼎張 博士

Prof. Ting-Chang Chang

國立交通大學

電子工程學系 電子研究所

碩士論文



Submitted to Department of Electronics Engineering and
Institute of Electronics

College of Electrical and Computer Engineering

National Chiao Tung University

in partial Fulfillment of the Requirements

for the Degree of

Master

in

Electronics Engineering

July 2011

Hsinchu, Taiwan, Republic of China

中華民國一〇〇年七月

新穎材料 DyMn_2O_5 在電阻式記憶體上的機制研究 與應用

研究生：黃偉立

指導教授：施敏 院士

張鼎張 博士

國立交通大學電子工程學系電子研究所碩士班

摘要

電阻式記憶體具備了可微縮化，低功率的消耗，快速操作特性以及穩定的容忍度的這些特點，使得它能夠成為下一世代的記憶體結構。在這篇論文研究中，我們將進一步的去研究這種金屬-介電質-金屬 $\text{Pt/DyMn}_2\text{O}_5$ (DMO)/TiN 的電阻式記憶體的結構。

在這篇論文裡，這類新型材料 DMO 的特性和電性特性的是藉由 XPS，TEM 等材料分析系統和安捷倫 B1500 電性測量系統所分析得到。在第二章描述中，可經由 X-射線光電子能譜 (XPS) 觀察到一些氧空缺存在於原始 DMO 的薄膜層中。我們的元件也可藉由變溫的電性量測方式測得低電阻狀態 (LRS) 是較屬於金屬的特性而在高電阻狀態下則是偏向半導體類特性機制。我們也可經由容忍度測試以及開關特性的穩定度於高溫狀態下，來探討此類的電阻式記憶體的可靠度，從它的容忍度可達到十萬次的操作下，一樣可以維持穩定的開關特性，而它的開關特性也可以在高溫 (85°C) 環境下，穩定維持到 10^4 秒的。

以 DyMn_2O_5 為基底下的電阻式記憶體，其電流電壓特性有出現一個特殊的現象，稱為負微分電阻 (NDR) 現象。事實上，NDR 的現象是由於氧離子斷鍵，飄

移和聚集所造成的現象。這種 DyMn_2O_5 組成的電阻式記憶體可以產生出雙重電阻轉態機制行為也可以經由電性量測方式觀察到。事實上雙極電阻開關的雙重轉態的特性是由於金屬絲和介面的轉態的機制所共存在的一種現象，然而我們也可經由不同的操作電壓來產生出這兩種轉態機制的出現。甚至它可以經由不同的厚度元件而產生單一主導的轉態機制。

在最後一章節裡，我們針對它的容忍度作進一步的研究發現，氧離子與氧空缺結合時間與熱的效應，也是影響整個容忍度的一項重要因素。因此，我們採用不同的脈衝週期條件，來提升容忍度的效應，甚至可讓我們的元件達到 10^7 的操作次數的測試，這類物理的研究而能夠優化我們元件特性。



The Researching Mechanism and Application of The Novel Material DyMn₂O₅ (DMO) in Resistive Random Access Memory

Student : Wei-Li Huang

Advisor : Prof. S. M. Sze

Prof. Ting-Chang Chang

Department of Electronics Engineering and Institute of Electronics

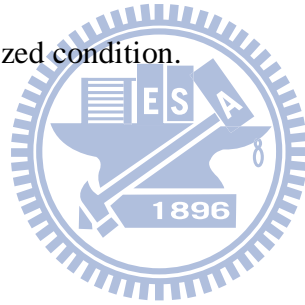
National Chiao Tung University



The resistive switching random access memories (RRAMs) possess some advantages of scalability, low power consumption, fast operating time and stable endurance. The RRAM with these advantages has high potential for next generation memory applications. The switching mechanism and electrical characteristics of Pt/DyMn₂O₅ (DMO)/TiN RRAM devices are investigated by material analysis and electrical measurement system. In chapter1, some oxygen vacancies are observed in the pristine DMO film through x-ray photoelectron spectroscopy (XPS). The low resistive state (LRS) of RRAM is found metal-like and the high resistive state is semiconductor-like properties by electric measurement at different temperatures. The endurance of the RRAM can achieve 10⁵ times and its retention time can also achieve 10⁴ seconds under high temperature (85⁰C) thermal stress.

For the DyMn_2O_5 -based RRAM, the current-voltage characteristics possess a special phenomenon which is called Negative Differential Resistance (NDR). In fact, the NDR phenomenon is due to the breaking bond, migration and accumulation of oxygen ions. The dual resistive switching behaviors are also observed in the device structure. The dual bipolar resistance switching behaviors of filament-type and homogenous-type can coexist in the devices by applying appropriate sweep voltages. It can be found that the thicker DMO films possess only homogenous-type mechanism.

In last chapter, we can find that the recovery time of oxygen and oxygen vacancy is an important factor for the endurance of the RRAM devices. Therefore, we apply different pulse conditions to enhance the endurance and the device can achieve 10^7 times endurance tests at optimized condition.



Acknowledgement

時間過得飛快,才覺得考上研究沒多久,到現在也經過兩年了,在新竹修課然後再到高雄做實驗,我所經歷,我所得到的不僅僅只是課業上的理論,也讓我體會到很多待人處事的道理,我十分感謝施敏老師以及張鼎張老師,總是不厭其煩的在 group meeting 中教導相關的知識,使我在半導體相關的領域可以懂得更多,看得更廣,以及在我研究上的指導與論文的修改,使得當我在困難以及不知所措時可以得到解決。

在我做實驗的時候往往能夠得到學長姊的幫忙,使得研究不會毫無目標的亂做一通,因此我非常感謝的是所有實驗室的學長姐,尤其是蔡侑廷學長,在他帶我做實驗的過程中,我學到很多思考的方式,做實驗的態度,知識成長以及數據分析,還有一點是他都很有耐心執導我,在做實驗過程中很感謝他對我的鼓勵以及建議,也很感謝一起走過這段日子的同學們:柔妙、岳恆、奕介、志誠、儀憲、凱弘、冠任、菟琳、雅琪、承瑋、國孝、祐松以及慶恩等,總是可以在我實驗碰到瓶頸的時候陪我聊天運動以及加油打氣,以及碩一的學弟妹們:昌蓓、明諺、君昱、峻豪、華茂、哲丘以及天健等,和你們嘴砲讓可以讓我有紓壓的功效,看你們在實驗室專心的準備期中期末考,讓我看到實驗室未來之光,還有真的很感謝遠在新竹的慶恩Q博,在我們來高雄做實驗的期間,總是很辛苦地幫我打點好學校一些大大小小的事情,讓我不用來回奔波,以及新竹的學弟謝謝你們幫我們簽名。

最後要感謝的是我親愛的家人,在爸爸媽媽姐姐的鼓勵下,是我最大的精神支柱,也是因為你們讓我有繼續升學的衝勁,謝謝你們給我好的讀書環境,讓我無憂慮的專研學業。因為有你們的幫助,得以讓我完成此本論文,感謝~~再感謝大家。

黃偉立 謹識

交通大學

2011 年

Contents

Chinese Abstract	I
Abstract	III
Acknowledgement	V
Contents	VI
Figure Captions	IX
Table captions	XIV
Chapter 1 Introduction	1
1-1 The Evolution of Memory	1
1-2 The Novel Memory Device	2
1-2.1 FeRAM.....	2
1-2.2 PCRAM.....	3
1-2.3 MRAM.....	4
1-2.4 RRAM.....	5
1-2.5 The Switching Mechanism of RRAM.....	7
1-2.6 The Conduction Mechanism of RRAM.....	11
Chapter 2 Basic material characteristics and electrical properties of DyMn₂O₅	22
2-1 Process Flow	22
2-1.1 Substrate Prepare.....	22
2-1.2 Sample fabrication.....	22

2-2 Materials Analysis of Pt / DMO / TiN (STD)	23
2-2.1 X-ray Photoelectron Spectroscopy (XPS).....	24
2-2.2 Fourier Transform Infrared Spectroscopy (FTIR).....	24
2-2.3 Transmission Electron Microscopy (TEM)	24
2-3 Electric Characteristic Measure	25
2-3.1 Forming Process.....	25
2-3.2 Current-Voltage after Forming Process.....	27
2-3.3 The Carrier Conduction Mechanism Fitting.....	27
2-3.4 Temperature effect of LRS and HRS Characteristic.....	28
2-3.5 Reliability	28
2-3.5-1 Retention.....	28
2-3.5-2 Endurance.....	29
Chapter3 Coexistence of Filament and Homogenous Resistive Switching for DyMn₂O₅ film	40
3-1 Electric Characteristic Measure before Forming	40
3-1.1 Temperature Effect.....	40
3-1.2 Constant Voltage Sampling Effect.....	41
3-1.3 Thinckness Effect.....	42
3-1.4 Mechanism of the Phenomenon of NDR before Forming	42
3-2 Electric Characteristic Measure after Forming	45
3-2.1 Normal Operation.....	45
3-2.2 Temperature Effect for sub-RRAM	46
3-2.3 Fitting Mechanism for sub-RRAM after Forming	47

3-2.4	Normal Switching Mechanism after Forming Process (coclusion)	47
3-2.4-1	Original - RRAM	48
3-2.4-2	sub- RRAM	48
3-3	Forming-Free Switching Mechanism	50
3-3.1	Operating Current-Voltage before Forminf	51
3-3.2	Pure Interface-type Operated Mode	52
3-4	The thin DMO+Nitrogen (DMON) Layer Effect	54
3-5	Conclude Coexistence of Interface and Filament Mechanism	56
Chapter 4	Investigation of Improving Endurance Performance by Using Fast Measurement systems	73
4-1	The Observation of Current by Using Pulse Current-Voltage	73
4-2	Pulse Cycle Effect	74
4-2.1	Less Pulse Cycle Effect	74
4-2.2	Many Pulse Cycles Effect-Part One	75
4-2.3	Many Pulse Cycles Effect-Part Two	76
4-3	300ns and 900ns for The Reset Time Effect	79
4-4	The Result of Best Endurance	79
Chapter 5	Conclusion	90
Reference		92
Resume		96

Figure Captions

Fig-1.2.1-1. The ABO_3 structure.....	15
Fig-1.2.1-2. The curve is P-V hysteresis.....	15
Fig-1.2.2-1. The main memory data storage part is in the middle layer of GeSbTe (GST) thin film.....	16
Fig-1.2.2-2. The main memory data storage part is in the middle layer of GeSbTe (GST) thin film.....	16
Fig-1.2.2-3. The heating time and transitional process. [8].....	16
Fig-1.2.3-1. The MRAM structure.....	17
Fig-1.2.3-2. The “1” state and “0” state of MRAM.....	17
Fig-1.2.4-1. The forming process.....	18
Fig-1.2.4-2. The reproducible behavior of RRAM.....	18
Fig-1.2.4-3. The rupture and formation process of filament [34].....	19
Fig-1.2.4-3. The unipolar current voltage curve, the left-side is log scale and the right-side is linear scale. [25] [26].....	19
Fig-1.2.4-4. The oxygen ions migrate to the electrode and the oxygen vacancies remain in the film.....	20
Fig-1.2.4-5. The bipolar switching behavior. The left-side is log scale and the right-side is linear scale[34].....	20
Fig-1.2.4-6. The interface model [34] [37].....	21
Fig-2.1.1. The substrate cross-section.....	31
Fig-2.1.2. The device structure of sample1.....	31
Fig-2.1.3. The cross-section of the sample2.....	32
Fig-2.2.1. the XPS Dy 4 <i>d</i> core-level photoemission spectrum[39].....	32

Fig-2.2.2. The O 1s spectrum[40].....	33
Fig-2.2-3. The spectrum of Far-FTIR for STD DMO film.....	33
Fig-2.2-4. The mid-FTIR	34
Fig-2.2-5.The MIM device cross-section.....	34
Fig-2.3-1. The probes contact with pads.....	35
Fig-2.3-2 .The forming of STD device.....	35
Fig-2.3-3.Typical current-voltage characteristics of STD device.....	36
Fig-2.3-4. The carrier conduction mechanism are at a piece of I-V curve.....	36
Fig-2.3-5. Two different characteristics, one is metal-like at LRS and the other one is semiconductor-like at HRS.....	37
Fig-2.3-5.The retention of our device and kept the thermal stress at 85 °C.....	37
Fig-2.3-6. The endurance characteristics between HRS and LRS of STD device.....	38
Fig-2.3-7(a). The condition of reverse bias pulse.....	38
Fig-2.3-7(b). The condition of reverse bias pulse.....	38
Fig-2.3-7(c). on/off pulse cycles.....	38
Fig-2.3-8.The on / off ratio is about 100 resistance, the HRS fluctuation is acute than LRS.....	39
Fig-3.1-1. The NDR voltage depend on temperature.....	59
Fig-3.1-2. The voltage of NDR depends on temperature.	59
Fig-3.1-3. Normal relation between current and time.....	60
Fig-3.1-4(a). The current time curve are at 303k.....	60
Fig-3.1-4(b). The current time curve are at 323k.....	60
Fig-3.1-4(c). The current time curve are at 343k.....	60
Fig-3.1-4(d). The current time curve are at 363k.....	60

Fig-3.1-5. These relations of current-time in the same plot and then compares them with each other.....	61
Fig-3.1-6. The forming processes of four different thicknesses into the same plot...61	
Fig-3.1-7. The NDR voltage and makes a plot recording the distribution of NDR voltage with different thickness.....	62
Fig-3.1-8 (a). The first step of oxygen ions model in pristine state.....	62
Fig-3.1-8 (b). The second step of oxygen ions model and the bonds are broken and migrate by applying voltage.....	62
Fig-3.1-9 (a). The oxygen ions will accumulate near TiN interfacial and form an oxygen-rich region.....	63
Fig-3.1-9 (b). The oxygen ions drift into TiN electrode by applying forming voltage and the filament is formed in the bulk, finally.....	63
Fig-3.1-10 (a). The flat band is at original state.....	63
Fig-3.1-10 (b). The step of breaking bond and migration of the oxygen ions.....	63
Fig-3.1-10 (c). The oxygen ions accumulate near the interface and bend the band upward.....	63
Fig-3.1-11. The larger cell size device has larger leakage than the small cell size.....	64
Fig-3.2-1(a). Original current was higher than later current, it is like reset Phenomenon.....	64
Fig-3.2-1 (b). The voltage was swept from 0V to -1.8V and then swept from -1.8V to 0V.....	64
Fig-3.2-2 (a). The device is operated between SHRS and HRS for 100 cycles.....	65
Fig-3.2-2 (b). The DC endurance HRS/ SHRS ratio was about 1.5 orders.....	65
Fig-3.2-3 (a). The SHRS is different between at 80 ⁰ K and at RT by applying the same Condition.....	65
Fig-3.2-3 (b). The V _{stop} condition was changed from 0.7V to 0.9V at 80 ⁰ K.....	65

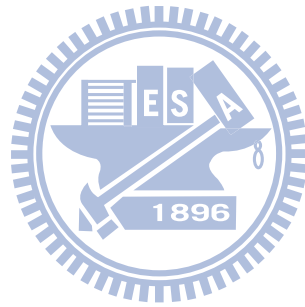
Fig-3.2-4. The conduction mechanism of carrier by fitting	66
Fig-3.2-5(a). The status of forming CP.....	66
Fig-3.2-5(b). The reset process.	66
Fig-3.2-5 (c). The NDR phenomenon.....	67
Fig-3.2-5 (d). The set process.....	67
Fig-3.2-6 (a). The migration of oxygen ion.....	67
Fig-3.2-6 (b). The accumulation of oxygen ion.....	67
Fig-3.2-6 (c). The oxygen ions migrate to bulk and the oxygen-rich layer is vanished when we apply reverse bias.....	67
Fig-3.2-7. SHRS and HRS depended on cell size but LRS was independent to cell Size.....	68
Fig-3.3-1(a). The swept loop from 0V → 5V → 0V.....	68
Fig-3.3-1(b). The swept loop from 0V → -5V → 0V.....	68
Fig-3.3-1 (c) The state is not at on- state.....	68
Fig-3.3-2 (a). The sub-RRAM the operating condition is at forward bias of 0.6V and at about reverse bias of -1.8V.....	69
Fig-3.3-2 (b). The operating mode before forming, and we discover V_{stop} was about 5V at forward bias.....	69
Fig-3.3-3 (a). The properties also possessed the NDR phenomenon and the NDR voltage was at about 2V.....	70
Fig-3.3-3 (b). The state is transition from ON state to OFF state.....	70
Fig-3.3-3 (c) the current was different from OFF state.....	70
Fig-3.3-3 (d) indicates the state transition from OFF state to ON state.....	70
Fig-3.3-4. The phenomenon of size effect.....	71
Fig-3.3-5(a). The oxygen accumulate nearing interface	71

Fig-3.3-5(b).The oxygen went back to bulk	71
Fig-3.3-5(c). The Schottky barrier is bend the band upward.....	71
Fig-3.3-5 (d). The Schottky barrier is bend the band upward and downward.....	71
Fig-3.4-1. The huge NDR phenomenon characteristic at forming process.....	72
Fig-3.4.2(a) The DMON possess the huge NDR than the DMO.....	72
Fig-3.4.2(b) The sub-RRAM HRS and SHRS ratio for DMON and DMO.....	72
Fig-4.1-1. The current-voltage of pulse.....	81
Fig-4.1-2. The current-voltage of pulse of set process.....	81
Fig-4.1-3(a). The three kinds condition of voltage pulse.....	82
Fig-4.1-3(b). The current value is detected by voltage pulse	82
Fig-4.1-3(c). The state is read under low bias.....	82
Fig-4.1-4. The resistance increases with temperature increasing.....	83
Fig-4.2-1(a). The endurance reset pulse width is 300 ns.....	83
Fig-4.2-1(b). The endurance of reset pulse width is 900ns.....	83
Fig-4.2-2. The endurance test under many pulse cycles.....	84
Fig-4.2-3. The statistics of different pulse cycles effect.....	85
Fig-4.2-4. The reset process of oxygen ions.....	85
Fig-4.2-5. The oxygen vacancies still exist in the bulk.....	86
Fig-4.2-6. The width between reset and set is called “a” and the width between set and “next reset” is called “b”	86
Fig-4.2-7. Each pair of parameters possesses some different effects.....	87
Fig-4.2-8. The width between reset and set is extended.....	87
Fig-4.2-9. The on/off ratio is enlarged with the a-region lengthening gradually.....	88
Fig-4.3-1.The endurance of different reset width in many pulse cycles.....	88
Fig-4.3-2. The different width phenomenon affects the state of device.....	89
Fig-4.4-1. The STD device represent the endurance can achieve 10^7 times.....	89

Table Cptions

Table 4-1. The endurance test condition of giving less pulse cycles.....83

Table 4-2. The endurance test condition of giving many pulse cycles.....84



Chapter 1

Introduction

1-1 The Evolution of Memory

In recently, Dynamic RAM (DRAM), Static RAM (SRAM) and Flash Memory have been widely used in our live. These memories have existed the development of numerous electronic systems especially for computer, communication and consumer applications (3C). Generally, these memories can be divided into two different types, one is the volatile-type memory and the other one is the non-volatile-type memory (NVM). Volatile memories cannot store any data without power. In other words, the information disappears once the system power is turned off, such as DRAM and SRAM. And the other type NVM is able to store the data (information) without power, such as the Flash memory. The NVMs have become more and more important because NVMs have widely been used to store information in the portable electronic system such as MP3, Cell Phone etc. Examples of NVMs include Read-Only-Memory (ROM), EEPROM (electrically-erasable programmable read-only memory), and the flash memory. The flash memory has been more and more important since 1990. The first programmable non-volatile memory is the floating-gate MOSFET, invented by D. Kahng and S. M. Sze in 1967 [1]. But the floating gate MOSFET possesses some disadvantages such as scaling limitation, high operating voltage, and long write/program speed. We have to improve the floating gate device or create some novel NVMs structure. A limiting of the floating gate structure is the MNOS (metal-nitride-oxide-semiconductor) structure which is formed when the floating gate

thickness approach zero. First, The MNOS has been evolved to form SONOS and TANOS.

Second, some novel NVMs structures are invented one by one. Generally, they can be divided into four species: FeRAM (Ferroelectric RAM), MRAM (Magnetic RAM), PCRAM (Phase Change Memory) and RRAM (Resistive RAM). In these novel-RAM we have to select a type of devices need to possess some advantages such as fast access time, scalability, low power consumption and high endurance/retention. The RRAM is a promising candidate for the next-generation device to be next-generation memory because it has many outstanding attributed. For example, its switching time can be less than 10 ns, its cell structure can less than $8F^2$, it has simple structure, and its density can be increased high. However, RRAM still has many issues to the resolves of many characteristic to be improved.

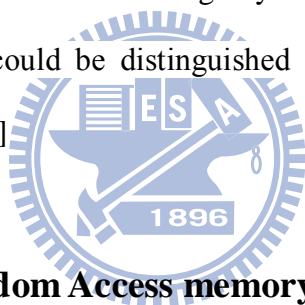
1-2 The Novel Memory Devices

In this part, we would discuss the four kinds of novel memory structures. And then we can compare them with each other.

1-2.1 Ferroelectric Random Access Memory (FeRAM)

Ferroelectric random access memory (FeRAM) has been widely researched because it can perform as a non-volatile memory. [2][3][4] It can be fabricated by using ferroelectric material to construct a FeRAM structure. The ferroelectric atomic arrangement has a crystal structure type of ABO_3 . Fig-1-2.1-1 shows the ABO_3 structure. The ferroelectric interior atomic arrangement structure would be changed if we apply an external field to the FeRAM device. In fact, the B-type atom can be

driven upward or downward in the interior arrangement. Besides, the electric dipole is induced because of the position of ion modulation by applying external field. For example, the B-type atom would be driven to upper position if we apply an upward field to the ferroelectric layer. On the contrary, the B-type atom would be driven to lower position if we apply a downward field. The atomic displacement cannot be changed and the atomic arrangement is still a stable state when we remove external field. We can understand the phenomenon from the polarization-voltage curve. The Fig-1.2.1-2 clearly shows the curve is P-V hysteresis. The electric dipole cannot disappear after removing the operating voltage that phenomenon called remnant polarization (P_r). The hysteresis curve is following counter clockwise curve. And the remnant polarization direction is able to change by changing different external field. The signals of “1” and “0” could be distinguished from the direction of remnant polarization, i.e., P_r and $-P_r$. [5]



1-2.2 Phase Change Random Access memory (PCRAM)

Phase-change memory (PCM, PRAM and Ovonic Unified Memory) is studied as a candidate for next generation non-volatile memory. The concept of phase change RAM was proposed by R.G. Neale, D.L. Nelson and G.E. Moore as early as in 1970s. [6] [7] And the depositing materials are known as chalcogenide and the materials after absorption thermal energy can transfer two different types, one is amorphous and the other one is poly-crystal. This material can achieve the memory storage ability because its characteristic possesses two different resistive characteristics by thermal effect changing the structure of material. The state would not be changed with time once we don't heat it again by external thermal stress so it can store the information for a long time. Therefore, PCRAM is also able to belong to non-volatile memory.

The Fig-1.2.2-1 and Fig-1.2.2-2 clearly depicts the memory data storage situation is in the middle layer of GeSbTe (GST) thin film. It just only needs a simple two-terminal point metal-GST-metal structure so we also only need to control the locally current flow the thin film. And achieve two different kinds of resistance. The Fig-1.2.2-3 shows the heating time and transitional process. [8]

1-2.3 Magnetic Random Access Memory (MRAM)

The Magnetic RAM (MRAM) was discovered in 1972. It is construct a prototype and display by Honeywell in 1992. Magnetic random access memory (MRAM) is not similar to conventional RAM technologies; it is that information/data is stored by magnetic storage elements rather than by electric charges or different atomic structure. In fact, the mechanism of program/erase is the electric spin orientation is changed in magnetic material layer by the electric current pass the top and bottom both conductive metal layers to induce the magnetic field. And then the magnetic field can change the spin orientation of middle layer which is called tunneling magneto-resistance (TMR) or Giant-Magneto-resistance (GMR) cell. We can see Fig-1.2.3-1 shows the MRAM structure. The barrier layer is deposited by Al_2O_3 . [9] [10] The top conductive metal layer is as the bit line, and the bottom conduction metal layer is as the word line. The MRAM cell will affect the polarization direction shift in free layer if we applied a pulse current to bit line because the bit line current induced magnetic field. On the contrary, we apply a pulse current in word line and then the induced magnetic will change the polarization direction of free layer completely. Therefore, the polarization of two ferromagnetic layers will be forward arranged. On the other hand, we can define the lower state as “0” state when the magnetic resistive is low. In other words, the polarization of two ferromagnetic layers is

reverse arranged and the magnetic resistive is higher, so we can define it as “1” state.

Fig-1.2.3-2 shows the “1” state and “0” state of MRAM.

1-2.4 Resistive Random Access Memory (RRAM)

The resistive random access memory (RRAM) is a type of RAM by controlling voltage or current to make the device inducing different resistance, i.e., it can be at high or low resistive state by external field. RRAM is a simple metal-insulator-metal (MIM) structure and its operating mode is easily to achieve the transitional process. The device can be operated after we apply the breakdown voltage of device which is called forming voltage and the process we call forming process. We have to set compliance current in order to avoid hard-breakdown and make the device produce the phenomenon of soft-breakdown. Fig-1.2.4-1 shows the **forming process**. And then we can apply bias to make the state of device from high resistive state (HRS) to low resistive state (LRS) and the process we called **reset**. On the contrary, we can also apply bias to make it from HRS to LRS which is called **set**. Therefore, it can produce reproducible behavior through set and reset process, i.e., we can turn the device on or turn it off. Fig-1.2.4-2 depicts we mention above. The ON state and OFF state can be as “1” and “0” so it is also a novel NVM. However, the RRAM device possesses some advantages than other novel RAM. The operating speed of RRAM can is less than 10ns. (Reference), the structure and cell size are simple and small, the operating voltage is low and hence it can be used in low power consumption. [12] [13] [14] [15] Finally, the RRAM structure still has many problems to solve them. We will focus on the issue of RRAM device. Therefore, we will divide into three different parts to discuss the materials, switching mechanisms of RRAM, and conductive mechanism of carriers.

1-2.4-1 The materials of RRAM

There are some kinds of insulators can be used in RRAM. They are the perovskite-type, the binary transition metal oxide and so on. The two species materials we mentioned above are common RRAM materials.

1-2.4-2 Perovskite-Type

The structure of Perovskite-type is ABO_3 . The type A atom in the structure is a cation and sits at cubic corner position (0,0,0) with the larger radius and the type B is also a cation and sits at body center position (1/2, 1/2, 1/2) with the smaller radius. The type O means the oxygen atom and it sits at face center position (1/2, 1/2, 0). In the common unit cell, type A occupies at the 8 corner positions, type B occupies at the body center position and O occupies at the 6 face center positions, like the Fig-1.2.1-1 . There are some common Perovskite structures such as $PrCaMnO_3$ (PCMO) [16] [17], $SrZrO_3$ (SZO) [18], and $SrTiO_3$ (STO) [19].

1-2.4-3 Binary Transition Metal Oxide-Type

There are some famous transition metal oxide materials such as TiO_2 , NiO and so on; they have been applied for thin film research for many years. S. Seo and coworker reported reproducible resistance switch of the NiO thin films deposited on $Pt/Ti/SiO_2/Si$ substrate in 2004. [20] There are still other type transition metals oxides have been widely used to match CMOS devices. Thus they can also compatible with modern CMOS process. However, this material group of binary oxides has simpler element components. It is easier to control the proportion of metal and oxygen

elements.

1-2.5 The Switching Mechanism of RRAM

In this part, we will introduce some different switching mechanisms of RRAM. Presently, the RRAM switching mechanism is not yet clear. But, there are many ideas and papers to offer some reasonable interpretations. Generally, the switching mechanism can be divided into two parts: one is bulk control type and the other one is interface control type. In bulk control type, the switching mechanism is relative to the insulator layer, i.e., the material characteristic is changed in the bulk. And the interface control type switching is relative to interfacial layer which is between the electrode and insulator layer. The transition of bulk is belonged to filamentary or conduction paths (CPs) model and the interface transition phenomenon is belonged to modified Schottky barrier model. We will discuss these mechanisms respectively.

1-2.5-1 Bulk type mechanism

1-2.5-1.1 The Filament type

First, we have to apply forming voltage to produce the breakdown phenomenon of device and the current value will suddenly increase which is called forming process. Next, we apply a bias to make the current reducing which is called reset process. Subsequently, we apply a bias to the device again and the current increasing sharply is like forming process we called set process. The switching phenomenon cause the filament is formed in the insulator layer. And the filament can also be ruptured and formed again and again so that the device possesses switching behavior. [21] [22] [23] Fig-1.2.4-3 illustrates what we mean. In addition, the device has to compliance the

current value ($<10\text{mA}$) to avoid the device becoming hard breakdown at the forming if we produce reproducible switching behavior. There are some reasons can explain the phenomenon of formation and rupture the filament result from thermal effect (Joule heating effect), reactive-oxidation (redox) processes by anion migration to the interface between the metal electrode and the insulator layer. And then we will discuss them respectively.

1-2.5-1.2 Thermal Effect (Joule Heating Effect)

This typical resistive switching behavior based on thermal effect shows in the unipolar characteristics. The unipolar characteristic operating mode is independent polarization. On the other hand, the device state can be changed the state from LHS to HRS or from HRS to LRS by applying forward bias. On the contrary, we can also apply reverse bias to transit the device state from LHS to HRS or from HRS to LRS. [24] Fig-1.2.4-3 depicts the unipolar current voltage curve. [25] [26] The device can turn on and turn off because the filament ruptures and forms when we apply a voltage to the device. At first, we apply the forward bias to make the device building the filament and the current increase suddenly to higher current. The device can transit from HRS to LRS because the filament is formed. Subsequently, we observe the device can transit from LRS to HRS if we apply the smaller forward bias but we don't compliance the current in this operating. Because we don't set the current limit, the crowd of electrons will induce heat and melt the filament at the local area in the bulk. The phenomenon is called electron migration. On the contrary, we can produce the same phenomenon under the reverse bias. In addition, there is another similar to electron migration effect such that the structure rearrange because current flow the film induce heating. Most of the current will easily pass the local area, so the

temperature is very high at local area. Therefore, the higher temperature at the local area can easily form or rupture the filament. In other words, it is a type of Joule heating effect and makes the filament rupture and formation because of electron migration or structure rearrangement by heat. [27] [28]

1-2.5-1.3 Redox Processes induced by Anion Migration

Another filament type is redox processes induced by *Anion* migration. The mechanism is the bond between oxygen and other metal will be broken by external electric field when we apply the forward bias on the bottom electrode at first. The oxygen will become the oxygen ion in the bulk and then the oxygen ion possesses free migrated ability. The oxygen ion will follow external field and move to the cathode. The oxygen vacancies can also provide spaces and the electron hop the vacancies through external field. Finally, the oxygen vacancies connect each other, and form a conduct path when we apply a larger bias. [25] [29] Fig-1.2.4-4 shows the oxygen ions migrate to the electrode and the oxygen vacancies remain in the bulk. Next, the device can transit from LRS to HRS if we apply a reverse bias. We have to use an opposite polarized, i.e., forward bias, to change the state from HRS to LRS. In other words, the set and reset process depend on polarization. It means that we apply forward bias to achieve set process and the device has to be applied reverse bias to achieve reset process. The operating mode is bipolar switching behavior. Fig-1.2.4-5 depicts the bipolar switching behavior. M. Fujimoto and coworker [30] observed that resistive switch is dependent on the operated polarity by using Pt/TiO₂/TiN/Pt devices in 2006. C. Yoshida and coworker [31] also found the bipolar resistive switching with the same structure of devices in 2007. In fact, the phenomenon is a type of redox

reaction because a bond between other atoms and oxygen transit to oxygen ions and then migrate to TiN electrode. First, the oxygen ions will react with TiN if we apply a forward bias on TiN electrode. Next, the oxygen ions will go back to bulk if we apply a reverse bias on TiN. The role of bottom electrode TiN is as an oxygen reservoir. [32] [33] It is a reaction and oxidation process. [30]

1-2.5-2 Interface Type Mechanisms (Modified Schottky Barrier Model)

The insulator contact with the metal electrodes will produce some interfacial characteristics in the metal-insulator-metal (MIM) structure. We have to deposit different metal electrode in MIM structure if the device perform the interface-type model. The device can possess the interface effect due to the work function are different between these two electrode such as Pt and TiN. Many papers research the interfacial problems by different working function in MIM system. [34]-[37] Generally, the interface contact which is between metal and insulator condition can be divided into two types, one is Ohmic contact and the other one is Schottky contact. The Schottky contact model plays a very important role In RRAM conductive mechanism models. A. Sawa and coworker earliest brought up the mechanism of Schottky barrier model. [17] [34] The device structure is Ti/PCMO/SRO and PCMO is p-type semiconductor. The Schottky contact occurs in the interface of Ti/ PCMO. We are able to know one important that Ti material possess a very strong attraction for oxygen ions in many papers researching. [32] [33] Ti electrode will catch many oxygen ions at the interface between Ti and PCMO if we apply a bias to make the bond between metal and oxygen breaking caused the interface. Therefore, there are many oxygen vacancies generation in the bulk. Oxygen vacancies perform the positive charge; they will bend the energy band. We will use oxygen vacancies

(oxygen ions) to think about the model. First, for p-type PCMO, a large amount of oxygen vacancies migrate to the interface between SRO/PCMO when the Ti electrode is given a positive bias (reverse field). In other words, it means the oxygen ions can drift to the Ti/PCMO interface by external forward field. And then the energy band is bent downward because the oxygen vacancies accumulate in the interface between SRO/PCMO. [17] The step is called reset process. Fig-1.2.4-6 depicts we mentioned above. [34] Second, the oxygen vacancies will migrate back to bulk when we apply a negative bias (forward) to the Ti electrode. On the other hand, the oxygen ions can drift back to the bulk through external reverse field. And then the energy band is bent downward because the oxygen vacancies do not accumulate in the interface between SRO/PCMO and go back to the bulk. The step is called set process. It is shown in the Fig-1.2.4-6. They think that the more or less of charged ions can change the Schottky barrier height or width and the reason will cause the resistance to become high or low.

1-2.6 The Conduction Mechanism of RRAM

Transition metal oxides can be divided into three different materials; one is insulators, second is semiconductors and third is metals oxide materials. Therefore, the carrier conductive characteristic may be different from each other due to their different chemistry, structure and physics. Generally, the most materials which were discussed in RRAM application belong to insulators, semiconductors and metal oxides according to the constitution and stoichiometry and the carriers conductive mechanisms mostly involved are Ohmic conduction, Schottky emission, Frenkel-Poole emission and Tunneling emission. Following we mentioned above, we will introduce these type carrier transport. [38]

1-2.6-1 Ohmic Conduction

Ohmic conduction transportation can divide into two different circumstances; first-type is at OFF state, second-type is at ON state. First, we introduce the first-type Ohmic transportation which takes place while the injected carrier density is less than the thermally-generated carrier density. In other words, the most carriers are from the valence band of material excited to conduction band by thermal effect so the carriers can drift to the other side from one side along the direction of external field. Generally, it can be applied to low electric bias to drive the carrier which are thermally generated transportation are dominate in Ohmic conduction. Second, the filament-type mechanism which is like metallization process (conduction paths) so the carriers can transport through filaments. And then the carriers' transportation is also an Ohmic mechanism because of metal (conduction paths). The current-voltage curve property in Ohm's law is the current passing through a resistor is proportional to the voltage drop cross the two points. Therefore, the temperature effect is also relation to Ohmic conduction behavior because the electron and phonon scattering effects. So the conductivity increases with increasing temperature for conduction in semiconductor while with decreasing temperature for metal conduction. The following is the expression for Ohmic conduction:

$$J \propto E_i \exp\left\{\frac{-\Delta E_{ac}}{kT}\right\}$$

, where E_i is the electric field and ΔE_{ac} is the activation energy of electrons. [38]

1-2.6-2 Tunneling carrier transportation

There is a conduction mechanism in high electric field it is tunneling effect. And it also often appears in insulator current conduction. The primary theory of tunneling conduction effect is quantum mechanical theory that the electrons can pass through any kinds of barrier. Tunneling emission possess a strong relationship with the apply voltage and less relationship with the external temperature so it appears in high voltage. Subsequently, tunneling emission can be divided into two types: direct tunneling effect (DT) and Fowler-Nordheim tunneling effect (F-N T). Direct tunneling is relation to the thickness of film. And Fowler-Nordheim tunneling is not relation to thickness of barrier. So we introduce the tunneling emission formula:

$$J \propto E_i^2 \exp\left[-\frac{4\sqrt{2m^*}(q\phi_B)^{3/2}}{3q\hbar E_i}\right] \text{ or } J \propto V^2 \exp\left(\frac{-b}{V}\right)$$

Where the E_i is electric field, the ψ_B is barrier height and m^* is effective mass. [38]

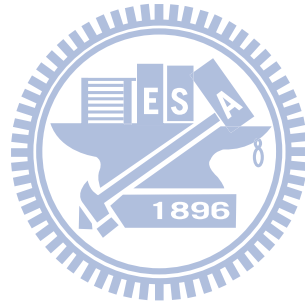
1-2.6-3 Schottky Barrier Emission

In the tunneling effect, we emphasize the field effect and affect the barrier for device but there is another type emission is the electron hop through the metal/insulator interface barrier height by the thermal effect. It is called Schottky barrier emission. In the type emission, the thermal effect is larger than field effect. The Schottky emission possesses a strong relationship with temperature and the image charge lowering the barrier height effect caused the electrons can hop through the barrier height easily. The barrier height is determined by the band of set between the work-function of material and metal work function which contact. And the interface trap, defect, carrier density, process condition can make the barrier height changing.

The electrons can easily jump the lower barrier height, and the electrons are difficult to jump to the higher barrier height. Following is the formula of Schottky emission.

$$J = A^{**} T^2 \exp\left[\frac{-q(\phi_B - \sqrt{qE_i/4\pi\epsilon_i})}{kT}\right] \text{ or } J \propto T^2 \exp\left[\frac{q}{kT}(a\sqrt{V} - \phi_B)\right]$$

Where A^{**} is effective Richardson constant, $\epsilon_i = \epsilon_r \epsilon_0$, ϵ_r is dielectric constant, and ϕ_B = barrier height. [38]



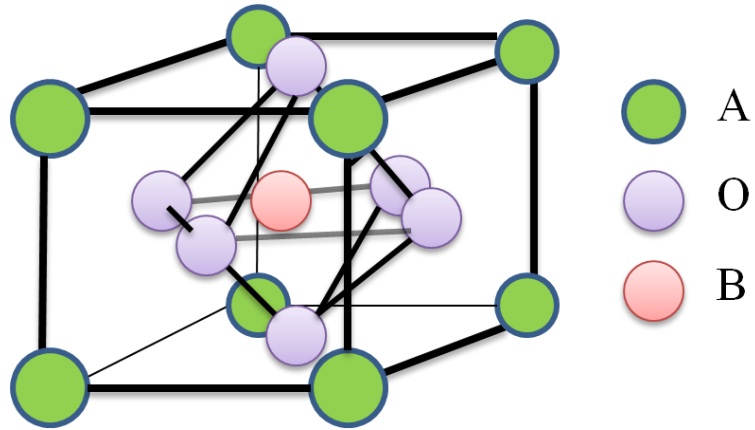


Fig-1.2.1-1 shows the ABO_3 structure.

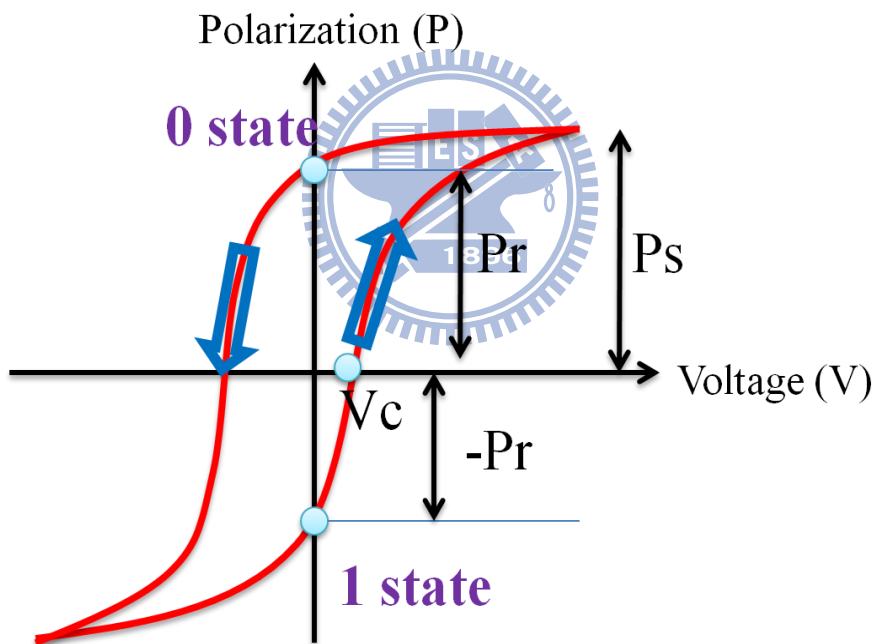
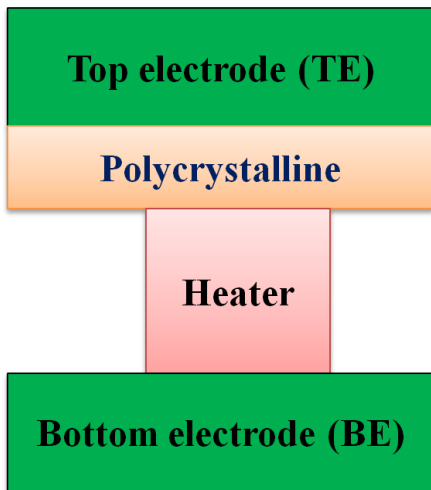


Fig-1.2.1-2 shows the curve is P-V hysteresis

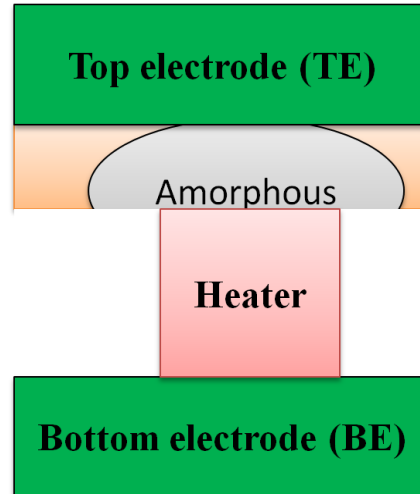
(Pr = Remnant Polarization, Ps = Saturation Polarization,

Vc = Positive Coercive Voltage).



0 State
Low Resistive State

Fig-1.2.2-1



1 State
High Resistive State

Fig-1.2.2-2

Fig-1.2.2-1 and Fig-1.2.2-2 clearly depicts the main memory data storage part is in the middle layer of GeSbTe (GST) thin film.

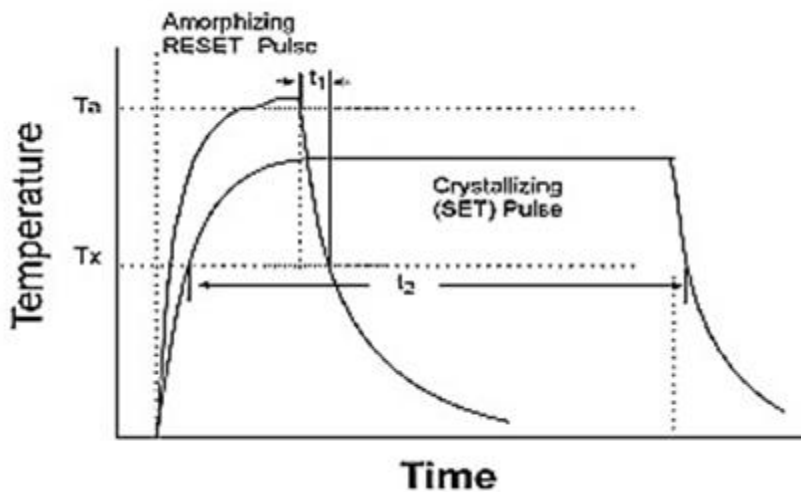


Fig-1.2.2-3 shows the heating time and transitional process. [8]

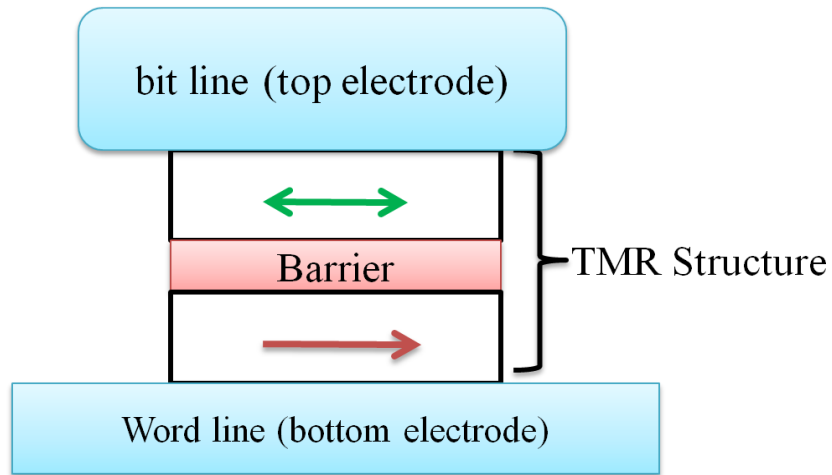


Fig-1.2.3-1 shows the MRAM structure

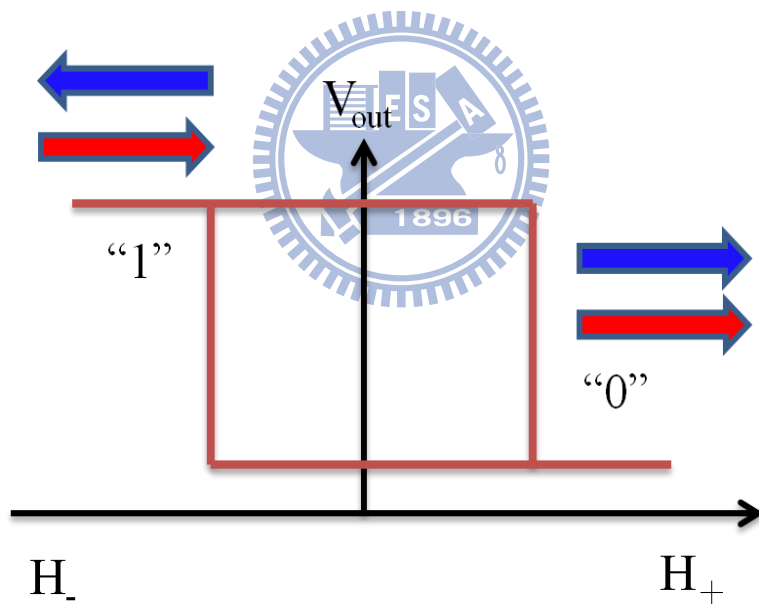


Fig-1.2.3-2 shows the “1” state and “0” state of MRAM.

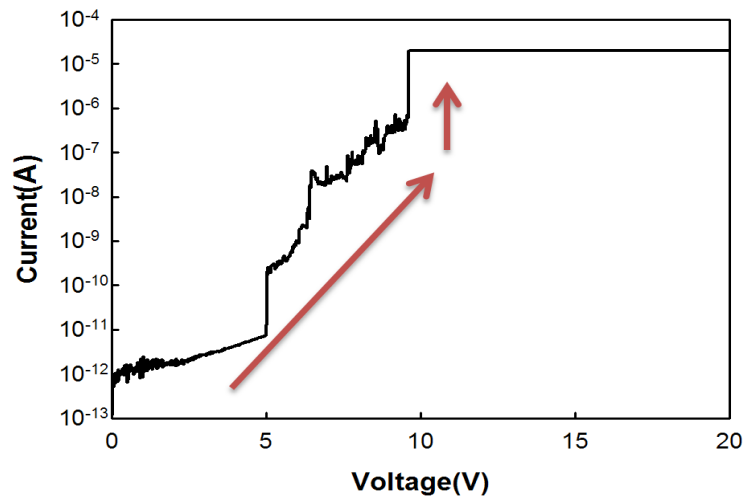


Fig-1.2.4-1 shows the forming process.

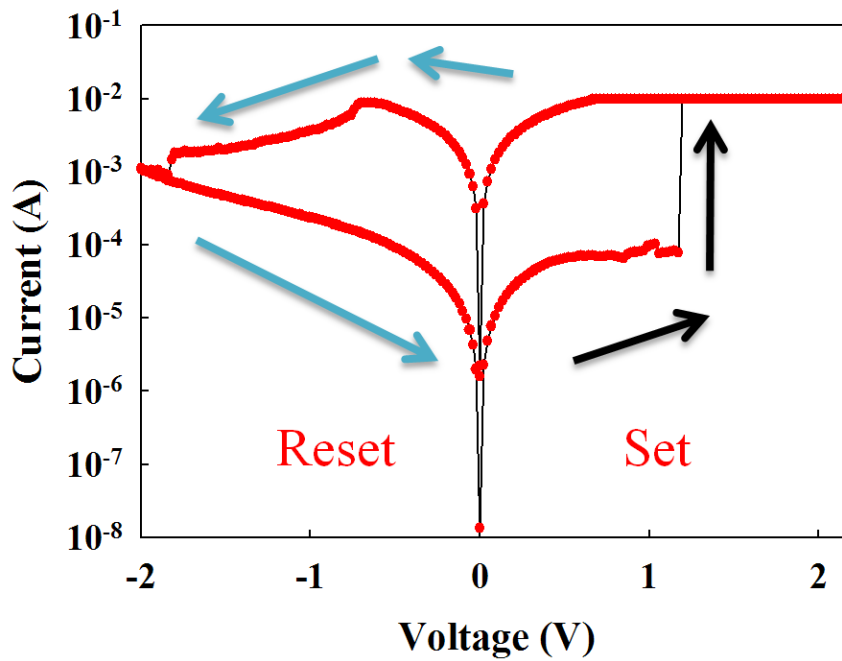


Fig-1.2.4-2 shows the reproducible behavior of RRAM and the current is large we call LRS or ON state and the current is small we call HRS or OFF state.

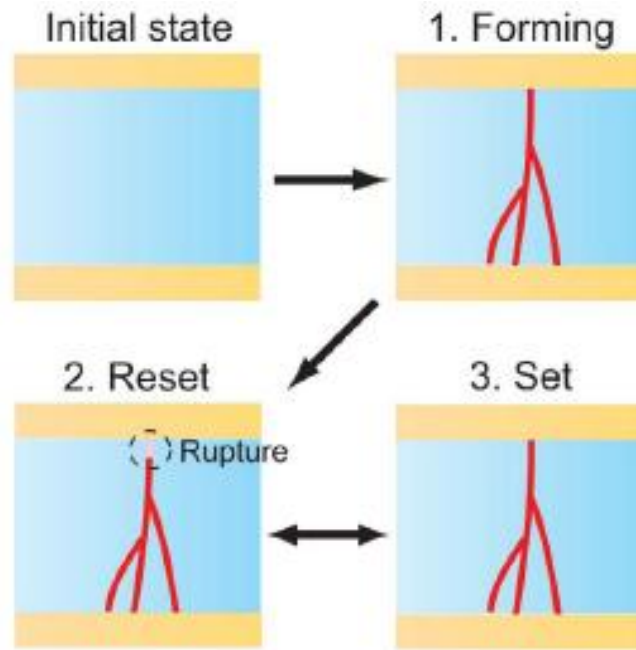


Fig-1.2.4-3 depicts there is no any filament in the film at initial state. **1.)** The device produces filaments in the film after forming process. **2.)** These filaments rupture after reset process by applying bias. **3.)** The filaments formed again after set process. [34]

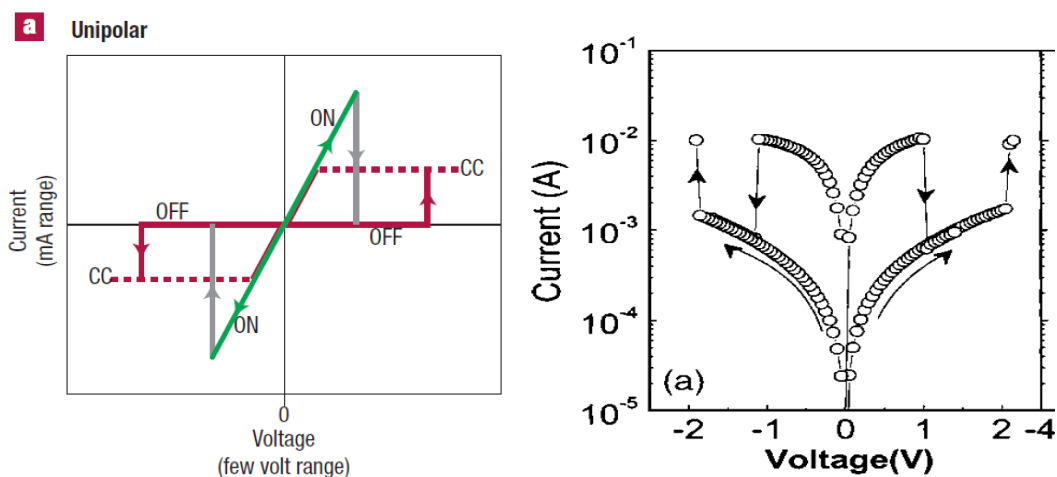


Fig-1.2.4-3 depicts the unipolar current voltage curve, the left-side is log scale and the right-side is linear scale. [25] [26]

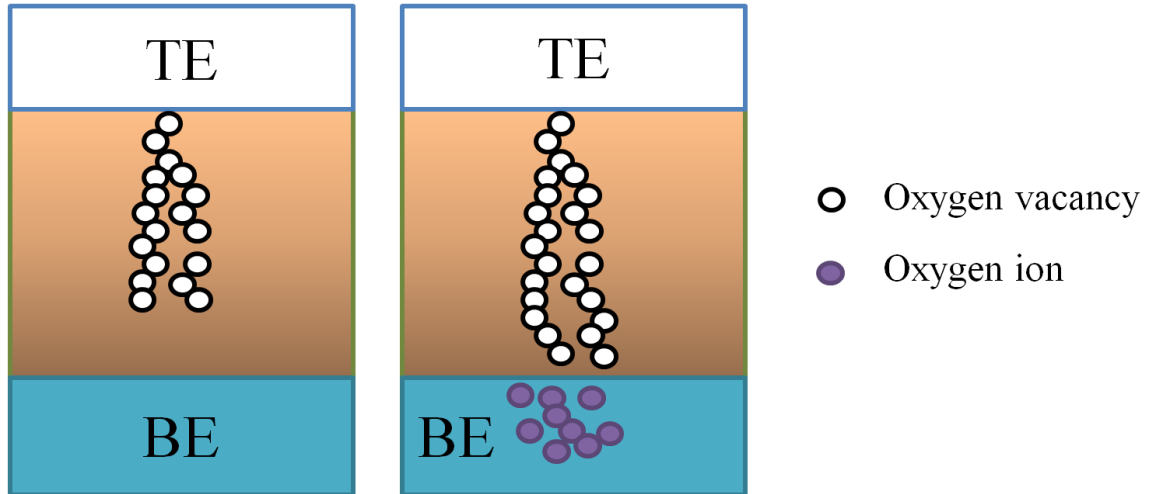


Fig-1.2.4-4 shows the oxygen ions migrate to the electrode and the oxygen vacancies remain in the film.

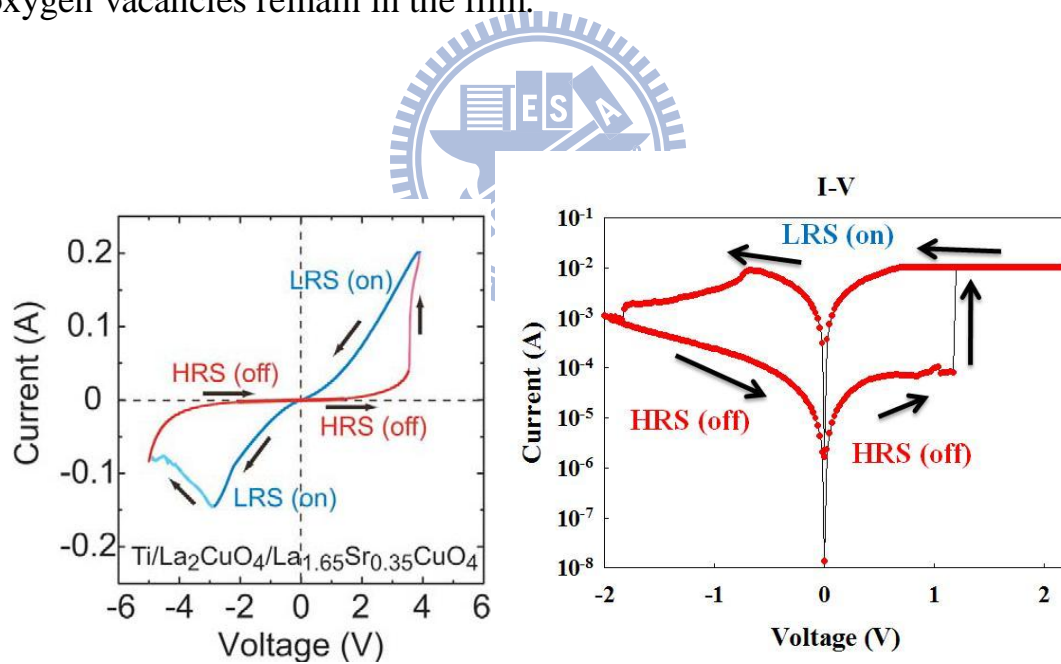


Fig-1.2.4-5 depicts the bipolar switching behavior. The left-side is log scale and the right-side is linear scale. [34]

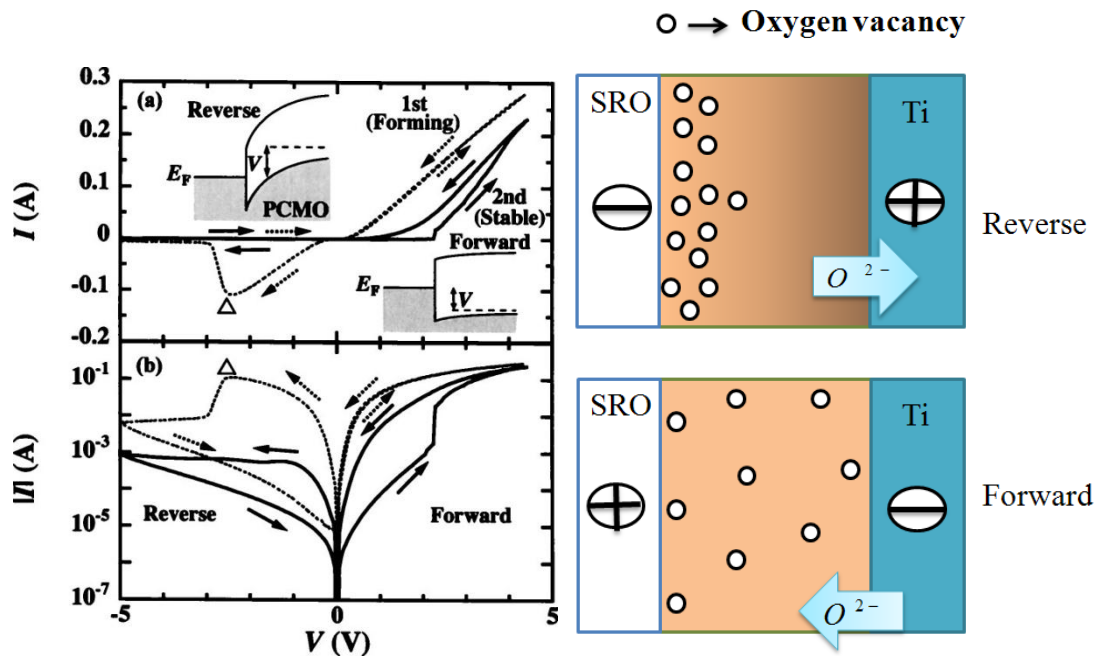
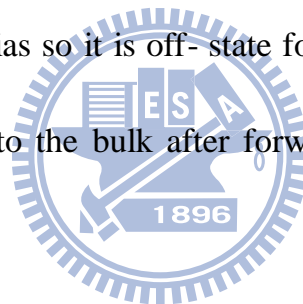


Fig-1.2.4-6 depicts, first, the oxygen vacancies accumulate at the interface of SRO/PCMO after reverse bias so it is off- state for p-type PCMO. Second, the oxygen vacancies go back to the bulk after forward bias so it is on-state for p-type PCMO. [34] [37]



Chapter 2

Basic material characteristics and electrical properties of DyMn_2O_5

In this chapter, we will introduce the process flow, materials analysis and basic properties of our device.

2-1 Process Flow

2-1.1 Substrate prepare

In this work, the structure of $\text{TiN}/\text{Ti}/\text{SiO}_2/\text{p}^+\text{-Si}$ was used as substrate. Subsequently, low temperature Oxide (LTO) is deposited on TiN film. But this structure was divided into two type morphology on TiN film which is bottom electrode. One was covered by photo-resist is called bottom electrode. The other one was not covered by photo-resist is called via hole which can be formed device area. And then the substrate will be used to deposit other film. Fig-2.1.1 depicts the substrate cross-section.

2-1.2 Sample fabrication

2-1.2-1 Sample1 *Pt / DMO (10nm) / TiN*

First, DyMn_2O_5 (DMO) material is used as the insulator of sample1, and then the film of DMO by radio- frequency (RF) magnetron sputter is deposited on the substrate. The magnetron sputter was carried out in an ambient of argon (30 sccm)

with power of 120 W and the working pressure of 5 mtorr. The thickness of DMO film is about 12nm. Afterwards Pt was the top electrode of sample1, and the thickness of Pt film is about 100 nm was deposited by magnetron sputter. Finally, the sample 1 was lifted off by acetone. Fig-2.1.2 shows the device structure of sample1. The sample1 will be used as the standard (STD) Metal-Oxide-Metal (MIM) structure device for RRAM researching. There are also many different kinds of the via hole size in the sample1. The via hole sizes are $64(\mu\text{m}^2)$, $16(\mu\text{m}^2)$, $4(\mu\text{m}^2)$, $1(\mu\text{m}^2)$, and $0.64(\mu\text{m}^2)$.

2-1.2-2 Sample2 Pt / DMO (10nm) / DMO+NH3 (2.4nm) / TiN

The sample2 used the same substrate to fabricate a contrastive device. It is a double layer structure. The substrate was putted into magnetron sputter system. First, magnetron sputter system was operated in an ambient of argon (30 sccm) and NH₃ (25 sccm) with power of 120 W and the working pressure of 10 mtorr. The switch gear of NH₃ pipeline was shut after 100 seconds, and only argon switch was opened until the thickness of DMO and Pt film were completed. Lift-off the sample2 was the ultimate step. Fig-2.1.3 shows the cross-section of the sample2.

2-2 Materials Analysis of *Pt / DMO / TiN (STD)*

For this topic, we would introduce our materials characteristic by X-ray Photoelectron Spectroscopy (XPS), Transmission Electron Microscopy (TEM), and Fourier Transform Infrared Spectroscopy (FTIR). We prepared many pieces of dummy wafer which has cleaned, and then we deposited the DMP film on different pieces of dummy wafer for analyzing the characteristic of materials and film

thickness.

2-2.1 X-ray Photoelectron Spectroscopy (XPS)

To confirm the composition of the DMO thin film, we have performed XPS analysis of DMO. Fig-2.2.1 shows the XPS Dy 4*d* core-level photoemission spectrum, which consists of two main peaks for the Dy-Mn and Dy-O bonds, respectively. [39] The O 1*s* spectrum is shown in Fig-2.2.2, and contains the two peaks of O-Mn and O-Dy. [40] From the XPS signal area ratio of three elements with sensitivity correction, the quantified composition ratio of the film is DyMn_{2.4}O_{4.6}. These results indicate that some oxygen vacancies exist in the pristine resistive switching film.

2-2.2 Fourier Transform Infrared Spectroscopy (FTIR)

First, we can observe the spectrum of far-FTIR for our DMO film from Fig-2.2-3. It shows the Dy-O bonds are near 458 cm⁻¹ and 550 cm⁻¹ and the Mn-O bonds are near 610 cm⁻¹ and 688 cm⁻¹. [41] [42] Second, we can see the chemical bonds in mid-FTIR. The mid-FTIR detects the longer frequency band range so there is some overlap wave peak. Therefore, we can observe the Mn-H-O bond is near 650 cm⁻¹. Fig-2.2-4 depicts the mid-FTIR. [41] [42]

2-2.3 Transmission Electron Microscopy (TEM)

We can direct analyze the material characteristic and thickness of STD by TEM. Fig-2.2-5 not only shows the STD device cross-section but also manifests the crystallinity of film. The Pt film shows a blacker region at the top, DMO film is under Pt film, and TiN is under the DMO film at the bottom. We got some other information of film. For instance, the thickness of DMO is about 12 nm and DMO was not

crystallization.

2-3 Electric Characteristic Measure

In this section, we measure the STD by Agilent B1500A and Agilent 4156C semiconductor characterization analyzer. The analyzer is controlled by the computer. First, we placed the STD device on the thermal chuck, and used probes contact with the pad of sample 1. Fig-2.3-1 shows the probes contact with pads. There are two pads in each device of STD, so one of pads is linked top electrode (TE) and the other one is linked bottom electrode (BE). Second, the computer is inputted parameters controlled the analyzer. We biased the bottom electrode and grounded the top electrode is like Fig-2.3-1. Here, the forward bias is defined by the current flow from TiN electrode to Pt electrode we called (by using a positive voltage to TiN), and the current flow from Pt to TiN is reverse bias (by using a negative voltage to TiN). Subsequently, we will observe three parts in the STD device, forming process, after forming process, and reliability.

2-3.1 Forming Process

For the STD device, the state of device is still an insulator at initial state before forming process. On the other hand, we bias the BE under small voltage and the current shows low value. However, the device is applied a forming voltage and the current will increase sharply. The forming process has mentioned above former chapter1 so we don't explain them again. Here, we will see our device during forming process. Fig-2.3-2 depicts the forming process of our STD device; we will divide into three regions during forming process. In region1, the voltage range is from 0V to 3V.

In region2, the voltage range is from 3V to 6V and the voltage from 6V to 8V is region3.

The region1 shows the state is high resistance and it is still original state because the electrons can't pass the insulator. Therefore, the current value is low under small bias in pristine film. The region2 illustrated two steps, one is a negative differential resistance (NDR) phenomenon from 3V to 4V and the other one is the current trend toward smooth situation when the voltage is from 4V to 6V. The NDR phenomenon means the current decreases with the voltage increasing. In region3, the device can achieve the breakdown condition near 7V and the current can increase sharply. We set the compliance current which is about 1mA to avoid hard-breakdown when the current increases sharply. The device had been changed its material structure after forming process.

Here, there are two different kinds of breakdown, one is called hard- breakdown and the other one is called soft-breakdown. The hard-breakdown is formed due to the insulator was produced a strong CPs which were consist of many defects, and the device is normally ON state. [28] [43] [44] And then it is difficult to recover a defect-rich conduction path by using of voltage when hard-breakdown is reached. It is different between soft-breakdown and hard-breakdown because soft-breakdown is reversible behavior. It mean that the device state can be changed by applying voltage from ON to OFF state. The device is able to recover the defects because the appropriate amount of bonds between oxygen and metal are broken. Soft-breakdown process is happened if we set compliance current condition. For hard-breakdown, it would be difficult to attract the ionic oxygen back by external bias, if the phenomenon is happen. [28] [43] [44]

2-3.2 Current-Voltage after Forming Process

Fig-2.3-3 shows typical current-voltage characteristics of STD device. We can divide into 6 steps in the Fig-2.3-3. After positive forming process, the state was at LRS. This is step1 when the device is given a negative bias from 0V to about -1 V and the state of device is still LRS. It is a little different step1 between step2 until the voltage is over -1V and the -1V is like a critical value which make device change the state. Step2 is swept from -1V to -1.8V. The swept range is from -1.8V to 0V is the step3. We discovered the sample1 shows two characteristic current curves, one is LRS and the other one is HRS. The bias is once over critical value (-1V), the state changed from LRS to HRS. When bias was increased from 0V to about +1V, this step we called step4. In step4, the current-voltage (I-V) curve possess NDR phenomenon near about 0.7V but the resistive switching behavior was still HRS. The current value increased rapidly when the voltage is over about 1V, and then the current achieved our set compliance current. The compliance current is 10^{-2} A . We sweep the voltage range from about 1V to 2V in the step5. The step6 swept voltage range is from 2V to 0V. The state is HRS in step4, but the state is changed from HRS to LRS through the step5.

2-3.3 The Carrier Conduction mechanism fitting

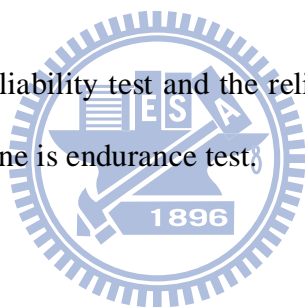
From Fig-2.3-4 we can discover the carrier conduction mechanism at a piece of I-V curve. First, we discuss the LRS carrier transportation. The carrier transportation mechanism is Ohmic conduction at LRS. Second, the carrier at HRS is also ohmic mechanism under small bias. Subsequently, the voltage range from -0.7V to -1.3V is Schottky barrier conduction mechanism and we also discover the voltage range from -1.5V to -1.8V is thermionic field emission.

2-3.4 Temperature effect of LRS and HRS characteristic

In order to verify the STD device transportation behavior we investigate the LRS and HRS with temperature effect. From Fig-2.3-5 depicts two different characteristics, one is metal-like at LRS and the other one is semiconductor-like at HRS. First, we observe HRS, the resistance state decrease with temperature increasing. It means the HRS is semiconductor conduction because the carriers have higher mobility under high temperature than under lower temperature. Second, the state increase with temperature increase at the LRS. It means the carriers have low mobility under higher temperature than under lower temperature.

2-3.5 Reliability

Here, we will discuss the reliability test and the reliability divide into two indices, one is retention and the other one is endurance test.



2-3.5-1 Retention

First, we observe the retention test. Retention is one of important reliability test for NVM device. The device is required retention time longer than 10 years for universal NVM. On the other hand, it has to maintain the state over 10 years if the device is on or off state. We test method is a kind of thermal stress so the retention time must to keep at thermal stress at 85⁰C. We would apply a smaller voltage from 0V to 0.2V read our device state. At 1s, 30s, 100s, 300s, 1000s, 3000s, 5000s, 7000s, 9000s, 10000s, the device would measure the current applying 0.2V in order to inspect the state is changed or not.

Fig-2.3-5 shows the retention of our device and kept the thermal stress at 85⁰C. On-Off ratio was still about 100 resistance ratio at 85⁰C. The state was stable over 10000

seconds. It indicated the state of our device was not changed by thermal stress at 85°C. It is a good appearance for our STD device.

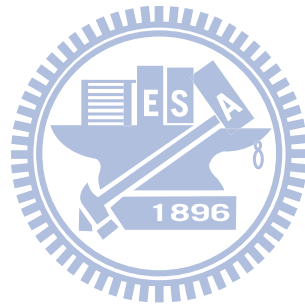
2-3.5-2 Endurance

The endurance is another important reliability test, and it is an indicator of reliability. For our device can divide into two different kinds of endurance, one is DC endurance and the other one is AC endurance. First, we chose DC endurance as simple analysis. We applied DC sweep to operate our device. And then the device is changed the state from HRS to LRS by applying forward bias when the state was HRS. Next, the device sweep reverse bias made the state from LRS to HRS. That we mentioned above, it is a sweep cycle (HRS→LRS, LRS→HRS) and the LRS and HRS can be read by 0.2V. Subsequently, Fig-2.3-6 depicts the endurance characteristics between HRS and LRS of STD device. The switch behavior of this device (on / off ratio) was about 100 resistance ratio at 0.2 V, and the resistance state was gradually stabilized over 100 times of cycles. From DC endurance, it is a good device for our sample.

Contemporary Non-Volatile Memory (NVM) shows resistive cycle times could achieve between 10^3 and 10^7 [45], and our DC measurement only achieve 100 cycle times. It is not enough to compare to modern NVM, so we have to use AC pulse measurement test application for our device. The AC measurement is different DC. I-V curve took on a full state (from HRS to LRS, or From LRS to HRS), and I-V curve is successive by DC measurement for our device.

First, the device state is at LRS and we apply a reverse bias pulse to change its state from LRS to HRS. Fig-2.3-7(a) shows the condition of reverse bias pulse. Next, we bias a smaller voltage to read its state. Second, we give a forward bias pulse to make HRS switching to LRS, and read it by 0.2V. Fig-2.3-7(b) depicts the condition of

reverse bias pulse. We applied thousands of forward and reverse bias pulse into the device at a time in order to reduce the time what we gave a pulse make it changed the state and read its state. It is like Fig-2.3-7(c). And then we gave a smaller bias to read its state again. Repeat the process for hundred times. It could obtain endurance of 10^5 times. The y-axis indicates resistance, the x-axis indicates switching times. Fig-2.3-8 shows the on / off ratio is about 10 resistance, the HRS fluctuation is acute than LRS. There were some error points in the AC endurance.



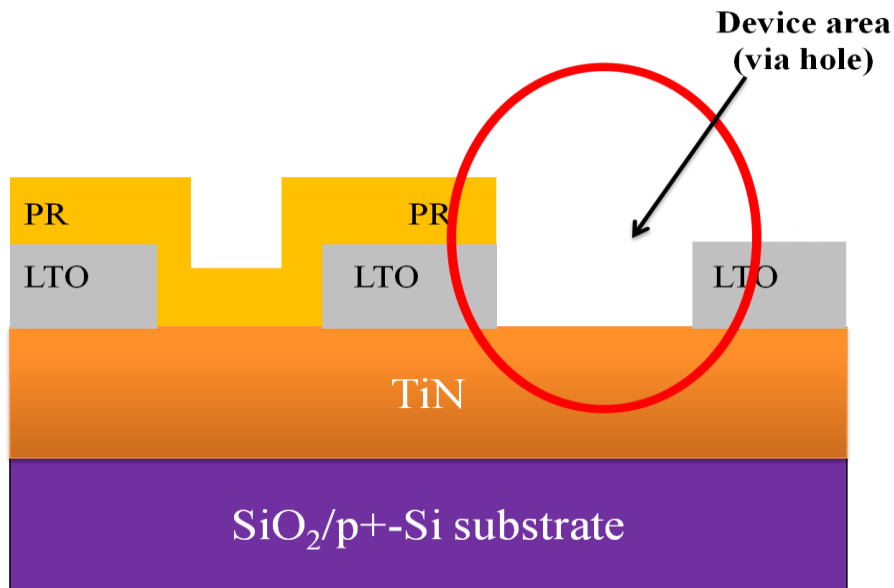


Fig-2.1.1 depicts the substrate cross-section.

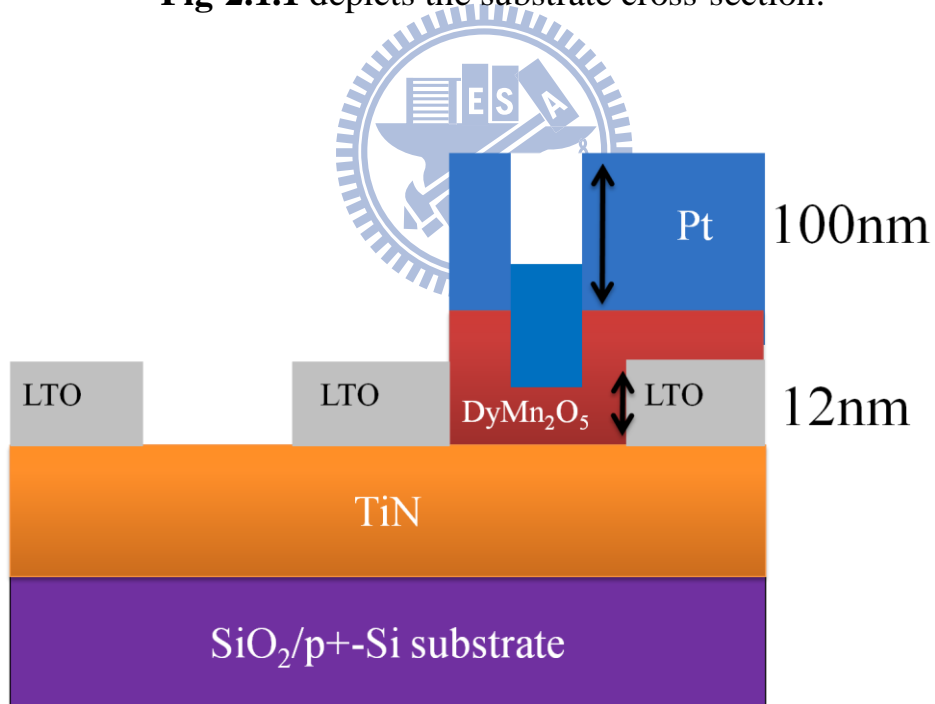


Fig-2.1.2 shows the device structure of sample1.

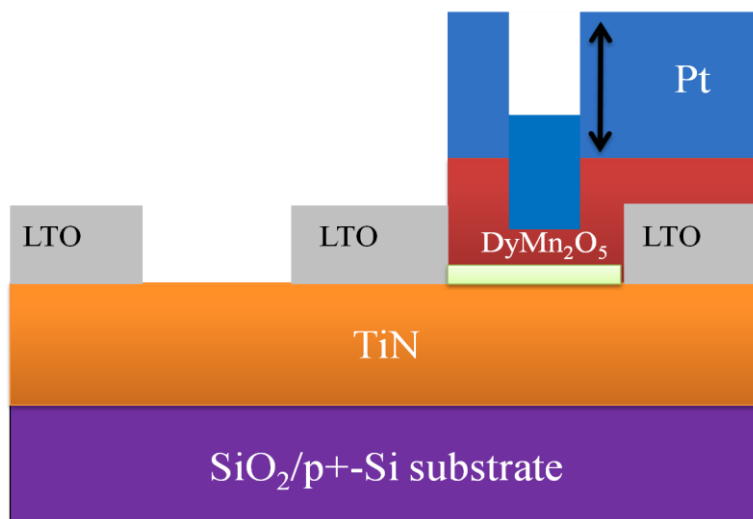


Fig-2.1.3 shows the cross-section of the sample2.

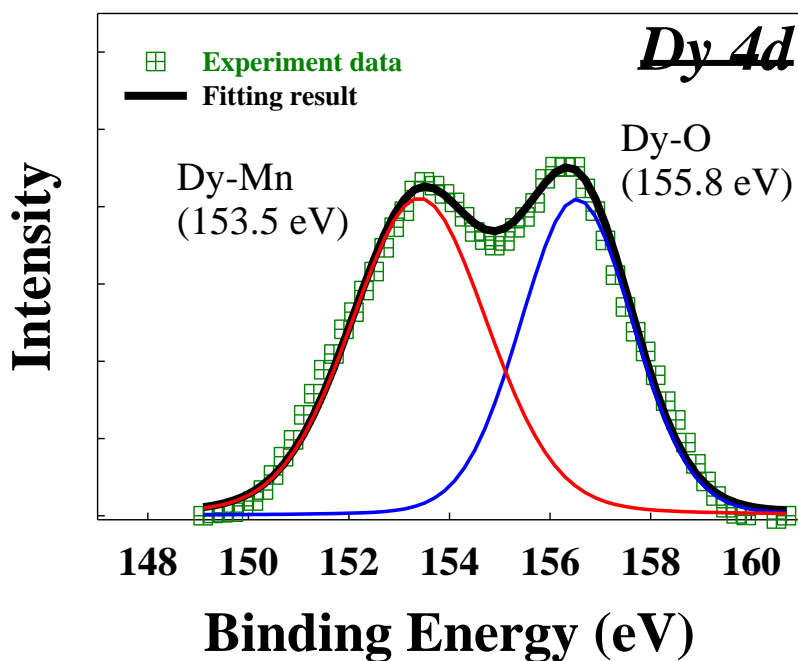
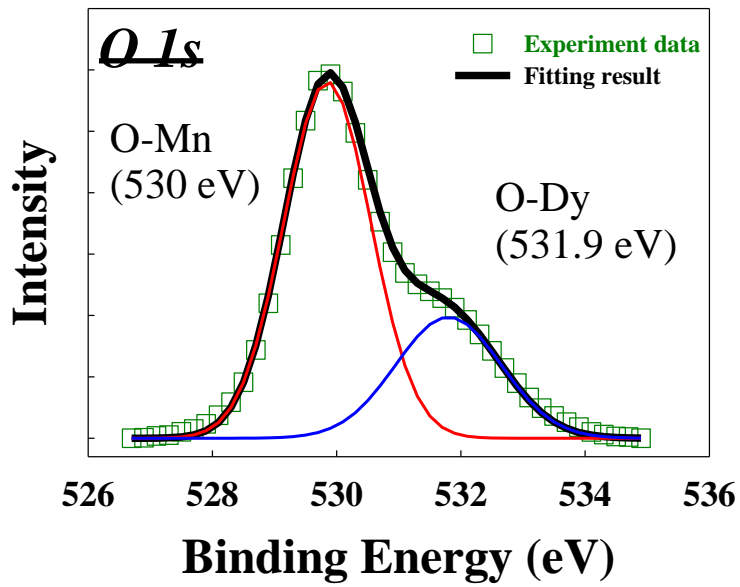


Fig-2.2.1 shows the XPS $\text{Dy } 4d$ core-level photoemission spectrum, which consists of two main peaks for the Dy-Mn and Dy-O bonds, respectively. [39]



The O 1s spectrum is shown in Fig-2.2.2, and contains the two peaks of O-Mn and O-Dy. [40]

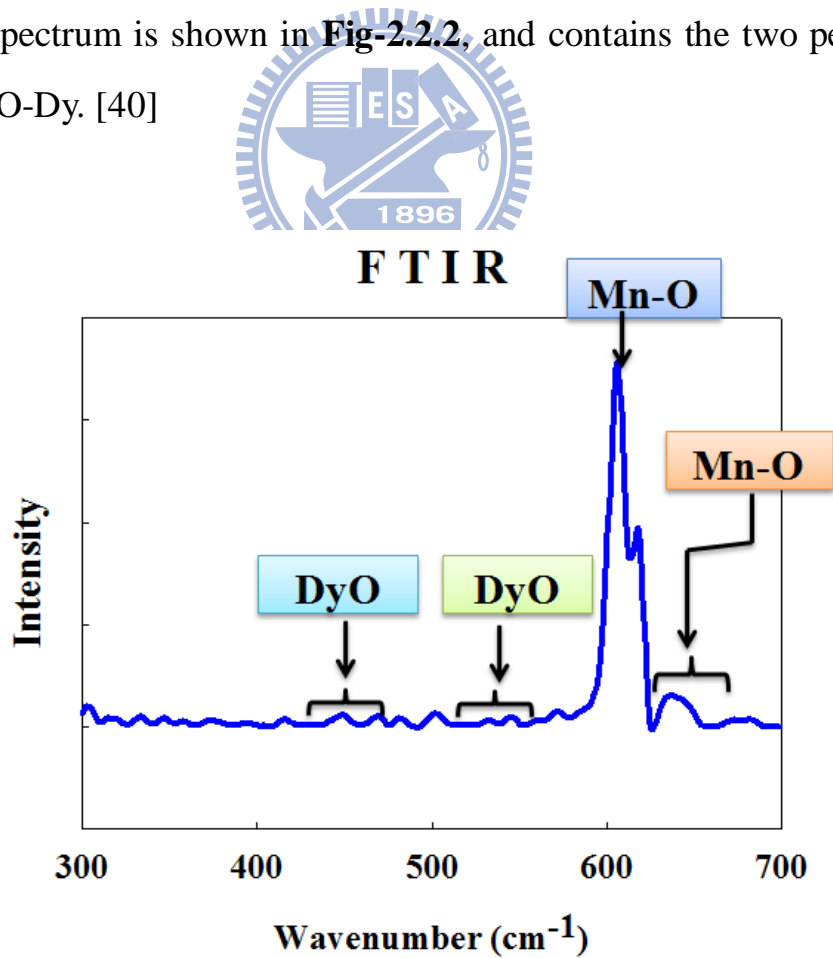


Fig-2.2-3 shows the spectrum of Far-FTIR for STD DMO film.

MID - FTIR

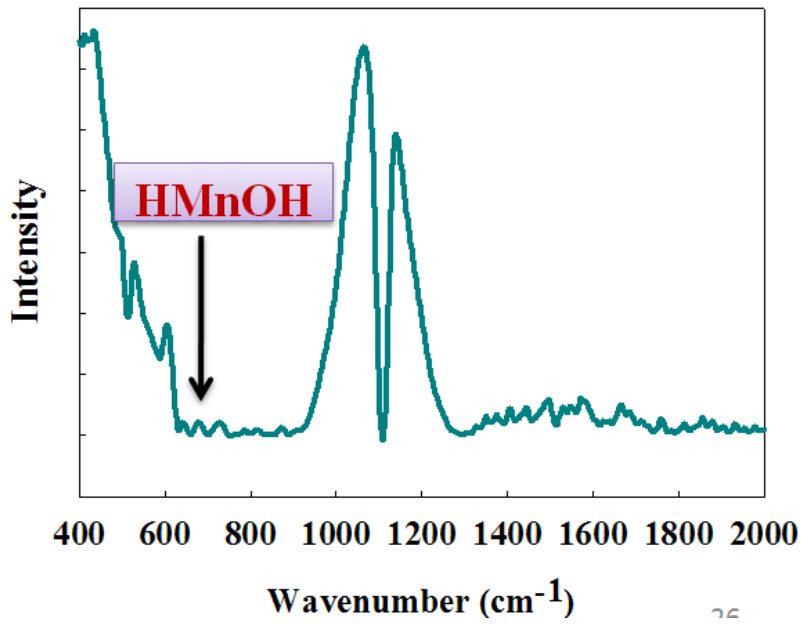


Fig-2.2-4 depicts the mid-FTIR.

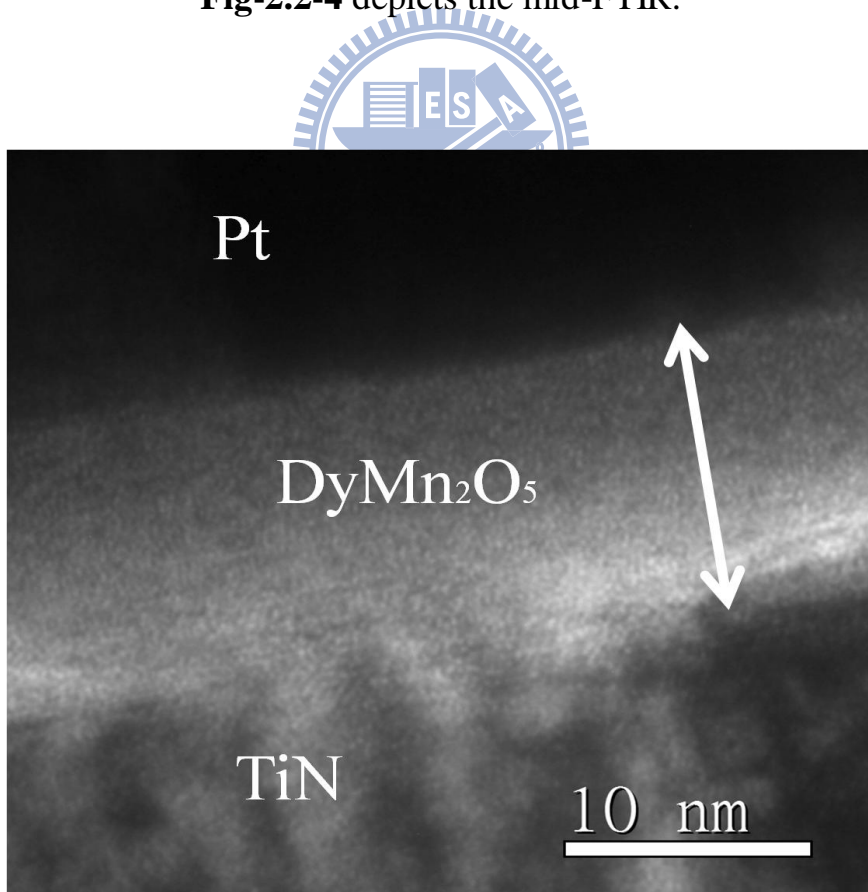


Fig-2.2-5 shows the MIM device cross-section.

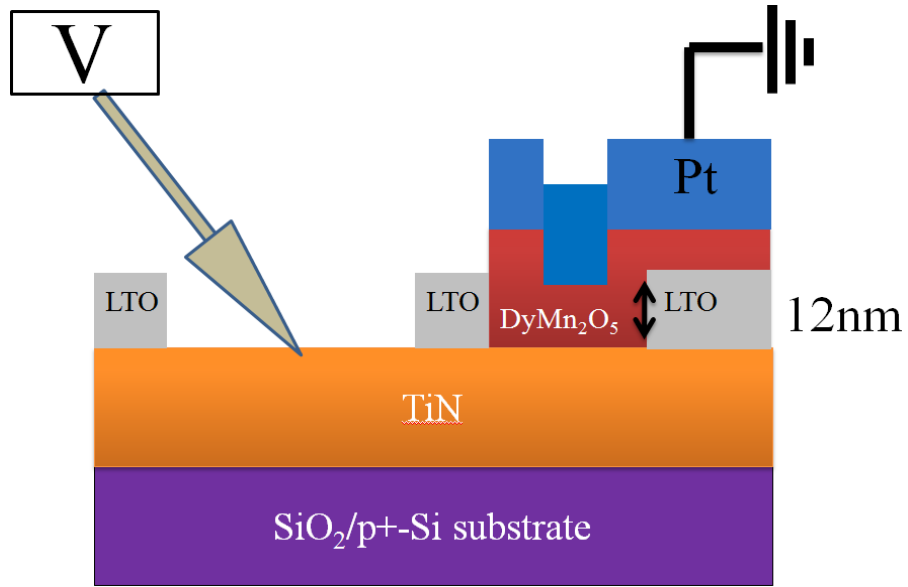


Fig-2.3-1 shows the probes contact with pads.

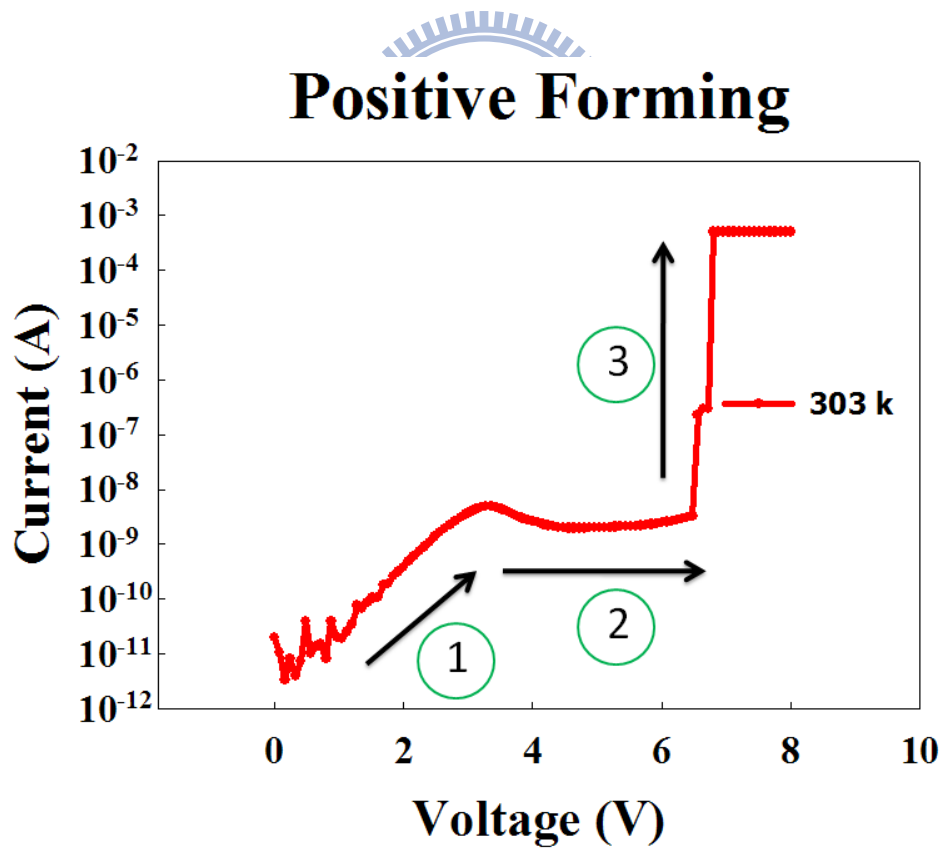


Fig-2.3-2 depicts the forming of STD device.

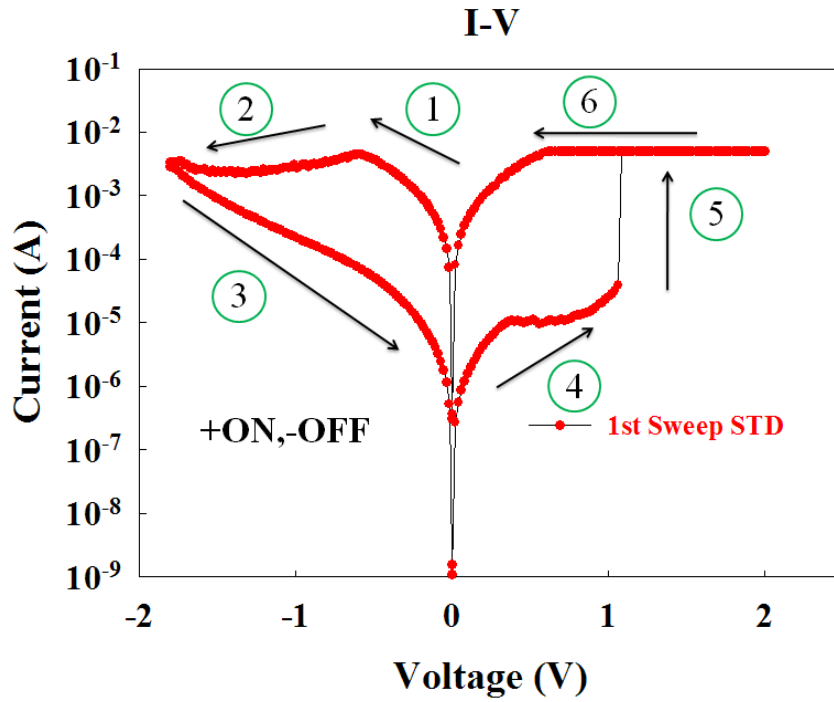


Fig-2.3-3 shows typical current-voltage characteristics of STD device.

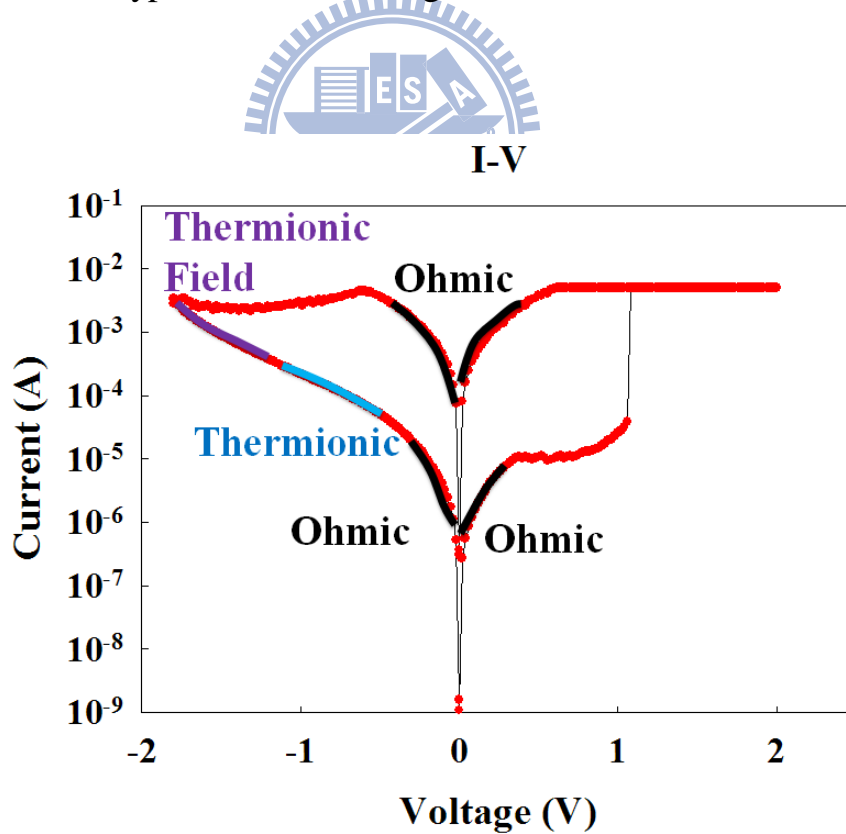


Fig-2.3-4 we can discover the carrier conduction mechanism at a piece of I-V curve.

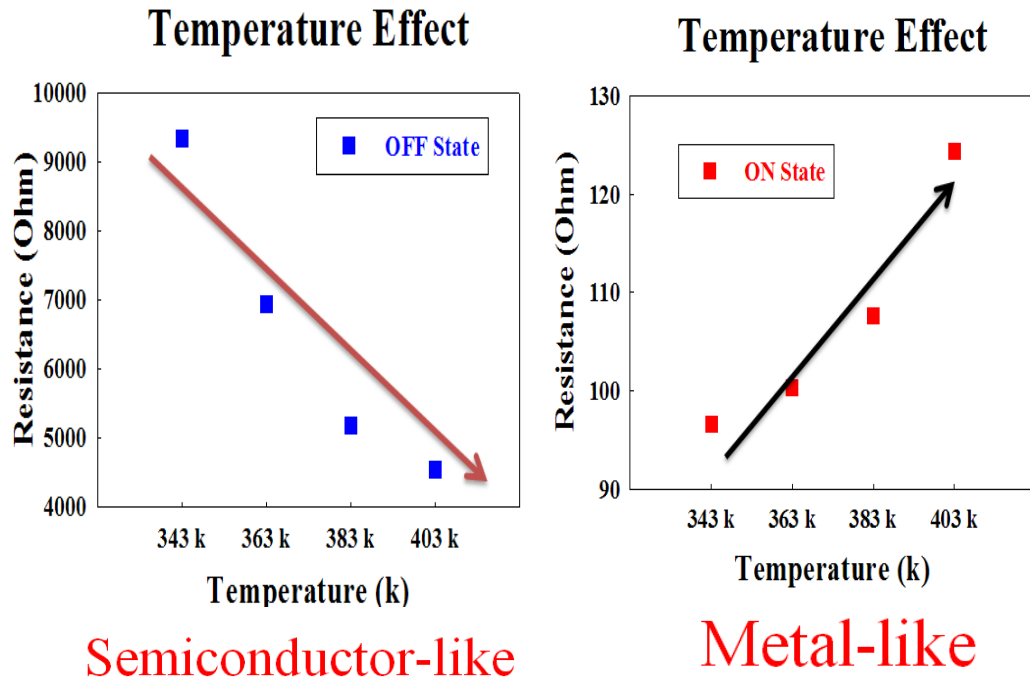


Fig-2.3-5 depicts two different characteristics, one is metal-like at LRS and the other one is semiconductor-like at HRS.

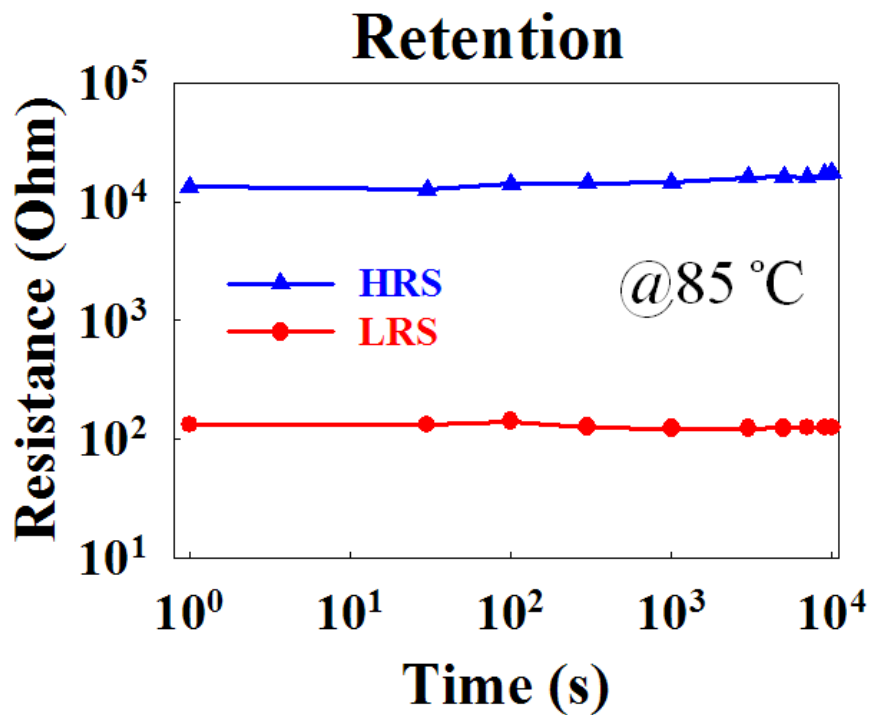


Fig-2.3-5 shows the retention of our device and kept the thermal stress at 85°C.

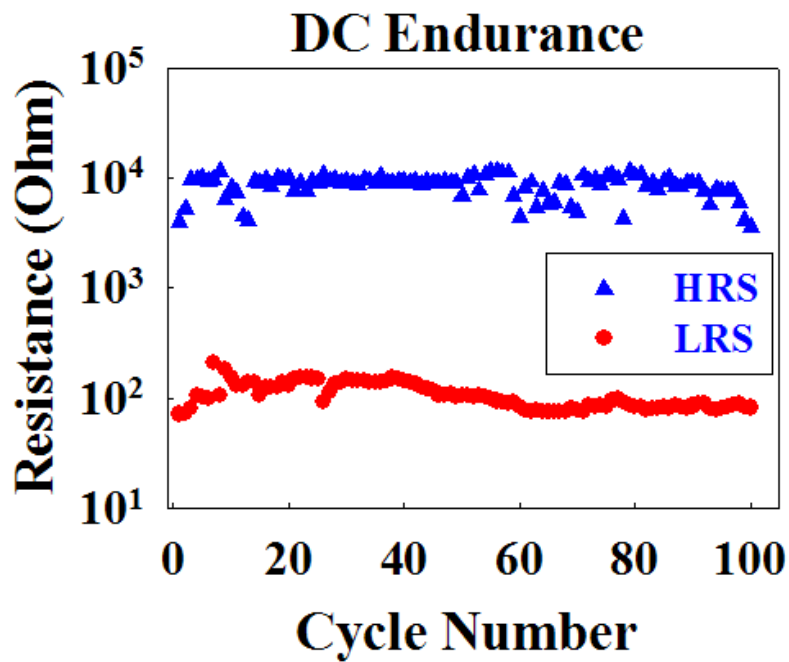


Fig-2.3-6 depicts the endurance characteristics between HRS and LRS of STD device. The switch behavior of this device (on / off ratio) was about 100 resistance ratio at 0.2 V, and the resistance state was gradually stabilized over 100 times of cycles.

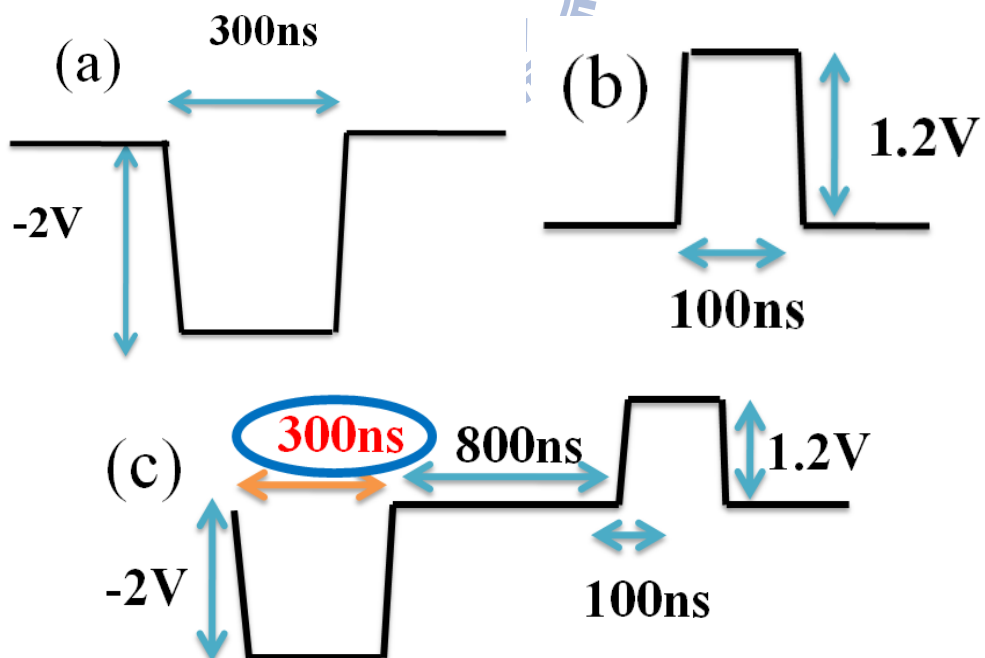


Fig-2.3-7(a) shows the condition of reverse bias pulse and **Fig-2.3-7(b)** depicts the condition of reverse bias pulse. **Fig-2.3-7(c)** shows on/off pulse cycles.

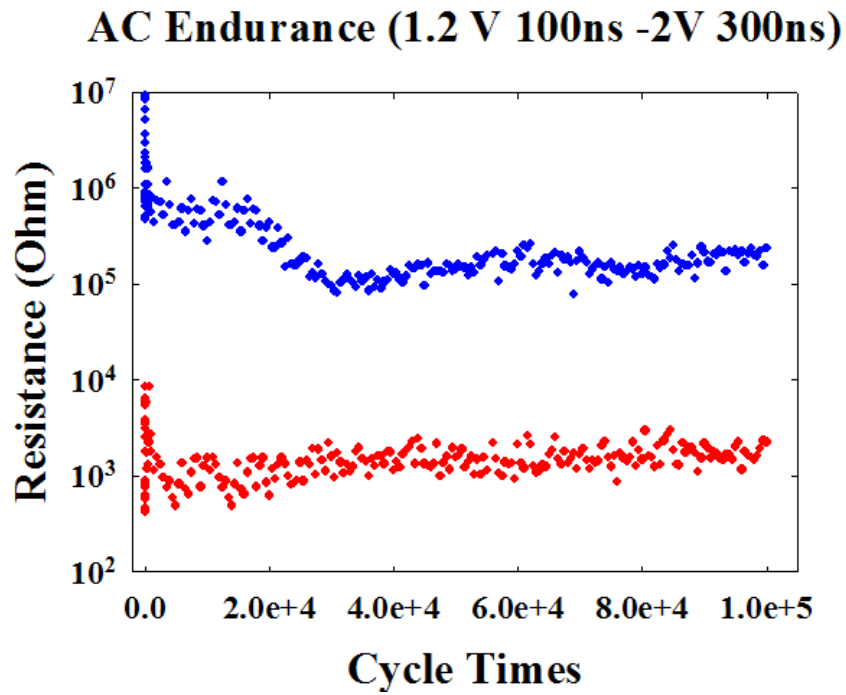


Fig-2.3-8 shows the on / off ratio is about 100 resistance, the HRS fluctuation is acute than LRS.



Chapter 3

Coexistence of Filament and Homogenous Resistive Switching for DyMn_2O_5 film

Resistive switching memories can divide into some mechanisms such as filament-type, interface-type and other types. However, our device I-V curve possesses a strange NDR phenomenon. Subsequently, we will investigate the NDR before forming, after forming and forming-free. Therefore, we discover the device possess filament and homogenous resistive switching behavior.

3-1 Electric Characteristic Measure before Forming

In the chapter3, we have observed a strange phenomenon from forming process. It is a little different from normal forming process because it exist the negative differential resistance (NDR) phenomenon nearly 3V. We will divide into three parts to discuss the NDR, one is temperature effect, another is constant voltage stress and the other is thickness effect.

3-1.1 Temperature Effect

We observed the forming process by using the STD sample in the experiment. First, we select same cell size devices which are on the STD device. And then we sweep the forming process condition at different temperature, i.e., 303k, 323k, 343k, 363k, 383k and 403k. We could observe a trend that the voltage of NDR depends on temperature. On the other hand, the voltage of NDR decreased with increasing temperature, i.e.,

303k is at about 4.2V, 343k is at about 2.7V, and 403k is at about 2V and so on. Fig-3.1-1 depicts what we mentioned above. We select the occurrence voltage of NDR and make a plot recording the distribution of NDR voltage. Fig-3.1-2 clearly shows the voltage of NDR depends on temperature and it shows the NDR voltage decrease with temperature increasing.

3-1.2 Constant Voltage Sampling Effect

In this experiment, we apply a constant voltage to stress the device which is a pristine film and then observe the current of device with time. First, the device is stressed through fixed 2V under different temperature, i.e., 303k, 323k, 343k and 363k. The current-time curve possess two kinds of curves, first is the current gradually increase with time increasing and second is the current possess smooth with time increasing. Fig-3.1-3 shows normal relation between current and time. Subsequently, we applied a fixed voltage 2V to the device. Fig-3.1-4(a) and Fig-3.1-4(b) shows current time curve at 303k and at 323k, respectively. We can observe the different between experiment and we think phenomenon. Under 303k and at 323k, the current-time possesses two trends, first is the current increase with time increasing and second is current decrease with time increase. Finally, the current achieve saturated current value. Fig-3.1-4(c) and Fig-3.1-4(d) depicts the current time curve at 343k and 363k, respectively. Fig-3.1-4(c) and Fig-3.1-4(d) are a little different from temperature under 303k and at 323k. Because there is no a step which is the current increase with time increasing under 343k and 363k. Therefore, we put these relations of current-time in the same plot and then compare them with each other. From Fig-3.1-5 we can discover the rate of current decrease to saturated state depend on the temperature, i.e., the current decay rate at higher temperature is faster than at

lower temperature.

3-1.3 Thickness Effect

We have four different thickness films 4nm, 7nm, 12nm (STD) and 15nm. We choose the same cell size ($8 \times 8 \text{ um}^2$) and then observe their forming behavior. Next, we put the four forming processes into the same plot and then compare with them. Fig-3.1-6 shows we mention above. The figure depicts an ordered phenomenon. The NDR phenomenon exist these different thickness in the same time. And the NDR voltage increased with the film thickness increasing. For example, the 4nm film was at 2.6V, the 12nm was about 4V and so on. We select the NDR voltage and make a plot recording the distribution of NDR voltage with different thickness. Fig-3.1-7 shows the trend we observed.

3-1.4 Mechanism of the phenomenon of NDR before Forming (Conclusion)

The NDR phenomenon depends on three effects: temperature, time and thickness effect. Therefore, we combine three effects that are like an ionic effect due to the ions possess the sensibility of temperature, field and time. However, the oxygen ions play an important role in most RRAM switching mechanism that we had described in chapter1. It is thought that the NDR phenomenon is contributed to the oxygen ions accumulation. In this study, we will bring up an oxygen ion model. The oxygen ions model is about the drifting and accumulating of oxygen ions which form an oxygen-rich region near the interface. [5] [15] [20] [46] The oxygen-rich film is a more insulating film than original so that electrons cannot easily pass through the oxygen-rich region. The NDR phenomenon occurs when the oxygen-rich region

becomes more insulated as larger voltage applied. Fig-3.1-8 (a) depicts the first step of oxygen ions model in pristine state. And Fig-3.1-8 (b) shows the second step of oxygen ions model and the bonds are broken and migrate by applying voltage. The bond between oxygen and metal is broke by external field so that the oxygen becomes oxygen ions. And then oxygen ion can drift to bottom electrode (TiN) by external electric field. Next, Fig-3.1-9 (a) depicts some oxygen ions accumulating are near TiN interfacial layer and then form an oxygen-rich region. But some oxygen ions still combine with TiN and form a TiON layer. The region blocks the carriers passing the interface so the current decrease when the voltage is increased. Fig-3.1-9 (b) shows the oxygen ions drift into TiN electrode by applying forming voltage and the filament is formed in the bulk finally so that the current sharp increase to compliance current at 1mA. The oxygen ions model can explain the phenomenon of NDR by using band diagram. Fig-3.1-10 clearly sees the band was bent upward by oxygen ions accumulating because oxygen ions are negative charge. Some electrons from Pt electrode and bulk were resisted when the band was bent by oxygen ions. It is a reason Schottky barrier height controlled the amounts of electrons pass film to the other electrode. Fig-3.1-10 (a) shows the flat band originally and Fig-3.1-10 (b) depicts the step of breaking bond and migration of the oxygen ions. Finally, Fig-3.1-10 (c) shows the oxygen ions accumulate near the interface and bend the band upward and block the carriers passing the layer.

Subsequently, we used the model to explain our device and applied three effects to confirm the model is feasible. First, we observe the temperature effect for our device. The NDR voltage decreased with increasing temperature. The bond between metal and oxygen can easily are broken and the oxygen ions are easily able to migrate to interface at higher temperature. Oxygen ions would receive more energy at higher temperature than at lower temperature so Fig-3.1-2 just shows the NDR voltage

decreased with temperature increasing. Second, time effect depended on chemical reactive and migratory time. Some bonds between metal and oxygen are weak and migrating to interface need more time. We observed the reactive time was about 50 seconds at 303k, but the reactive time just is about 10 seconds at 323k. It can't observe two parts current-voltage effect at 343k and 363k because the bonds have achieved critical broken bond condition at higher temperature. The effect is sensitive to temperature. And the current achieves the saturated state is sensitive to temperature so the current time relation is Fig-3.1-5. Third, the thickness affected the distribution of NDR voltage. The NDR voltage increases with the film of thickness increasing. We observed the phenomenon that the film is thicker one we have to provide more effective field to reach the NDR effect, and the thinner film don't need too much effective field to achieve the NDR phenomenon so the Fig-3.1-7 shows the NDR voltage decreases with the thickness increasing.

What do the oxygen ions accumulate near the interface? In fact, some oxygen ions accumulated nearing DMO/TiN interface due to one is the initial thin interfacial TiON layer formed on TiN electrode and the other one is low Gibbs free energy of Dy-O.

On the other hand, it needs to possess two effects to reveal the NDR. First, TiN electrode usually also acts as an oxygen reservoir role for the MIM structure^[32]. And then the oxygen ions can't pass the interface because thin interfacial TiON layer was a diffusion barrier for mobile oxygen ions^[33]. Second, Dy is rare-earth atom and its Gibbs free energy is low. Therefore, Dy attracted oxygen ions are similar to TiN so oxygen ions accumulating nearing interface is easily. Interface is formed an oxygen-rich region, and it was also a higher resistive region. Fig-3.1-9 (a) and Fig-3.1-10 (c) depicts we mention above.

However, that effects still needs some evidences to proof the oxygen migrating and accumulating cause by current-voltage are different between to another normal

forming process. It is forming size effect because the NDR is bulk effect, and we can see the obvious phenomenon from Fig-3.1-11. The larger cell size device has larger leakage than the small cell size because the defects generated the forming of leakage in bulk at initial state.

The NDR is not enough energy to make oxygen ions pass the TiON layer, but more of them would overcome the diffusion barrier into TiN electrode once device is applied larger voltage. The conduction path was able to connect the top and bottom electrode each other. Fig-3.1-9 (b) shows the filament is formed.

3-2 Electric Characteristic Measure after Forming

This part of our study, we would discuss basic current-voltage properties after forming. And then we observe operating the properties of DMO.

3-2.1 Normal Operation

First, we applied reverse bias to make the device transiting from LRS to HRS after forming. Subsequently, we can also apply forward bias to make the device transit from HRS to LRS. This forward set switching and reverse reset switching operations is called counterclockwise (CCW) BRS behavior. Fig-2.3-3 indicates we mentioned above. We observed the HRS at set side ($0V \rightarrow 2V \rightarrow 0V$), the NDR occurred in the same polarization. It could be discovered the phenomenon from Fig-2.3-3. The NDR voltage was not only lower than before forming process, but current was also higher than before forming.

First, in order to observe whether the NDR possesses a hysteresis phenomenon, the voltage was swept from 0 V to 0.7 V and then swept from 0.7V to 0V. It could be observed current exist different between original and later value. It meant there were

two different states. Fig-3.2-1(a) depicts different states. Original current was higher than later current, it is like reset phenomenon. Second, the voltage was swept from 0V to -1.8V and then swept from -1.8V to 0V. We could note the current value were different. It could see what we say from Fig-3.2-1 (b). The operating mode was 0V \rightarrow 0.7V \rightarrow -1.8V \rightarrow 0V. It exist reproducible sub-clockwise (sub-CW) parasitic switching mode, but at a current sub-cycle, a cycle (sub-CW) lower than standard LRS/HRS cycles. The resistance state is defined as super-high resistance state (SHRS) and high resistive state (HRS) was same as original RRAM and sub-RRAM or sub-CCW. (i.e. it is higher resistance for Original RRAM and lower resistance for sub-RRAM, their resistive state matched each other.) Fig-3.2-2 (a) shows that the device is operated between SHRS and HRS for 100 cycles and Fig-3.2-2 (b) shows the DC endurance ON (HRS)/OFF (SHRS) ratio was about 1.5 orders.

3-2.2 Temperature Effect for sub-RRAM

The part of experiments, we decreased temperature from room temperature (RT) to 80⁰K. And then we observe the trend of sub-RRAM (NDR). Fig-3.2-3 (a) depicts the SHRS is different between at 80⁰K and at RT by applying the same condition. And then we modified the V_{stop} condition at 80⁰K from 0.7V to 0.9V, the SHRS was able to achieve the same state with temperature was at RT. It could note the phenomenon from Fig-3.2-3 (b). We mentioned above the NDR before forming depended on temperature and the sub-RRAM (NDR) after forming depended on temperature, too. We can compare with fig-3.1-2. It cannot complete the NDR phenomenon cause by the SHRS state was not at lowest state. However, we have to change the condition in order to achieve the same state and proof we think about it so the condition is at 0.9V can achieve the lowest state.

3-2.3 Fitting Mechanism for sub-RRAM after Forming

Here, we would introduce carriers' conductive process and divide into two parts, part one is original RRAM and part two is sub-RRAM. And the original RRAM fitting mechanism has shown in chapter2 so we will mention sub-RRAM fitting mechanism.

<sub-RRAM>

Its ON state is the same with original-RRAM OFF state, so their mechanisms were the same too. We just only discuss the mechanism of SHRS from Fig-2.3-4. At reverse bias, the carrier conduction mechanism is thermionic field emission under large bias (from -1.5V to -1.8V) and then the carrier conduction was Schottky barrier emission at medium bias (from -0.7V to -1.3V). Finally, the carrier conduction was Ohmic transportation under the low bias.

3-2.4 Normal Switching Mechanism after Forming Process(conclude)

We mentioned the oxygen ions model in our device during forming process, and the NDR phenomenon result from oxygen ions migration and accumulation nearing the interface (DMO/TiN). However, we also observed the NDR phenomenon exist in IV curve after forming process. And the NDR phenomenon also implies the sub-RRAM behavior and temperature effect. We attribute these effects we mentioned above to be the oxygen ions effect. Therefore, we will use the model explain the original-RRAM and sub-RRAM.

3-2.4-1 Original-RRAM

At first, the bulk is formed CPs and then CPs connected two electrodes after forming process. Fig-3.1-9 (b) and Fig-3.2-5(a) shows the status of forming CP. We applied a reverse bias to reset the state from ON state to OFF state. The oxygen returned to bulk and then the recovered the CPs (i.e. the rupture the filament) so the carriers are difficult pass the film from one electrode to another. Fig-3.2-5(b) indicates the reset process. We can apply a forward bias to make the state from OFF to ON state again. However, the device will possess the NDR at lower forward bias. The reason is the oxygen will accumulate near interface at low bias. The CPs is formed once we apply large bias and the set process is produced. The state from OFF to ON state cause by oxygen migrated from bulk to electrode and formed filament (CP). Fig-3.2-5 (c) depicts the oxygen ions drift to interface and Fig-3.2-5 (d) shows the NDR phenomenon. And then Fig-3.2-5 (a) indicates the set process is achieved by applying large voltage.

We can go back to see the fitting mechanism. In the ON state, the carrier conduction is Ohmic because the CPs is formed. And then the carrier conduction is Schottky conduction mechanism at the OFF state because the oxygen ions migrated to the interface and accumulated near the interfacial layer. The electrons conduction is also verify the oxygen ions model.

3-2.4-2 sub-RRAM

Here, we explain the sub-RRAM switching mechanism. First, the device is operated at OFF state. And the NDR exist in IV curve by applying a low forward bias because the oxygen ions drift to the interface and accumulate near the interface. The

phenomenon shows Fig-3.2-6 (a) is the migration of oxygen ion and Fig-3.2-6 (b) is the accumulation of oxygen ion. The bias is swept back to 0V when the voltage is at 0.7V. We don't continue to apply larger bias to the device so the device cannot achieve the set process. Therefore, we can observe the state is changed to SHRS because the oxygen-rich layer is produced. Fig-3.2-6 (c) depicts the oxygen ions migrate to bulk and the oxygen-rich layer is vanished when we apply reverse bias. Therefore, the switching behavior results from the migration and accumulation oxygen ions.

We observed the main conductive mechanism of carrier dominated by thermionic emission from fitting result in sub-RRAM. In fact, the conduction mechanism verifies our oxygen ions model. Schottky emission dominated the conductive mechanism result from the oxygen ions accumulate at interface (DMO/TiN) and form an oxygen-rich layer. On the other hand, the barrier height can be bending the band upward or downward for sub-RRAM when we applied forward or reverse bias. And the different barrier height could be changed different state so the fitting conduction is thermionic emission. The current consequently were different between ON and OFF state because the capability of hopping the barrier was different for electrons. For example, the carriers can't easy hop the higher barrier and can easy hop the lower barrier.

The temperature effect is similar to the NDR is before forming. We observed the NDR voltage at 80⁰K was higher than at RT because the mobility and accumulative capability of oxygen ions were weak. The oxygen ions would get more energy from environments at higher temperature so they don't need external larger bias to achieve accumulation. On the contrary, they acquired more external lager bias we gave to achieve the accumulation of oxygen ions. In other words, the Schottky barrier was not complete formation by oxygen ions accumulating, and then the electrons could easily

cross through the bulk at lower temperature. The NDR phenomenon before or after forming is driven from the migration and accumulation of oxygen ions and filament is formed by oxygen vacancies. Therefore, the sub-RRAM implies interface switching mechanism. The original-RRAM possesses large current value is like a filament type switching mechanism.

Subsequently, we have to compare filament-type to interface-type. The conductive mechanism is filament-type if we apply a larger bias but the conductive mechanism is interface-type if we change the set stop (i.e. change sweeping voltage from 2V to 0.6V). The filament was not the important role because the filament is ruptured and the migration and accumulation of oxygen ions are just dominating transitional mechanism at OFF state. On the contrary, the interface-type was not a key role at filament-type operating. The size effect is an important evidence for the interface-type mechanism because the conductive circumstance is relative to the oxygen in bulk [34]. Fig-3.2-7 depicts SHRS and HRS depended on cell size but LRS was independent to cell size. It is independent to cell at ON state because filament was a cone-shaped configuration which was just a local shape. It depended on cell size effect because the oxygen dominated state (HRS and SHRS) for sub-RRAM. The current was larger when cell size was bigger, and the current was lower when cell size was smaller. In other words, the resistance was large when size was smaller. We observe the $0.64 \mu\text{m}^2$ of cell size was larger resistance and the $64 \mu\text{m}^2$ of cell size was lower resistive state. The resistance decreased with increasing cell size we could see the effect from Fig-3.2-7 again.

3-3 Forming-Free Switching Mechanism

In many papers, there is some interface-type which was not forming process such

as PCMO [17] [34], SZO [47] and STO [48]. The film existed to original resistive switching behavior or characteristic before forming process. However, we observe there is the NDR phenomenon before and after forming and the NDR possesses a hysteresis phenomenon after forming process. We think our device should possess the forming-free and pure interface-type mechanism behavior before forming process. Subsequently, we would investigate the characteristic before forming.

3-3.1 Operating Current-Voltage before Forming

First, we selected the STD device to experiment our study. And then we have to change the forming V_{stop} condition from 8V to 5V in order to avoid forming breakdown phenomenon. The V_{stop} is required a larger voltage than NDR voltage and then swept loop from $0V \rightarrow 5V \rightarrow 0V$. The current is detected the values shows Fig-3.3-1(a). Fig-3.3-1(a) shows the state possess two different state between original and later value. Next, we set the other polarization V_{stop} condition, and then swept loop from $0V \rightarrow -5V \rightarrow 0V$. Fig-3.3-1(b) depicts we mentioned above. From Fig-3.3-1(b) we can observe the states are also different so we read forward bias to check out whether the state turn on. Fig-3.3-1(c) depicts the state was not at ON state. Therefore, it is possible that the action of turning on have to apply larger reverse voltage to make our device achieving ON state. Therefore, we reset reverse V_{stop} from -5V to -8V, but the voltage (-6V) has achieved the film breakdown voltage. We cannot operate the characteristic before forming.

(Conclude)

First, Fig-3.3-2 (a) shows the sub-RRAM the operating condition is at forward bias of 0.6V and at about reverse bias of -1.8V. The turn-on voltage required larger voltage than the turn-off voltage. Therefore, the bias different is about 3 times. We go back to

see Fig-3.3-2 (b) indicates the operating mode before forming, and we discover V_{stop} was about 5V at forward bias. We have to apply larger voltage was about 15V ($5V * 3 = 15V$) to make our sample to turn on by the inference of sub-RRAM model. In other words, our devices have to endure -15V reverse bias so we have to change the characteristics of our device (DMO) to endure larger breakdown voltage. The simplest method is changed the thickness of film.

Subsequently, we calculated the film field. First, we confirmed one thing the film breakdown voltage for 12nm (STD) was about -6V. It is breakdown field about 5MV/cm for 12nm DMO film. We would deposit thickness of film was larger than 25nm DMO film if the DMO film has to endure to avoid breakdown under the larger voltage was about -12V~ -15V.

3-3.2 Pure Interface-type Operated Mode

We deposited the thicker DMO film was about 45 nm by using sputtering system. We use the sample to confirm whether our model is right. We calculated the breakdown voltage depended on breakdown again. We computed the breakdown voltage value was about 20V (i.e. $5(\text{MV}/\text{cm}) * 40(\text{nm}) = 20\text{V}$) under reverse bias. First, we sweep the sample by applied a forward bias condition was $0\text{V} \rightarrow 7\text{V} \rightarrow 0\text{V}$. Fig-3.3-3 (a) shows the properties also possessed the NDR phenomenon and the NDR voltage was at about 2V. Subsequently, we confirm the whether the state was transition from one state to another state. We repeated the same swept condition and observed the current value. Therefore, it was sure the state is transition from ON state to OFF state. Fig-3.3-3 (b) could know the NDR was a conversion process. Next, we applied a reverse bias to turn on state, so the sample was gave a voltage condition was $0\text{V} \rightarrow -12\text{V} \rightarrow 0\text{V}$. The device can be avoided the breakdown phenomenon after we

have calculated the breakdown voltage of thicker device is larger than -12V. Fig-3.3-3 (c) the current was different from OFF state, and we will do the same action to check out whether the state was transition. We applied the lower forward bias to read the state. Fig-3.3-3 (d) indicates the state transition from OFF state to ON state. The property was turning on was under the reverse bias and turning off was under the forward bias. The IV curve shows a reproducible characteristic. The polarization was the same with sub-RRAM, and the characteristic was just like an enlarged sub-RRAM. We have to connect the resistive switching behavior relationship with each other. We called the switching behavior was Super Low Current RRAM (SLC-RRAM). But the characteristics were some advantages and some disadvantages. The advantages were the current was very low, and resistive switching behavior was forming-free. The disadvantage was operating voltage was too high. The switching behavior still depended on cell size (The $0.64 \mu\text{m}^2$ cell size was higher resistance, and the $64 \mu\text{m}^2$ cell size was lower resistance); we could observe the phenomenon of size effect from Fig-3.3-4.

(Conclude)

Here, we absolutely discuss the SLC-RRAM model. The SLC-RRAM was like an enlarged sub-RRAM, so we thought the characteristic was relative to the migration and accumulation of oxygen ions. We would use the same model to explain the property. First, we can know the SLC-RRAM was a switching behavior was at ON state by using reverse bias and at OFF state by using forward bias before forming process. In some papers [34], the switching behaviors possess forming-free, size effect and low current usually called interface-type switching property. Our thicker device conformed to interface-type property, so we confirm the SLC-RRAM was interface-type. In fact, we explain the SLC-RRAM was also oxygen ions

accumulating at interface and forming an oxygen-rich layer. In other words, it was higher resistance region nearing interface (DMO/TiN) when we applied a forward bias. We see the oxygen ions model from Fig-3.3-5 (a) and Fig-3.3-5 (b). Fig-3.3-5 (a) depicts the oxygen accumulate nearing interface when we give forward bias and then form oxygen-rich region (i.e. form a thin higher resistance (THR)) at interface by gathering oxygen. The electrons were difficult to overcome the THR if the oxygen was gathered by external field. The current decreased with voltage because more oxygen was accumulated nearing interface with increasing voltage. And Fig-3.3-5 (b) shows the oxygen went back to bulk when the device was gave a reverse bias. The oxygen recover defect in the bulk, and the film was similar with original film which to the accumulation of oxygen ions, so the electrons was able to overcome lower resistive film to pass to the other electrode. We have to apply a reverse bias to turn on the device because the oxygen ions would go back to bulk.

On the other hand, the Schottky barrier is bend the band upward when the oxygen ions accumulate near interface and the Schottky barrier is bend the band downward when the oxygen ions go back to bulk. Fig-3.3-5 (c) and (d) In this part, we absolutely discuss the interface-type switching mechanism and there is no filament effect to affect our device, so the current was just lower. SCL-RRAM can compare with sub-RRAM, but the sub-RRAM current was very high to SCL-RRAM. We thought a reason which was the filament leakage was a little effect into to sub-RRAM. They possess the same mechanism was the accumulation of oxygen nearing interface.

3-4 The Thin DMO +Nitrogen (DMON) Layer Effect

In this study, we use the sample2 was a co-sputtered device and the sample2 we had described how to deposit the process flow by using sputter in chapter 2 experiment

process flow. The cross-section is like Fig-2.1-3. Here, we just only mentioned its characteristics of sample2 and the device is also an important evidence to conform the oxygen accumulation and migration model. The part of our studies, we will only discuss the sample2 sub-RRAM to compare with STD sub-RRAM.

First, the sample2 also needed to go through forming process, and the device possesses the huge NDR phenomenon before and after forming. We observed the Fig-3.4-1 shows the huge NDR phenomenon characteristic at forming process. We selected a STD NDR property (i.e. Fig-3.2-2 (a)) to compare with sample2. And then we combine two curves in the same scale in order to compare to each other. Fig-3.4.2 (a) depicts what we say. Fig-3.4.2 (a) indicated the triangle-up symbol is DMO+NH₃ (DMON) characteristic and the circle symbol is DMO (STD) characteristic. DMON and DMO both possess sub-RRAM property and the NDR voltages are similar to each other. We can observe the current of DMON and DMO are the same value under low forward bias but the current are different under the NDR voltage. Fig-3.4.2 (a) can depicts the DMON possess the huge NDR than the DMO and the DMON resistive state was lower than the DMO resistive state (i.e. DMON SHRS was lower than DMO). Fig-3.4.2 (b) indicates the sub-RRAM HRS and SHRS ratio for DMON and DMO. By the way, Fig-3.4.2 (b) indicates we selected 10~15 device from the STD sameple1 and the DMON sample2 and then acquired their ON/OFF ratio every device by sweeping 20 cycles and we combine all ON/OFF ratio to generate distribution. Fig-3.4-2 (a) depicts the DMO sub-RRAM ON/OFF ratio was about one order and the DMON sub-RRAM ON/OFF ratio was about two order.

Here, the DMON possessed a larger the NDR phenomenon because the nitrogen bond possess unpaired covalence bond so the film generate many traps in the film. In other words, the nitrogen can easy catch the oxygen ions when the oxygen migrated to interface. The oxygen model we mentioned above formed the NDR phenomenon so

the nitrogen bond increased the oxygen attraction in the bulk when we deposited a thin nitrogen layer. It is important evidence the oxygen accumulated nearing interface.

(Conclude)

The DMON device is also able to verify the oxygen ions model because the nitrogen unpaired covalent bond effect. And its sub-RRAM possessed some advantages, such as larger ON/OFF, lower current value and it could be formed multi-bit, scaling down.

3-5 Conclude Coexistence of Interface and Filament- type Mechanism

In part1, we introduced the forming process mechanism and then we observe a phenomenon was the NDR nearing 2~3V. So we do some experiments (thermal, thickness, and time) in order to result from what happen to them. Finally, we could understand the NDR was the migration and accumulation of oxygen ions, so we brought up the oxygen ions model by referring some papers [5] [15] [20] [46]. In DMO film, the Dy atom is one of key role because it possessed an attraction for oxygen-ions, and the TiN electrode was also one of important role for the NDR because it was a reservoir and diffusion barrier for oxygen. On the other hand, the NDR possessed two needs one is Dy attraction and TiON diffusion barrier under lower bias, and then the completely formed soft-breakdown under large bias. The oxygen no possessed more energy to pass the barrier and attraction under lower bias and the oxygen can overcome the barrier and attraction by large external field and temperature so we have to provide larger voltage and temperature. Therefore, temperature, thickness, and time affected the NDR.

In part 2, the basic properties still possessed the NDR after forming so we do a little

different operating condition. We attempt to operate the device before set process and we can discover the NDR also imply the existence of other RRAM. It is different from original RRAM so we called sub-RRAM. Subsequently, we investigated the sub-RRAM mechanism and it was similar to the characteristic before forming depended on temperature. We also analyze the conduction mechanism of sub-RRAM by fitting current-voltage curve and the carrier main conduction mechanism shows Schottky emission. The carrier fitting conduction could be thought sub-RRAM was interface-type and original was filament-type RRAM. We must confirm the sub-RRAM was interface-type by size effect and the original RRAM was filament through no size effect. We discovered the coexistence filament-type (original-RRAM) and interface-type (sub-RRAM) and then we investigated the conduction mechanism for the coexistence RRAM.

In part 3, we believed our devices possess interface-type RRAM property before forming (i.e. forming-free). First, we try to changed different forward bias V_{stop} condition from 8V to 5V, we can discover the state was different between original and later in STD device. Turning on process was fail because the film was too thin to endure the film breakdown so we try to deposit the thicker film (45nm) in order to avoid the film breakdown. The thicker film was operated by some conditions and it was forming-free switching behavior and we called super low current RRAM (SLC-RRAM). It was just like an enlarged sub-RRAM. We discovered the SCL-RRAM depended on size was the same with sub-RRAM. It could confirm a thing our oxygen accumulation model was possible.

We need more evidences to verify the oxygen ions model and could be application of sub-RRAM so we have to change some fabrication parameter to confirm the model. In part 4, we changed fabricated condition the sample 2 device was co-sputter nitrogen into film and formed a thin DMO-nitrogen thin film in order to confirm our

model. It could be discovered the NDR is huge than STD device because the nitrogen possess some unpaired covalence bonds. In other words, the bonds could catch more oxygen ions nearing interface result in the resistance was larger than STD or it could also say more oxygen accumulation nearing interface result in the Schottky barrier is increased. Therefore, the current of DMON were lower than DMO. We consider the larger ON/OFF ratio than the STD.

Concluding we mentioned, it is an important thing the interface-type conduction mechanism have existed for our device. Because the film thickness effect affects the film main conduction mechanism, the interface-type competes with filament-type mechanism when we operated in different conditions. We can observe the main interface-type mechanism in the thicker device because the breakdown voltage is higher than the SLC-RRAM turning on voltage (before forming). On the contrary, we can observe the filament-type in thin film because the SLC-RRAM turning on voltage is higher than breakdown voltage but we still are able to see the interface-type (sub-RRAM) in main filament mechanism. Such as the phenomenon (sub-RRAM is still in filament-type), we attributed the oxygen migration and accumulation still slightly affected our device. Therefore, we still observed the size effect of OFF-state and sub-RRAM after forming process.

We can obtain some the RRAM mechanisms from this study such as interface-type and filament-type. The interface-type compete to filament-type in different thickness DMO device because Dy and TiN electrode affect the RRAM switching behavior in the film. Wherefore, coexistence of interface and filament-type RRAM are possible and they don't contradict each other. These concerns maybe apply to novel RRAM.

Temperature Forming Effect

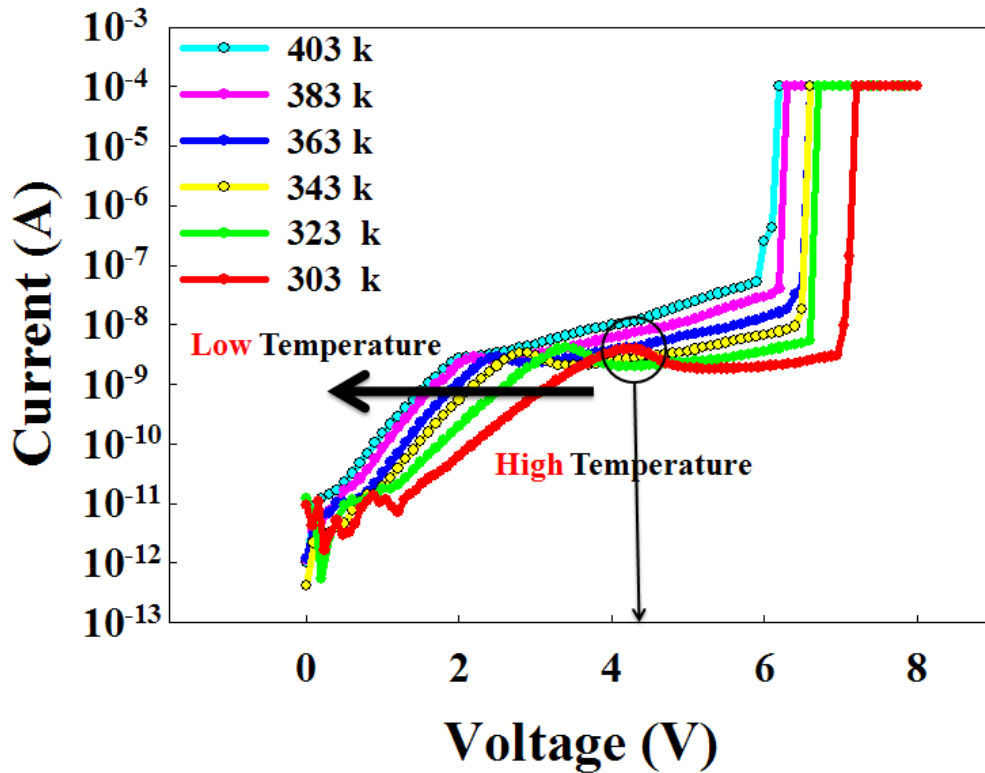


Fig-3.1-1 shows the NDR voltage depend on temperature

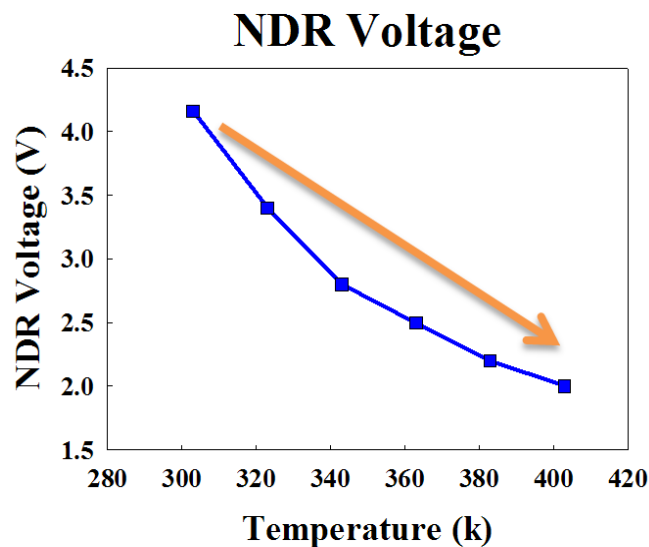


Fig-3.1-2 clearly shows the voltage of NDR depends on temperature and it shows the NDR voltage decrease with temperature increasing.

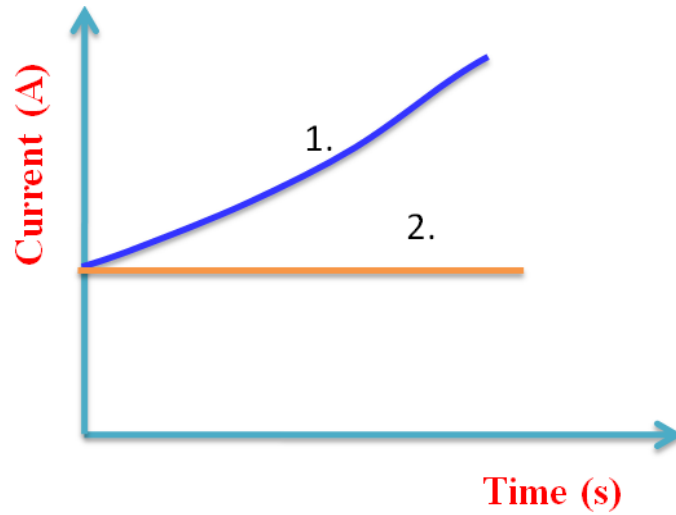


Fig-3.1-3 shows normal relation between current and time.

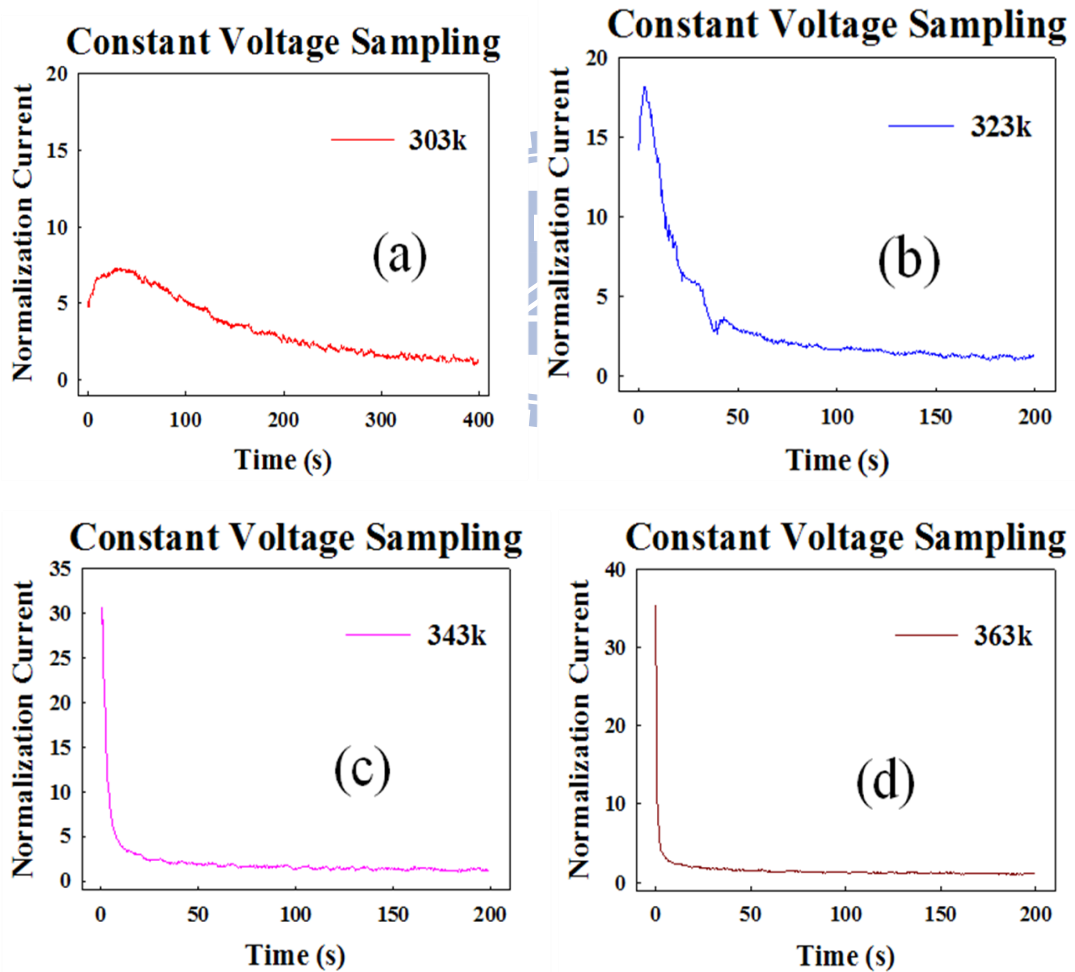


Fig-3.1-4(a) and Fig-3.1-4(b) shows current time curve at 303k and at 323k, respectively. Fig-3.1-4(c) and Fig-3.1-4(d) depicts the current time curve at 343k and 363k, respectively.

Constant Voltage Sampling

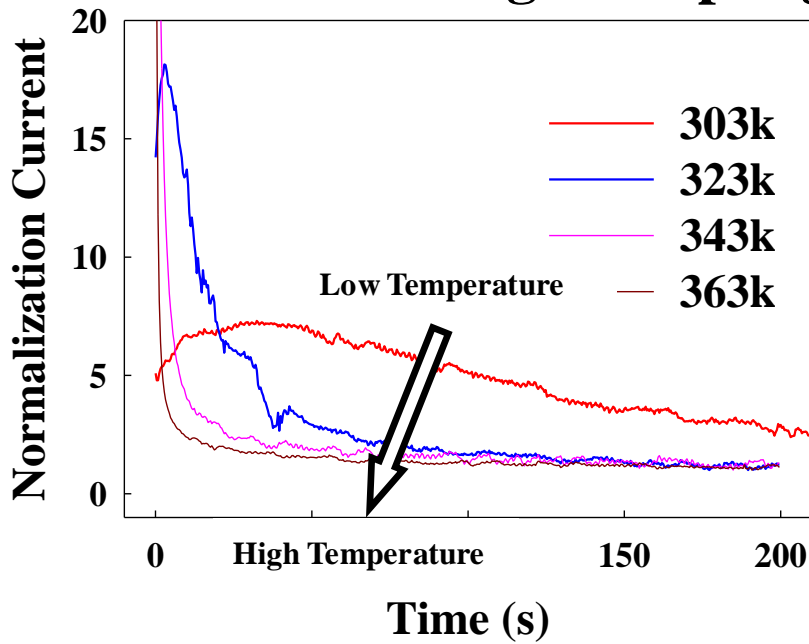


Fig-3.1-5 depicts these relations of current-time in the same plot and then compares them with each other. And the current decay rate at higher temperature is faster than at lower temperature.

Different Thickness Forming

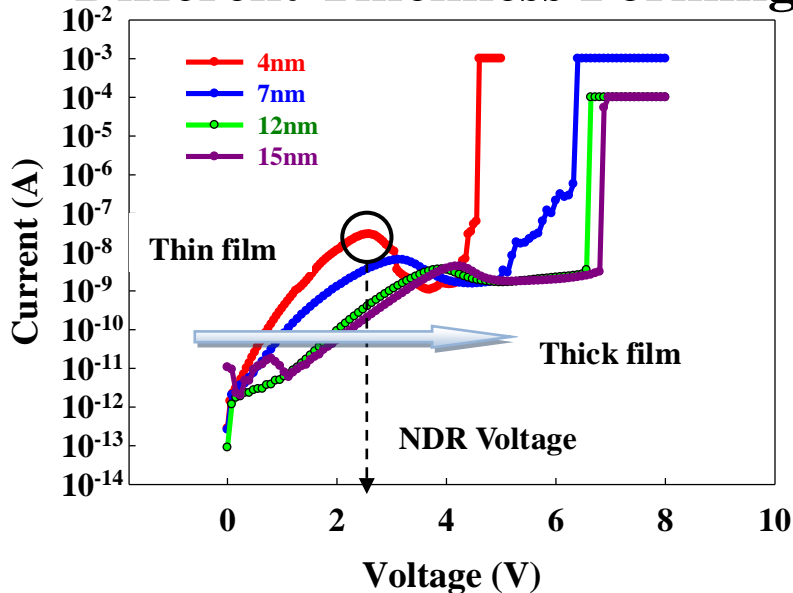


Fig-3.1-6 shows the forming processes of four different thicknesses into the same plot and then compare with them.

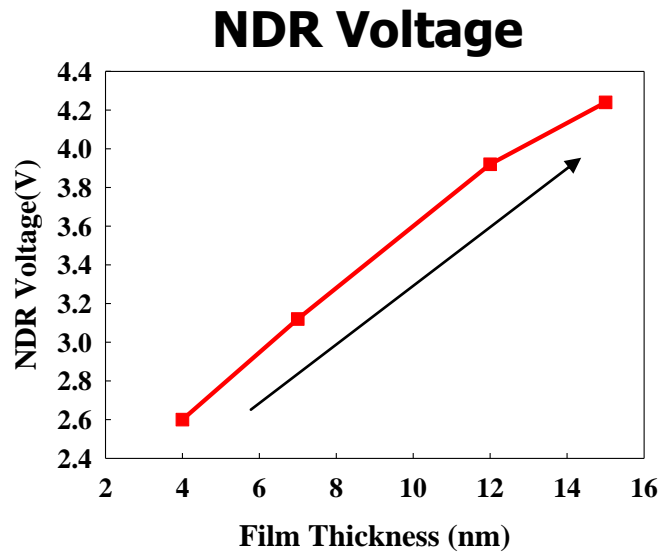


Fig-3.1-7 shows the NDR voltage and makes a plot recording the distribution of NDR voltage with different thickness, i.e., the NDR voltage increase with film thickness increasing.

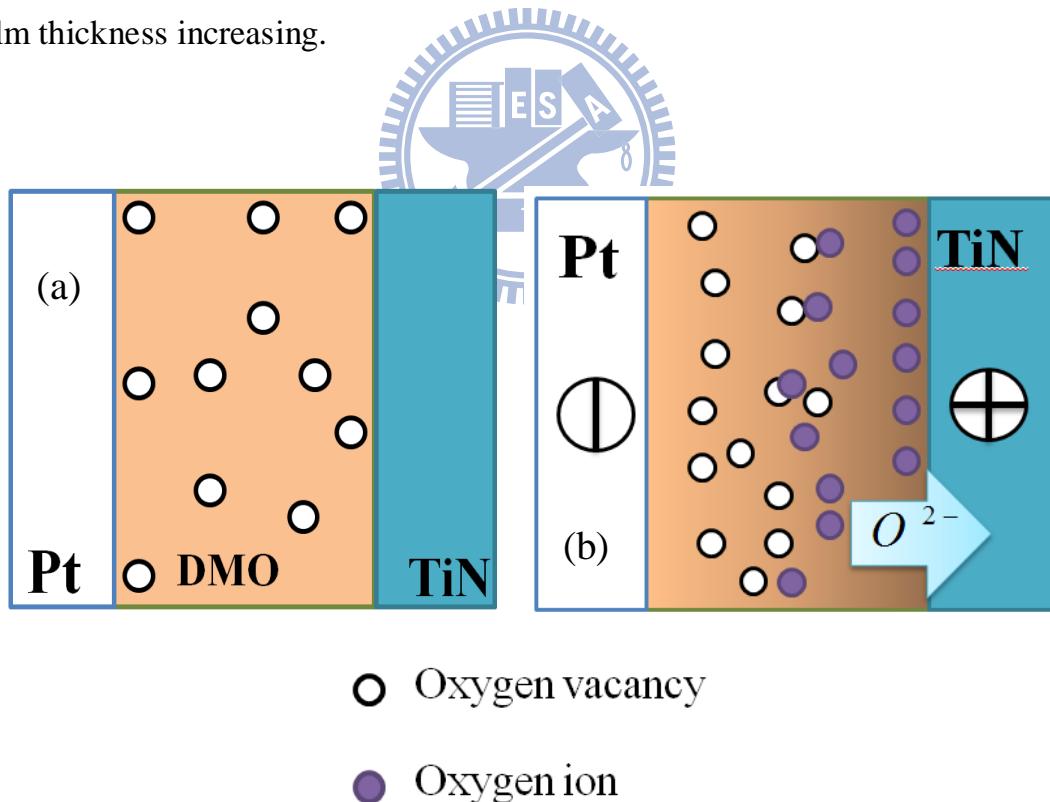


Fig-3.1-8 (a) depicts the first step of oxygen ions model in pristine state. And **Fig-3.1-8 (b)** shows the second step of oxygen ions model and the bonds are broken and migrate by applying voltage.

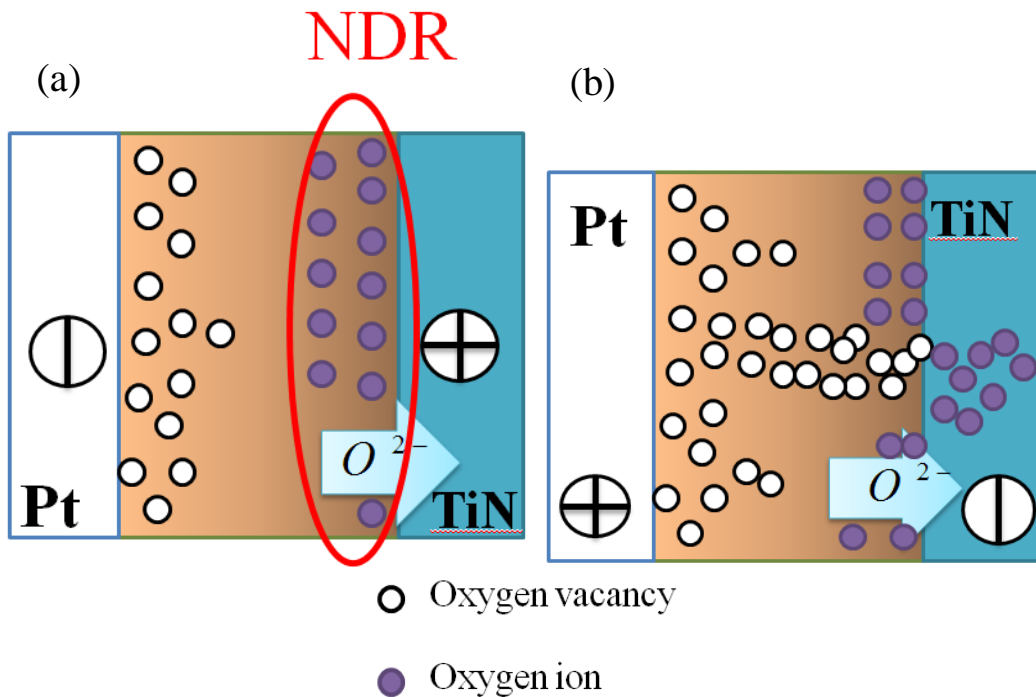


Fig-3.1-9 (a) depicts the oxygen ions will accumulate near TiN interfacial and form an oxygen-rich region. **Fig-3.1-9 (b)** shows the oxygen ions drift into TiN electrode by applying forming voltage and the filament is formed in the bulk, finally.

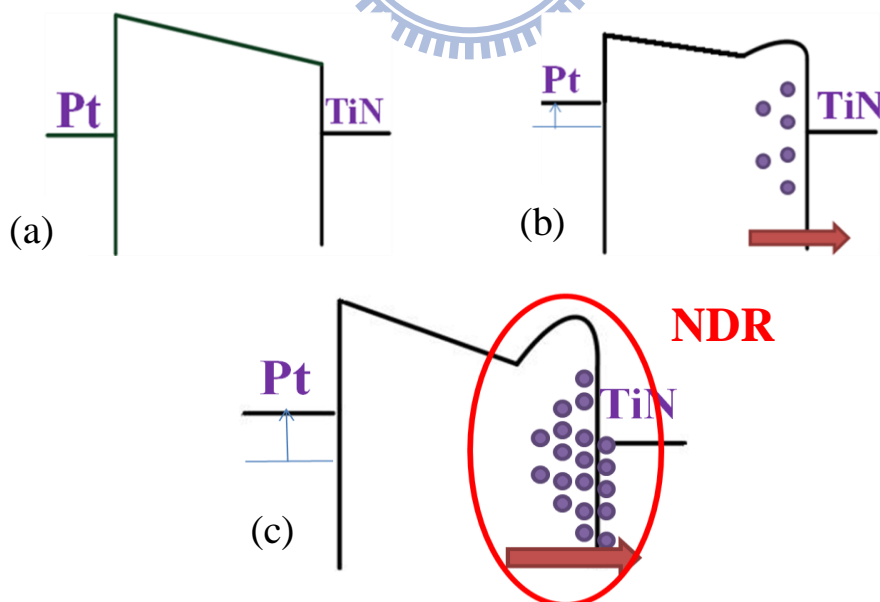


Fig-3.1-10 (a) shows the flat band originally and **Fig-3.1-10 (b)** depicts the step of breaking bond and migration of the oxygen ions. **Fig-3.1-10 (c)** shows the oxygen ions accumulate near the interface and bend the band upward.

Forming Size Effect

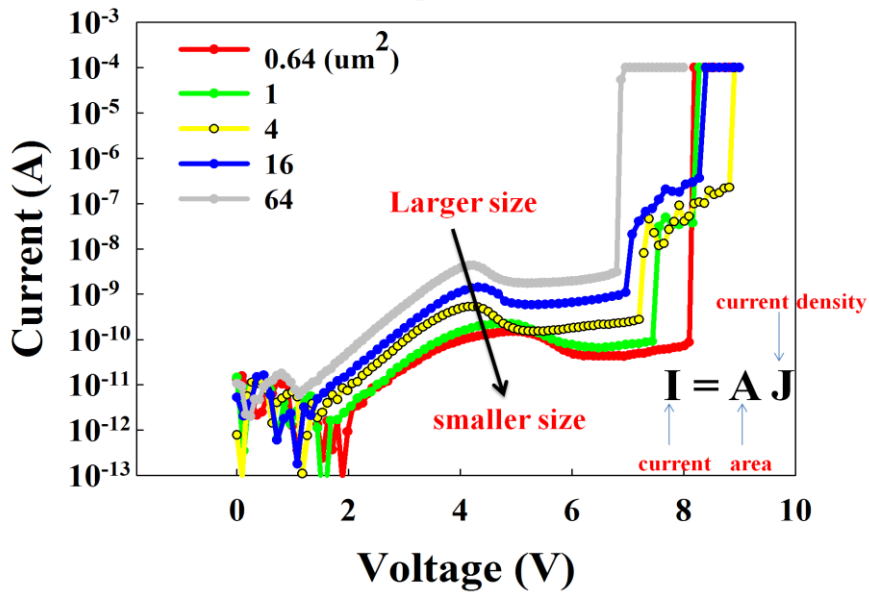


Fig-3.1-11 depicts the larger cell size device has larger leakage than the small cell size because the defects generated the forming of leakage in bulk at initial state.

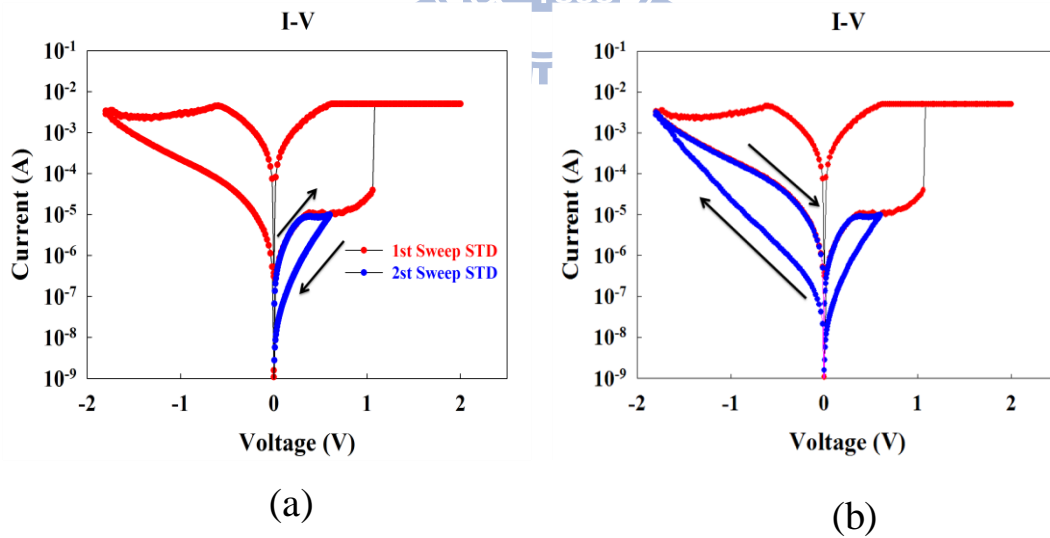


Fig-3.2-1(a) depicts different states. Original current was higher than later current, it is like reset phenomenon. **Fig-3.2-1 (b)** indicates the voltage was swept from 0V to -1.8V and then swept from -1.8V to 0V and we could note the current value were different.

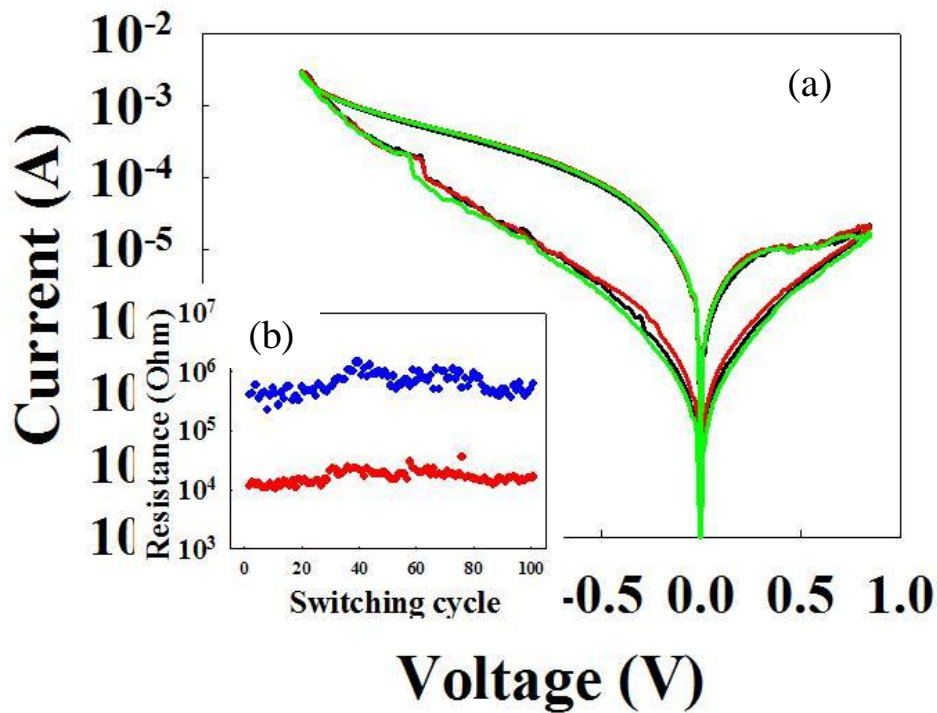


Fig-3.2-2 (a) shows that the device is operated between SHRS and HRS for 100 cycles and **Fig-3.2-2 (b)** shows the DC endurance ON(HRS)/OFF(SHRS) ratio was about 1.5 orders.

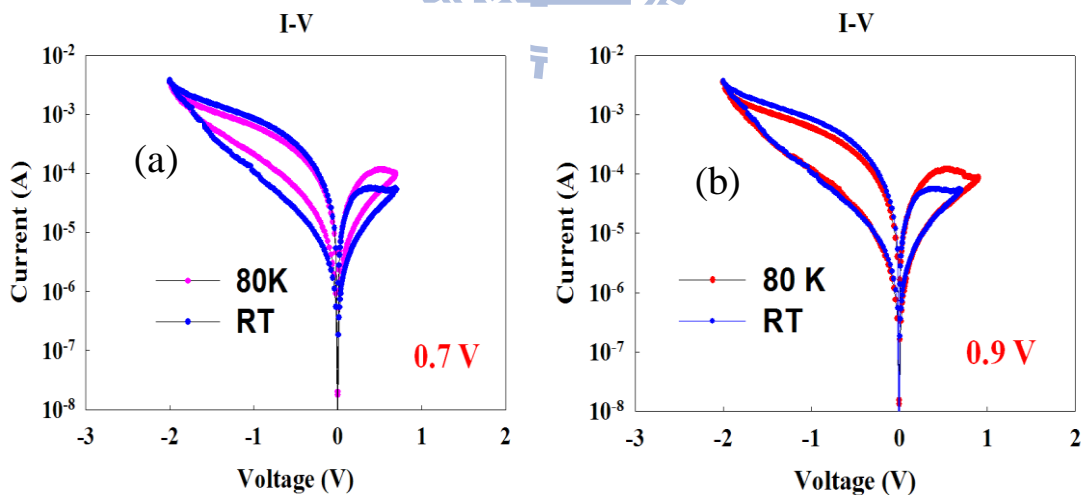


Fig-3.2-3 (a) depicts the SHRS is different between at 80⁰K and at RT by applying the same condition. And **Fig-3.2-3 (b)** shows the V_{stop} condition was changed from 0.7V to 0.9V at 80⁰K, the SHRS was able to achieve the same state with temperature was at RT.

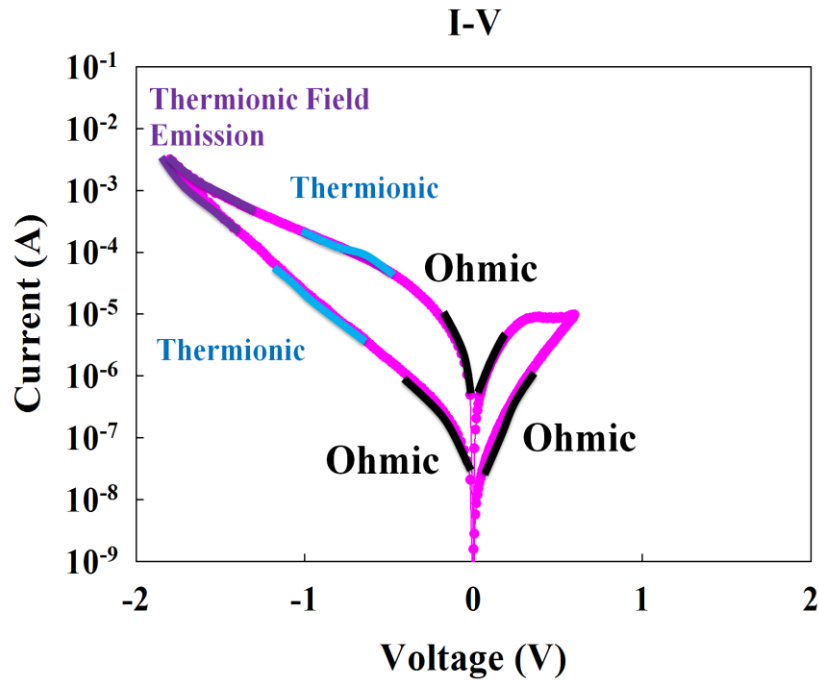
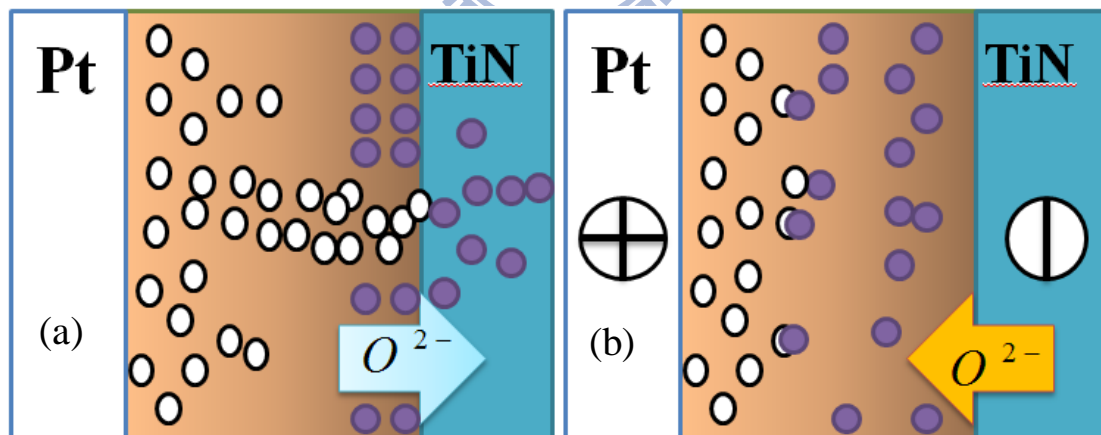


Fig-3.2-4 indicates the carrier conduction mechanism is thermionic field emission under large bias (from -1.5V to -1.8V) and then the carrier conduction was Schottky barrier emission at medium bias (from -0.7V to -1.3V). Finally, the carrier conduction was Ohmic transportation under the low bias.



- Oxygen vacancy
- Oxygen ion

Fig-3.2-5(a) shows the status of forming CP. **Fig-3.2-5(b)** indicates the reset process.

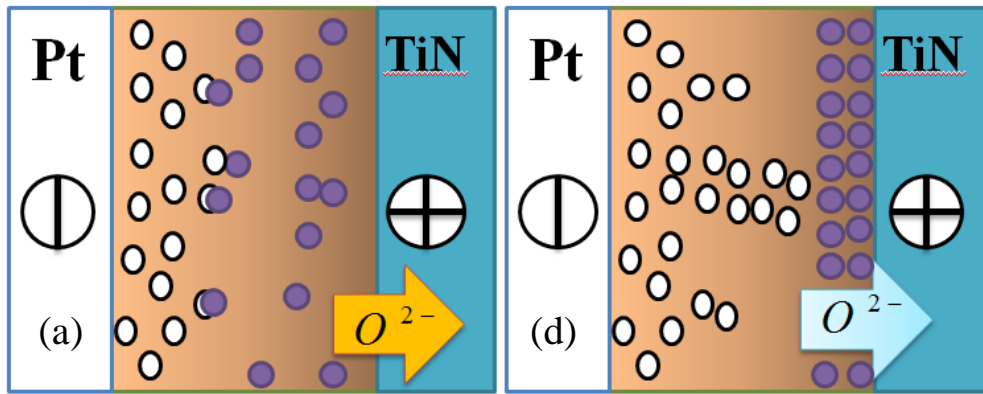


Fig-3.2-5 (c) depicts the NDR phenomenon and **Fig-3.2-5 (d)** shows the set process.

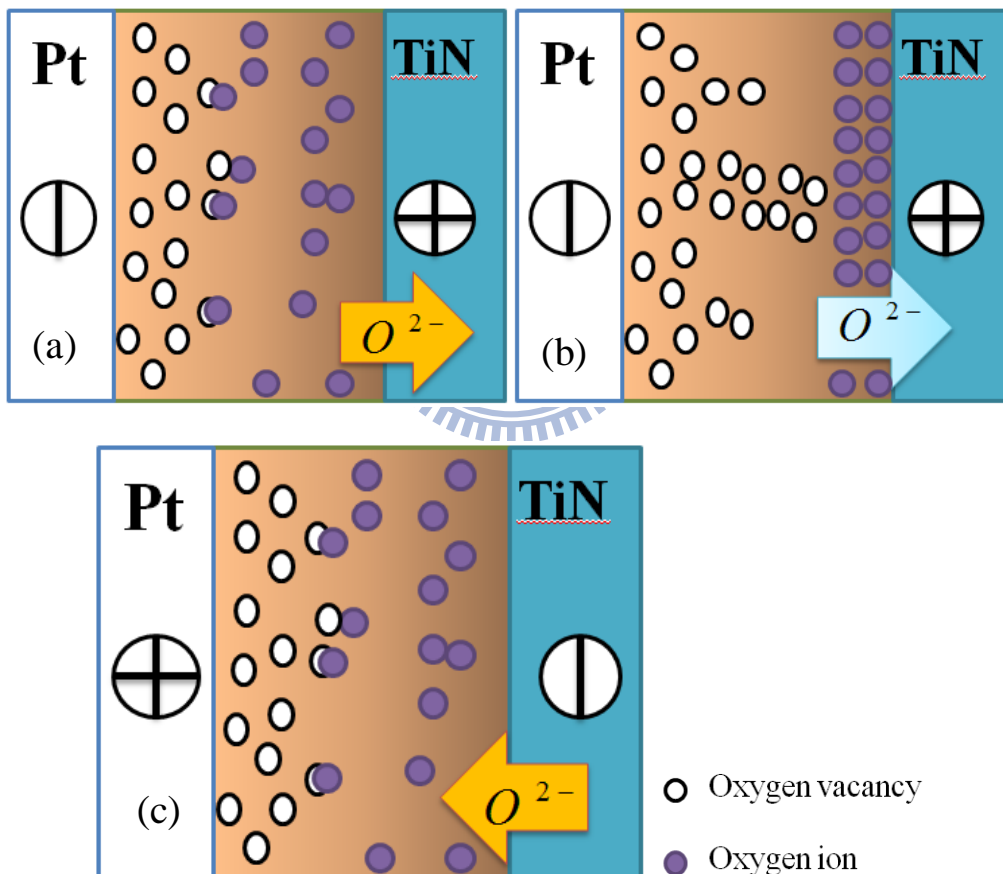


Fig-3.2-6 (a) is the migration of oxygen ion and **Fig-3.2-6 (b)** is the accumulation of oxygen ion. The state is changed to SHRS because the oxygen-rich layer is produced. **Fig-3.2-6 (c)** depicts the oxygen ions migrate to bulk and the oxygen-rich layer is vanished when we apply reverse bias.

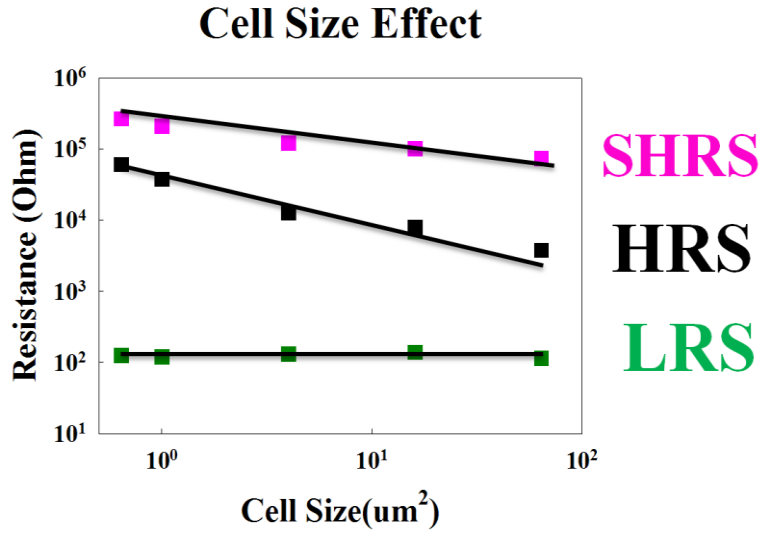


Fig-3.2-7 depicts SHRS and HRS depended on cell size but LRS was independent to cell size.

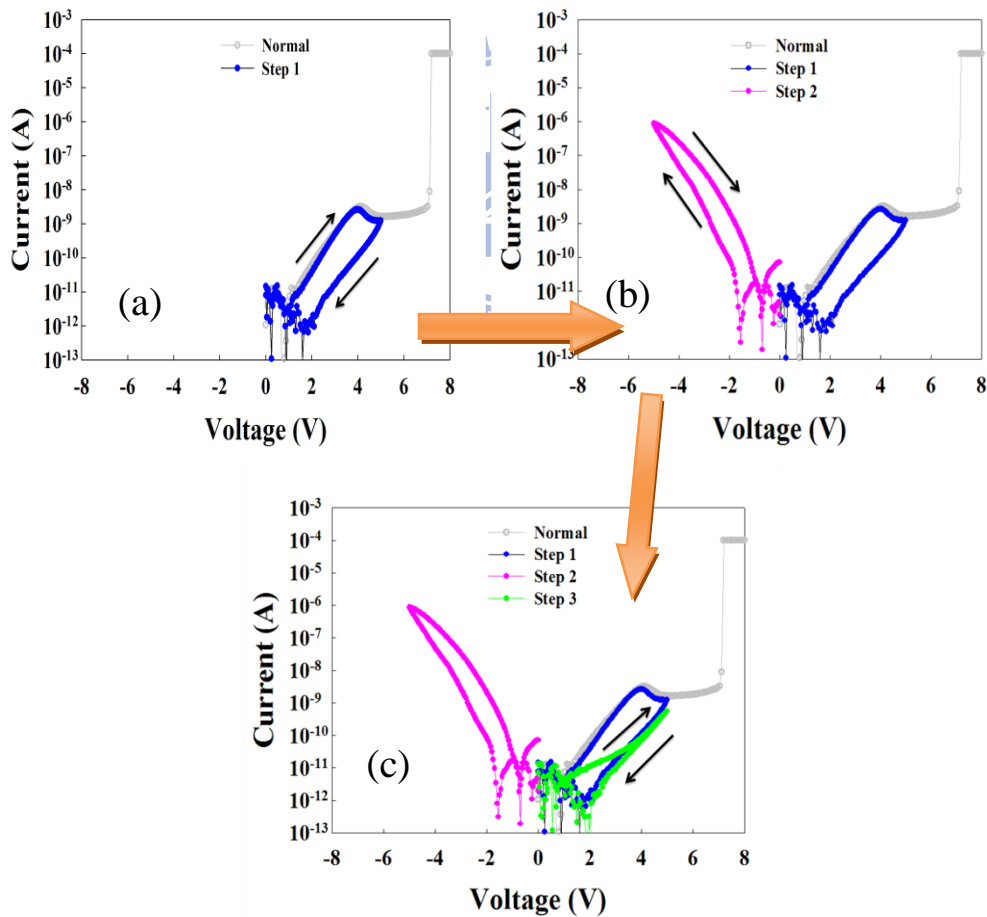


Fig-3.3-1(a) shows the swept loop from $0\text{V} \rightarrow 5\text{V} \rightarrow 0\text{V}$ and **(b)** depicts the swept loop from $0\text{V} \rightarrow -5\text{V} \rightarrow 0\text{V}$. **(c)** depicts the state is not at on- state.

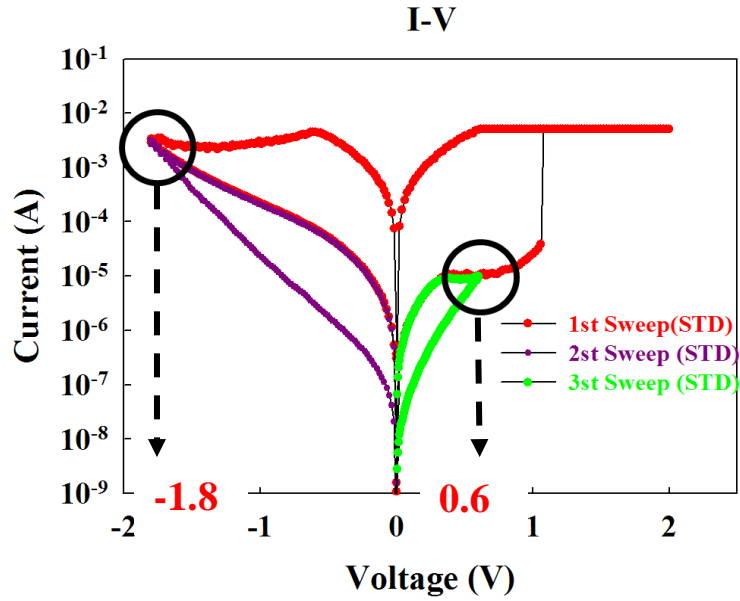


Fig-3.3-2 (a) shows the sub-RRAM the operating condition is at forward bias of 0.6V and at about reverse bias of -1.8V.

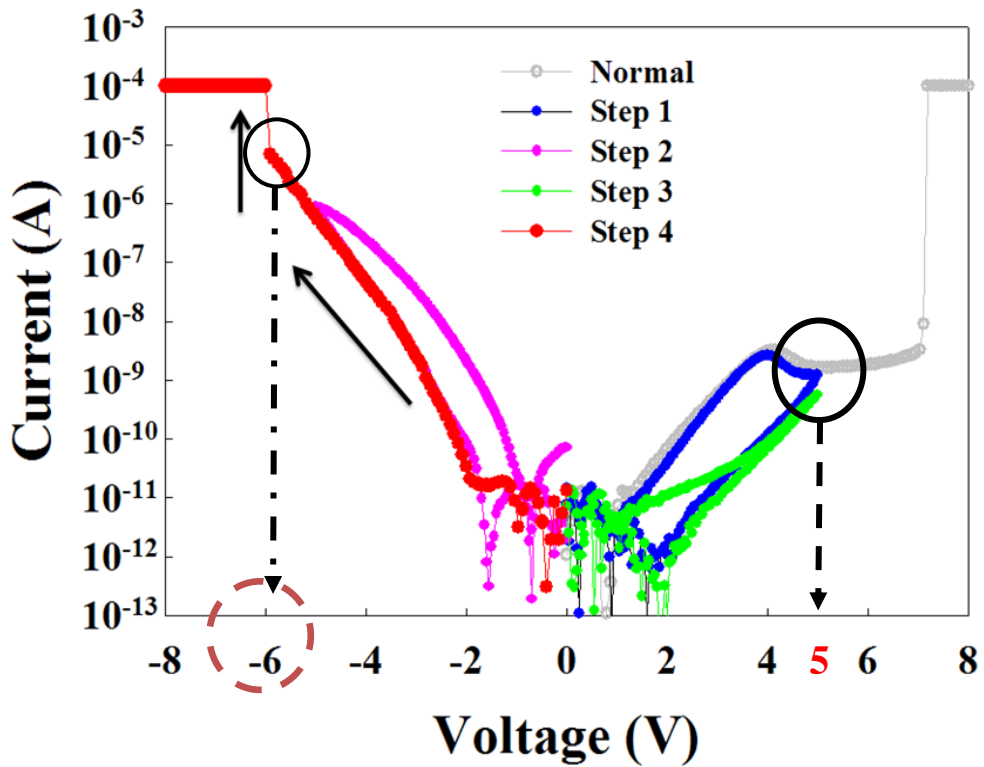


Fig-3.3-2 (b) indicates the operating mode before forming, and we discover V_{stop} was about 5V at forward bias.

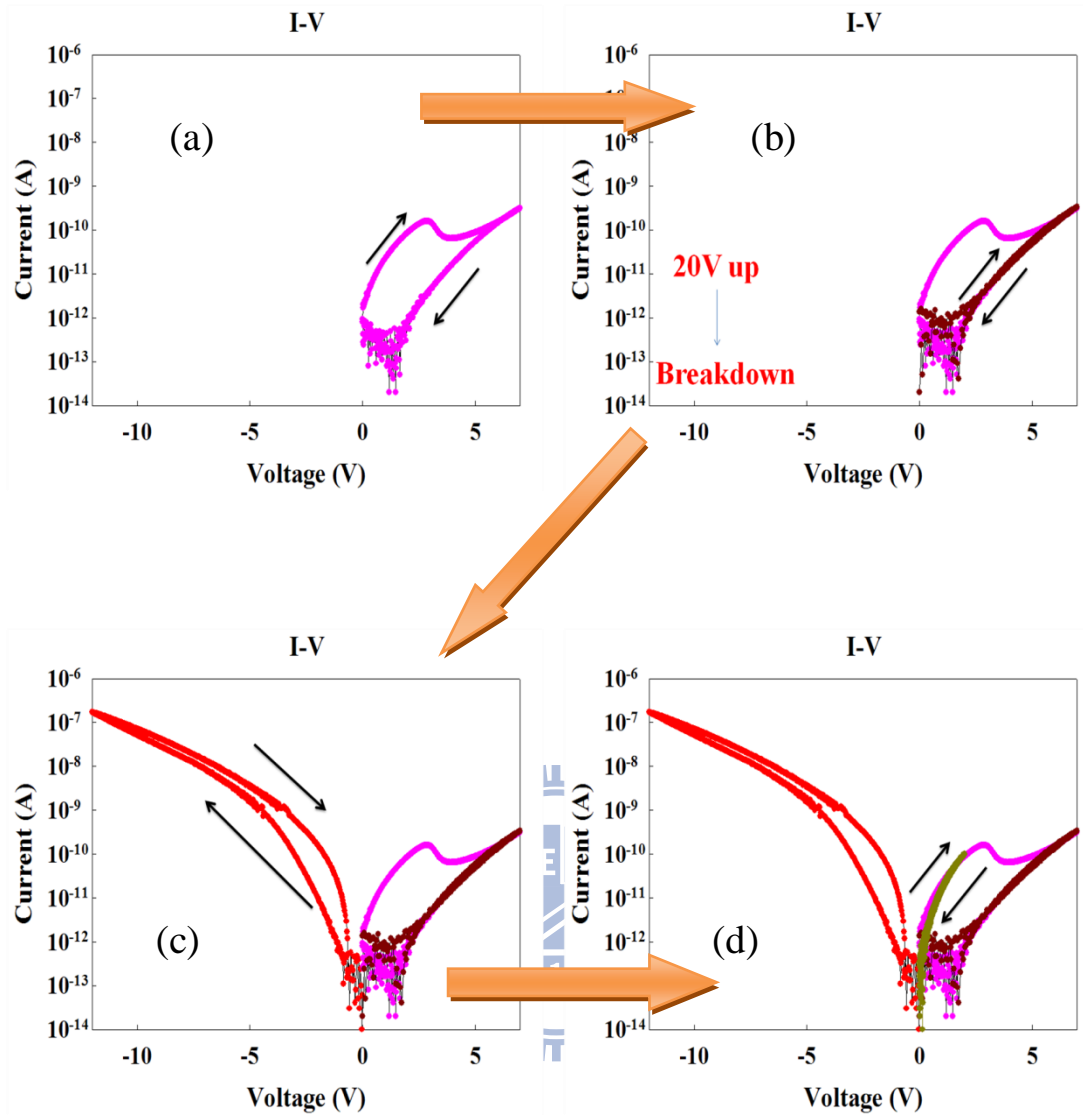


Fig-3.3-3 (a) shows the properties also possessed the NDR phenomenon and the NDR voltage was at about 2V. **Fig-3.3-3** (b) depicts the state is transition from ON state to OFF state. **Fig-3.3-3** (c) the current was different from OFF state, and we will do the same action to check out whether the state was transition. Therefore, **Fig-3.3-3** (d) indicates the state transition from OFF state to ON state.

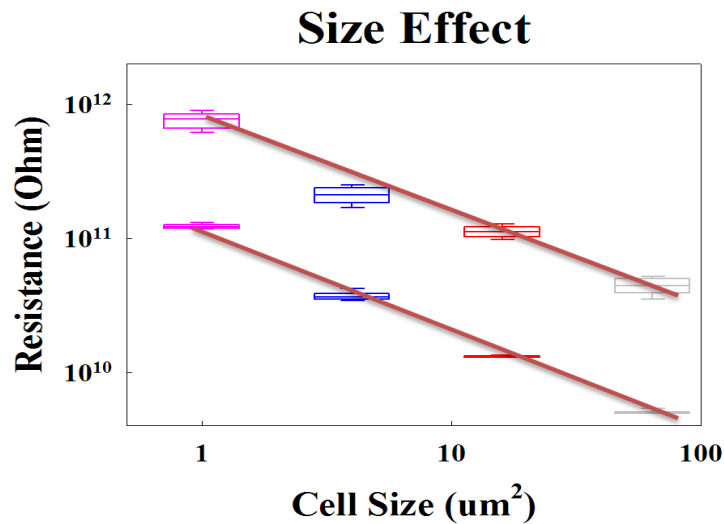


Fig-3.3-4 shows the phenomenon of size effect

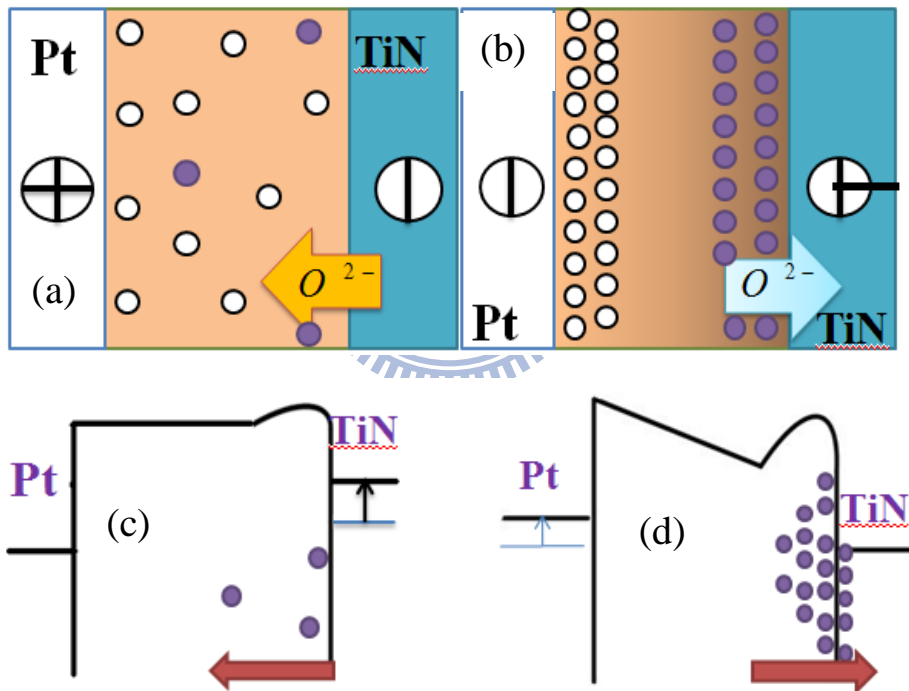


Fig-3.3-5 (a) depicts the oxygen accumulate nearing interface when we give forward bias and then form oxygen-rich region and **Fig-3.3-5 (b)** depicts the oxygen went back to bulk when the device was gave a reverse bias.

Fig-3.3-5 (c) and **(d)** indicate the Schottky barrier is bend the band upward when the oxygen ions accumulate near interface and the Schottky barrier is bend the band downward when the oxygen ions go back to bulk, respectively.

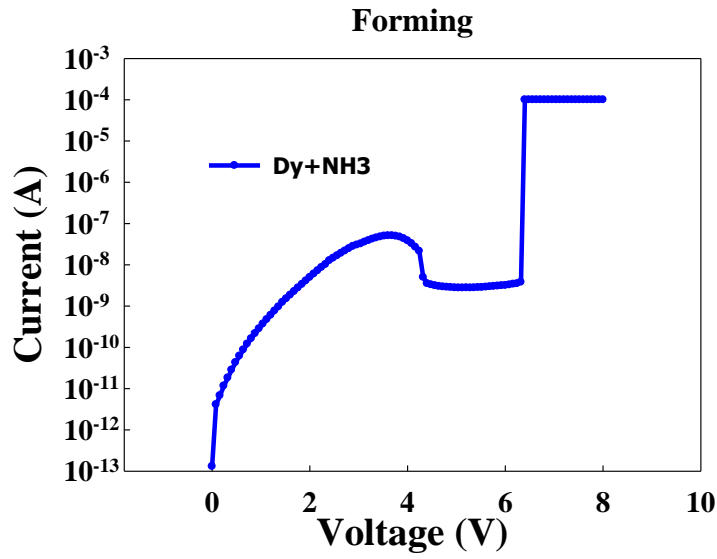


Fig-3.4-1 shows the huge NDR phenomenon characteristic at forming process.

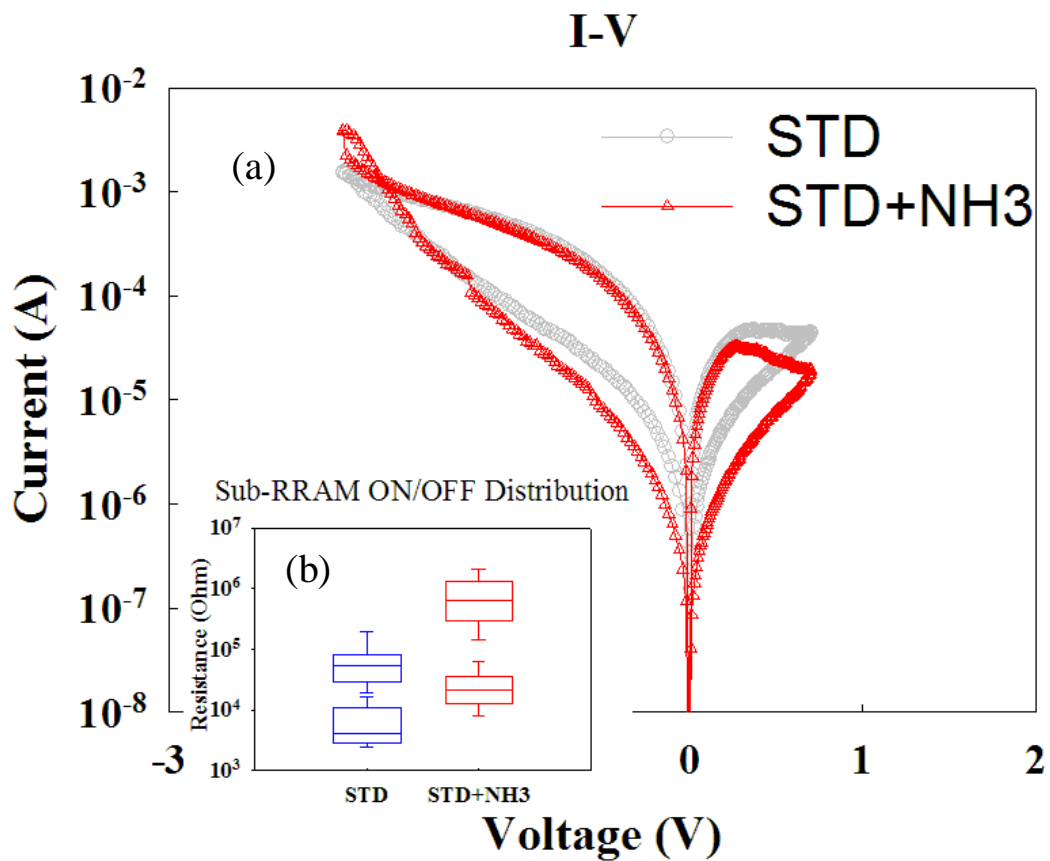


Fig-3.4.2 (a) can depicts the DMON possess the huge NDR than the DMO and the DMON resistive state was lower than the DMO resistive state. Fig-3.4.2 (b) indicates the sub-RRAM HRS and SHRS ratio for DMON and DMO.

Chapter 4

Investigation of Improving Endurance Performance by Using Fast Measurement Systems

In this section, we want to investigate one of reliabilities of our device and it is endurance test. However, the endurance test possess limit by DC measurement system. Therefore, we have to change the measurement method to achieve many on-off actions. Using Fast Measurement Systems is required for this section. Here, the pulse measurement will be used in this section.

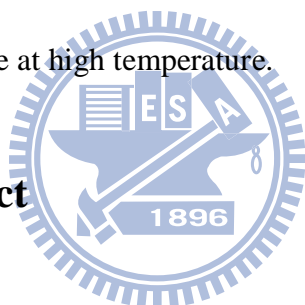
4-1 The Observation of Current by Using Pulse

Current-Voltage (Pulse IV)

The pulse IV means we apply a fixed voltage pulse and observe the current with extremely short time. Fig-4.1-1 shows we mention above. Here, we will see the relationship of current-time. Therefore, the current-time relationship can divide into two different situations, part one is the current of *set process* and part two is the current of *reset process*. At first, Fig-4.1-2 shows the current of set process but the current just increases with time. We will not discuss the set process effect in the section. Second, the current of reset of STD device is Fig-4.1-1, and there is a special phenomenon in the reset process. Fig-4.1-1 depicts the trend of current-time can be divided into three parts, first is peak1, second is peak2 and third is a smooth current. Therefore, we will discuss three effects whether the three parts affect the device switching behavior and endurance. First, we will pick three kinds of width, one is

100ns, another one is 300ns, and the other one is 900ns at 297k, 333k, 353k and 373k. Fig-4.1-3(a) shows the three kinds of voltage pulse; (b) shows the current value is detected and (c) depicts the device is read by applying low bias. Fig-4.1-3(a), (b) and (c) shows the current-time are at 297k. Here, we can discover the voltage pulse width which is 300ns and 900ns can make the device transition from on-state to off-state but the width is 100ns can't make the device changing the state. Therefore, we select the pulse width is 100ns at 297k, 333k, 353k and 373k and then we read the state of device by applying low bias. Fig-4.1-4 indicates the resistance increases with temperature increasing. On the other hand, the transition time of device is gradually short because the mobility of oxygen ions is increased by getting more energy at high temperature. Therefore, we can see the device which the condition is at 100ns can transit from on-state to off-state at high temperature.

4-2 Pulse Cycle Effect



In this section, we will discuss the endurance test. Generally, the endurance test can be divided into DC endurance and AC endurance test, but we have to spend more time by DC measurement. We have to use pulse measurement (AC) method in order to decrease test time.

4-2.1 Less Pulse Cycle Effect

In this part, we give two kinds of reset condition of voltage and width, one is -2V and 300ns and the other one is -2V and 900ns to the STD device. And the set transition condition of voltage and width is 1.2V and 100ns. Fig-2.3-7(a) and (b) shows we mentioned above. The method of endurance test is 1~10 times by single

pulse and then read the state of device, 20~100 times by 10 pulse cycles and then read the state of device, 200~1000 times by 100 pulse cycles and then read the state of device and 2000~100000 times by 500 pulse cycles. Fig-2.3-7 (c) shows the pulse cycle means the reset and set is continuous action and the condition of pulse cycle is like Fig-2.3-7(c). And the less pulse cycles means giving the most pulse cycles are applied under 500 times per time and then read the state of device. Table 4-1 shows we mentioned above. The reset pulse width is 100 ns can't make the device changing the state so we don't show the figure. And Fig-4.2-1(a) depicts the reset pulse width is 300 ns and (b) shows the reset pulse width is 900ns. The device reveals smooth state under 300 ns and 900 ns. The 10^5 times of endurance test is not enough to apply to modern NVMs so we have to gain the giving most pulse cycles per time.

4-2.2 Many Pulse Cycles Effect – Part One

Here, we will give the most pulse cycles are 10000 times per time and then read the state and the condition of pulse cycle is also like Fig-2.37(c). First, the 300ns condition is applied in the endurance test. And Table 4-2 depicts the condition of endurance test. Fig-4.2-2 shows the situation of endurance test under many pulse cycles. And we can discover a strange phenomenon at 10^4 times. The state of device reveals normally on-state phenomenon. In normally on-state, the most pulse cycles per time is 10000 cycles and we would like to make sure whether many pulse cycles cause the normally on-state phenomenon. Therefore, we gather statistics that shows different pulse cycles and how the different conditions affect the state of device. For example, we give single pulse cycle and then read the state of device by applying low bias. However, we operate 10 times at the same steps and gather statistics. Subsequently, we also give 100, 500, 1000, 1500 and 2000 pulse cycles to test the

STD device and then repeat what we mention above steps. Fig-4.2-3 indicates the statistics of different pulse cycles effect. We can discover a phenomenon that the on- or off-state of device possesses larger variation when the device is given the numbers of pulse cycles larger than 1000 cycles per time. Especially, the state of device achieves normally on-state when we give the pulse cycles equal 2000 cycles per time. Consequently, it is observed that the device can be influenced by giving the many pulse cycles per time.

(Conclusion)

In fact, we think the many pulse cycles affect the device state because the reset process not completed. For set process, the oxygen ions migrate direct to TiN by external field because the oxygen ions are not constrained to another reaction step. For reset process, the oxygen ions go back to bulk have to undergo two steps, first step is the oxygen ions migrate to bulk from TiN by external field and second step is the oxygen ions recombine with oxygen vacancies in the bulk. [49] [50] Fig-4.2-4 shows we mention above. But we think the normally on-state phenomenon because the oxygen ions can't recombine with the oxygen vacancies or the less oxygen ions recombine with the oxygen vacancies and then the filament still exist in the bulk. Fig-4.2-5 depicts the oxygen vacancies still exist in the bulk and then form a conduction path. The reasons of recombining failure can possess two factors, one is the time of recombination is not enough and the other one is heating effect. Therefore, we do some experiments to verify our conjecture in next section.

4-2.3 Many Pulse Cycles Effect - Part two

In this section, we will verify our conjecture and the condition is at 300ns still is used to in the experiment. At first, the normally on-state occurred because the time of

recombination is not enough and heating effect. We have to change the condition of pulse cycle and then make the device achieving the enhancement of endurance. Here, we define some parameters; one is the width between reset and set is called “a-region” and the other one is the width between set and “next reset” is called “b-region”. Fig-4.2-6 shows the condition. The changing condition a-region and b-region are extended or curtailed. Subsequently, we try to test the optimization condition and then apply the condition to analyze the effect, further. Therefore, we set three different a-region, $a_1=800\text{ns}$, $a_2=15\mu\text{s}$ and $a_3=20\text{ns}$ and the four different b-region, $b_1=800\text{ns}$, $b_2=20\text{ns}$, $b_3=20\mu\text{s}$, $b_4=15\mu\text{s}$. Next, five different compositions are applied to the device and then each pair of parameters is like Fig-4.2-7. The condition is inputted the device and is given 5000 cycles per time to the device. The device is biased ten times and then we gather statistics which is the distribution of on/off ratio. Fig-4.2-7 shows what we said the statistics. Each pair of parameters possesses some different effects from Fig-4.2-7. And Fig-4.2-7 indicates the optimization condition is the second pair of parameters (i.e. a_2 and b_2). This condition possesses lower leakage and larger on/off ratio so the condition is applied to the further experiment.

Subsequently, the long a-region and the short b-region are as the standard condition. Fig-4.2-8 depicts the new changeable condition. And the a-region is modified another width is at $3.5\mu\text{s}$, $4.5\mu\text{s}$, $5.5\mu\text{s}$, $7.5\mu\text{s}$ and $9.5\mu\text{s}$ and the b-region is modified width is fixed at 20ns . Fig-4.2-9 indicates a special phenomenon which the on/off ratio is enlarged when the a-region lengthening gradually. On the other hand, the on-state independent with various a-regions and the off-state depend on the various a-regions.

(Conclusion)

From Fig-4.2-7 and Fig-4.2-9, the phenomena verify our conjectural the model at the section is 4-2.2. Here, the pulse cycle effect is explained by the lattice and non-lattice oxygen model. The lattice oxygen ions are the oxygen ions bond with the

oxygen vacancies and the non-lattice oxygen ions are the oxygen ions don't bond with the oxygen vacancies. The amount of non-lattice oxygen ions is too many to rupture the conduction paths. On the contrary, conduction paths can be easily ruptured if the amount of lattice oxygen ions is more than the non-lattice because the non-lattice oxygen ions are simply captured at TiN. There are two reasons that can cause the non-lattice oxygen increasing, first is the time of recombination and second is heating effect. The transition process can be described by the oxygen ions reaction. First, we can see the set process. In fact, the set process is a single reactive step which means the oxygen ions are pushed to the electrode (i.e. TiN). However, the reset process has to possess two reactive steps, first is the oxygen has to hop to the barrier from TiN to bulk and second is the oxygen ion recombine with the oxygen vacancy. Consequently, the time of recombine is not enough and then the non-lattice oxygen ions are produced. Here, we think the first step of reset process has to bias to the device but the second step is unnecessarily biasing the device. We have to increase a-region in order to achieve complete recombination because the time of recombination time is longer. The non-lattice oxygen effect is not serious at less pulse cycles but the effect is serious at many pulse cycles. On the other hand, the conduction paths can't be ruptured because too many the non-lattice oxygen ions are captured. We can see Fig-4.2-5 shows we discuss the model. The heating effect existed in many pulse cycles but the effect makes the oxygen ions possess too high mobility to recombine with vacancy. Therefore, the recombination and the heating effect determine the pulse cycle effect so we have to solve the two problems to avoid the normally on-state phenomenon. The a- and b-region have to be extended to achieve steady state. However, we also find a better pair of parameters which is the combination of a_2 and b_2 . Fig-4.2-9 depicts we mentioned the model. The off-state increases with increasing the a-region because the amount of non-lattice oxygen ions captured at TiN is less.

The oxygen ion can achieve complete bonding with vacancy if the enough recombination time and decreasing heating effect so the amount of non-lattice oxygen is decreased. Fig-4.2-9 indicates the non-lattice ions are relative to the width of a-region. On the contrary, the ions can't achieve a situation of bonding with vacancy if the recombination time is not enough and the heating effect still exists. Consequently, the state will remain on the on-state in the condition of many pulse cycles. The phenomenon is like Fig-4.2-3.

4-3 300ns and 900ns for The Reset time Effect

Here, we observe the different reset time how they affect the endurance of device. The condition is the composition of long a2 and short b2 and then we apply a serious 5000 pulse cycles to the device. Fig-4.3-1 depicts the endurance of different reset width. In less pulse cycles effect, the two different reset time effects are at steady state. In many pulse cycles, the 300ns and 900ns effects possess some different phenomenon which is the 900ns possesses higher instable than the 300ns.

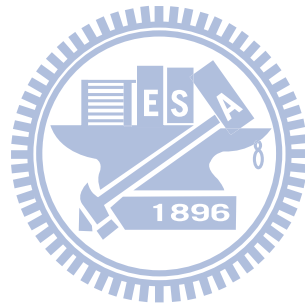
(Conclusion)

The different width phenomenon affects the state of device because the unnecessary energy can influence the stability of device. Fig-4.3-2 depicts the phenomenon. And the unnecessary energy cause increasing power consumption. The operating speed of 300ns is faster than 900ns. Therefore, the 300ns is batter condition than 900ns.

4-4 The Result of Best Endurance

Here, the two effects (i.e. the pulse cycles effect and the 300ns effect) are combined

an optimized condition and apply to the device. And then we observe the endurance test of STD device. The STD device can achieve 10^7 times operating and the on/off ratio can keep one order and stable. Fig-4.4-1 indicates the 10^7 the operating times.



Pulse I-V

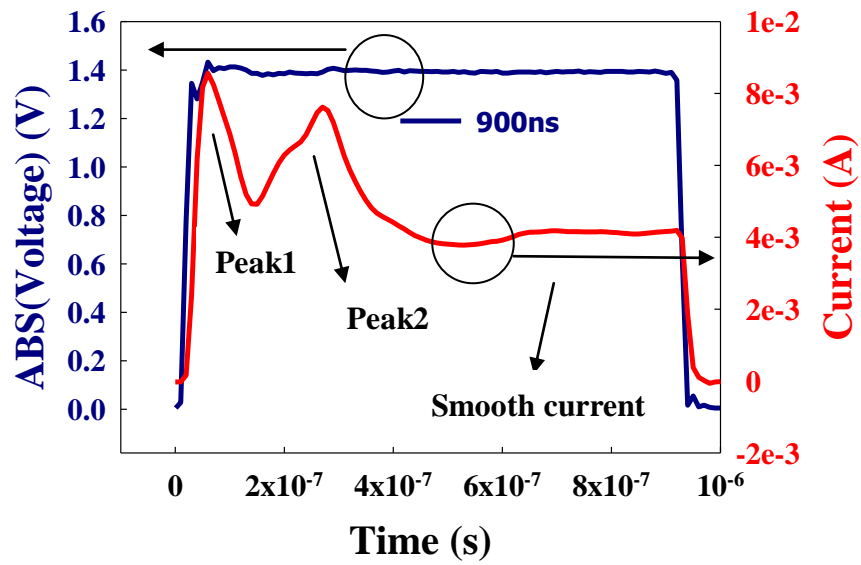


Fig-4.1-1 shows a fixed voltage pulse and detects the current with extremely short time.



Pulse I-V

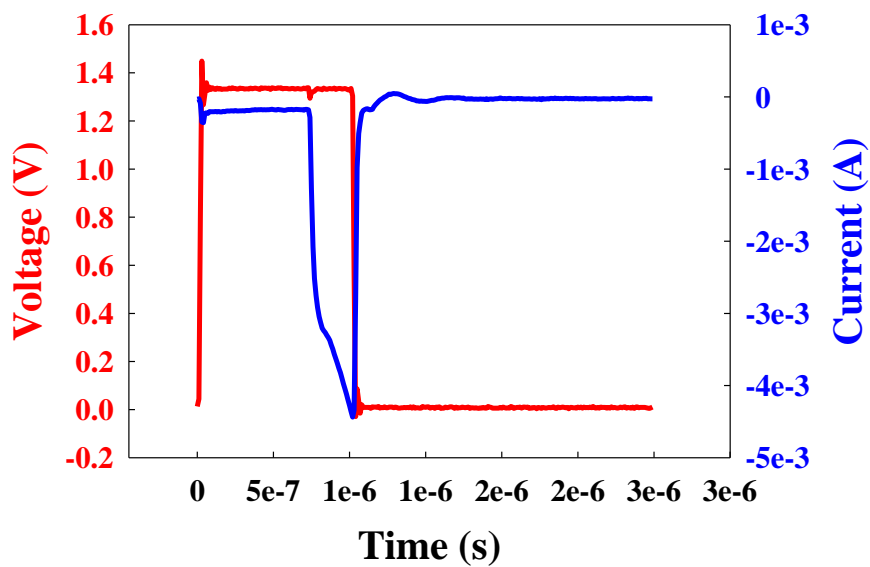


Fig-4.1-2 shows the current of set process but the current just increases with time.

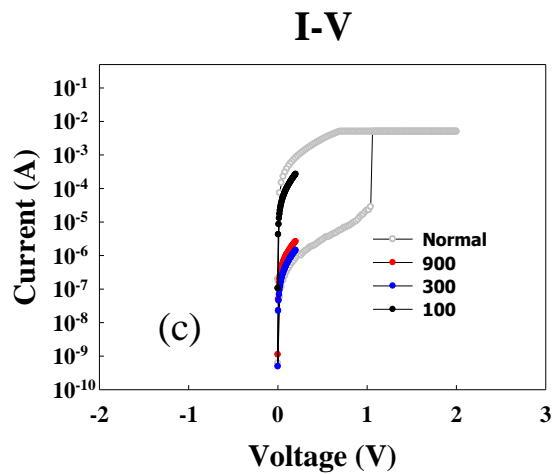
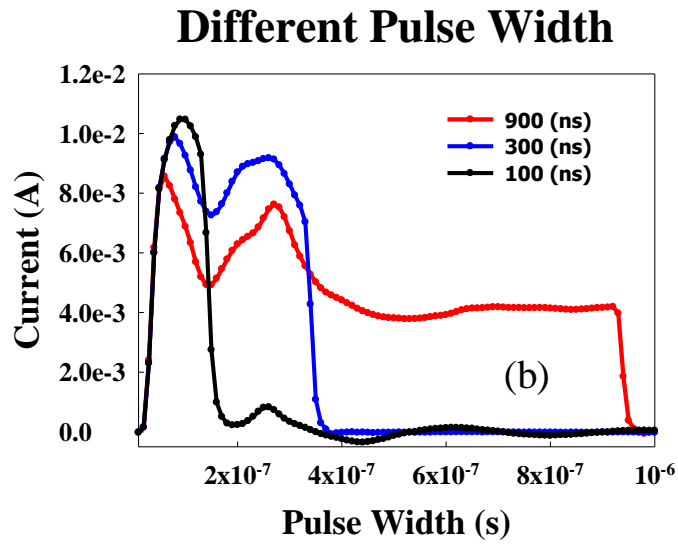
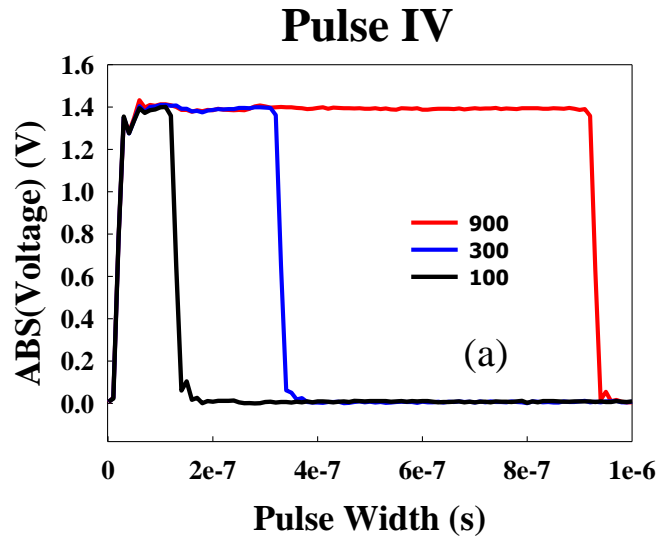


Fig-4.1-3(a) shows the three kinds of voltage pulse; **(b)** shows the current value is detected and **(c)** depicts the device is read by applying low bias.

Fig-4.1-3 (a), (b) and (c) are at 297k.

Temperature Effect (For Reset time 100ns)

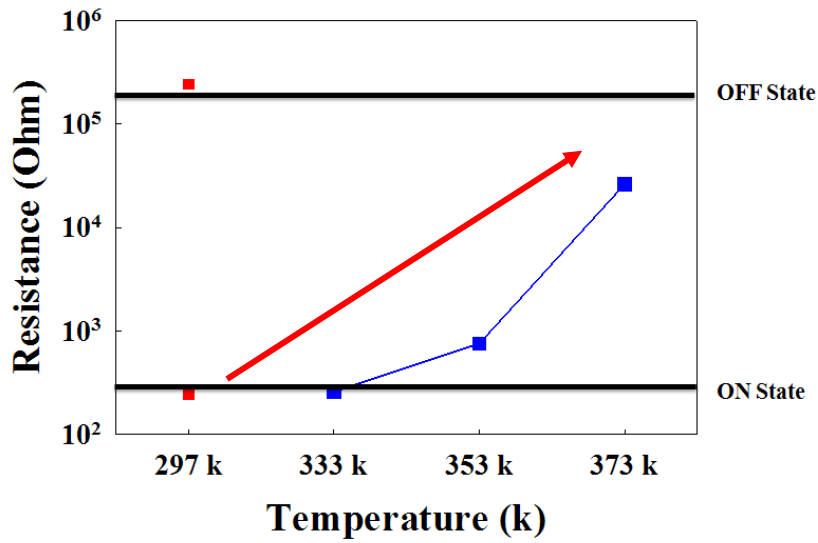


Fig-4.1-4 indicates the resistance increases with temperature increasing.

1. 1~10 by single pulse
2. 20 ~ 100 by 10 pulses cycles
3. 200 ~ 1000 by 100 pulse cycles
4. 1000~100000 by 500 pulse cycles

Table 4-1

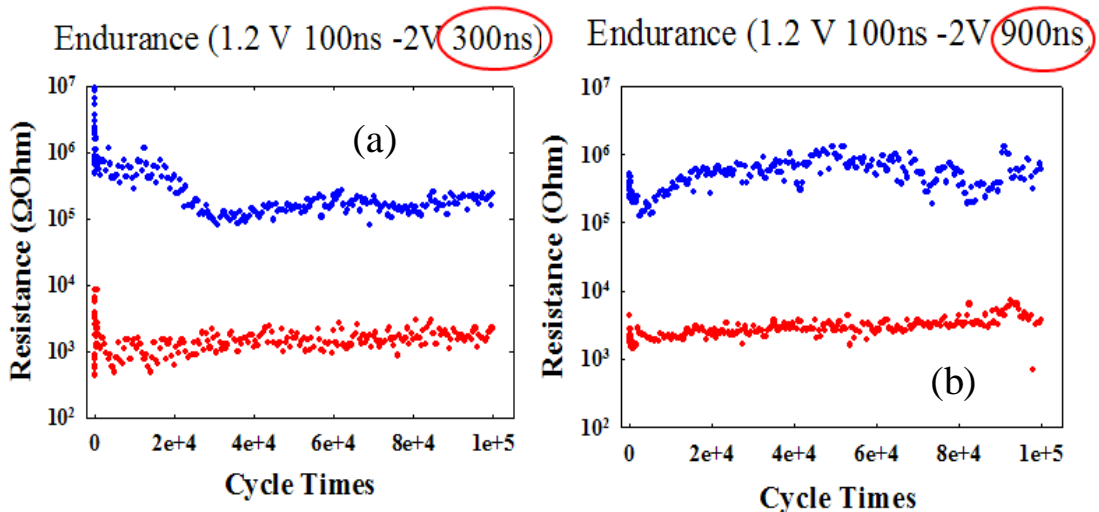


Fig-4.2-1 (a) depicts the endurance of reset pulse width is 300 ns and (b) shows the endurance of reset pulse width is 900ns.

1. 1~10 by single pulse
2. 20 ~ 100 by 10 pulses cycles
3. 200 ~ 1000 by 100 pulse cycles
4. 1000~10000 by 1000 pulse cycles
5. 10000~100000 by 10000 pulse cycles

Table 4-2

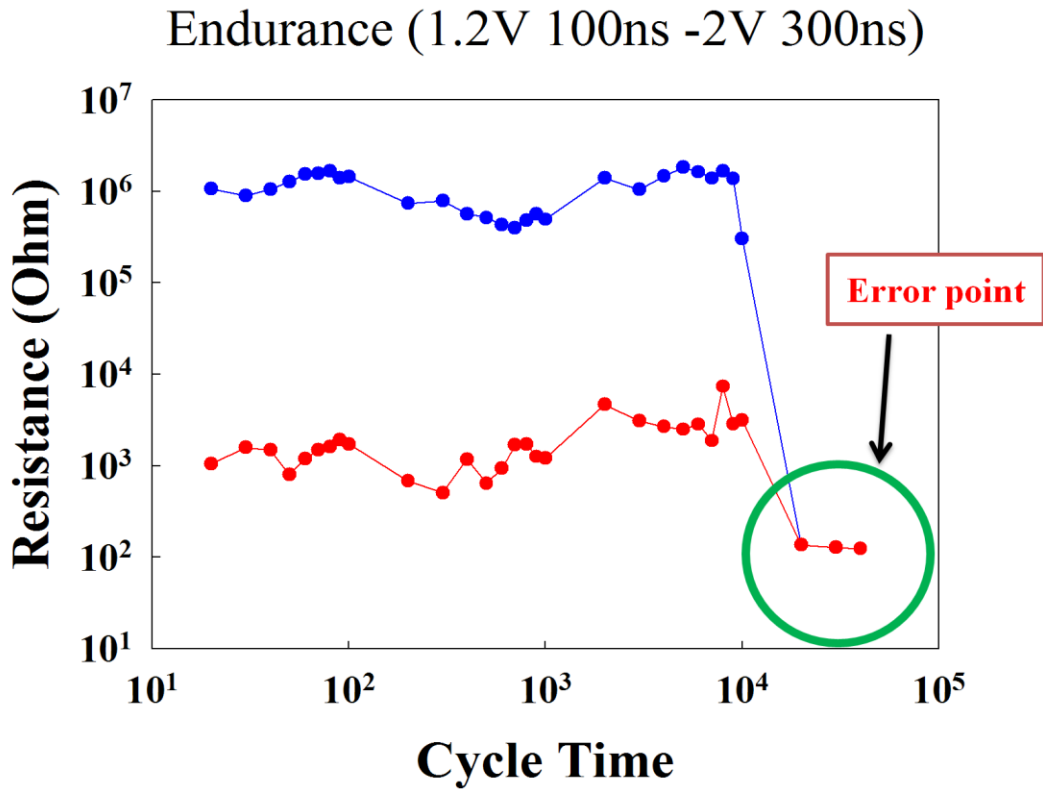


Fig-4.2-2 shows the endurance test under many pulse cycles.

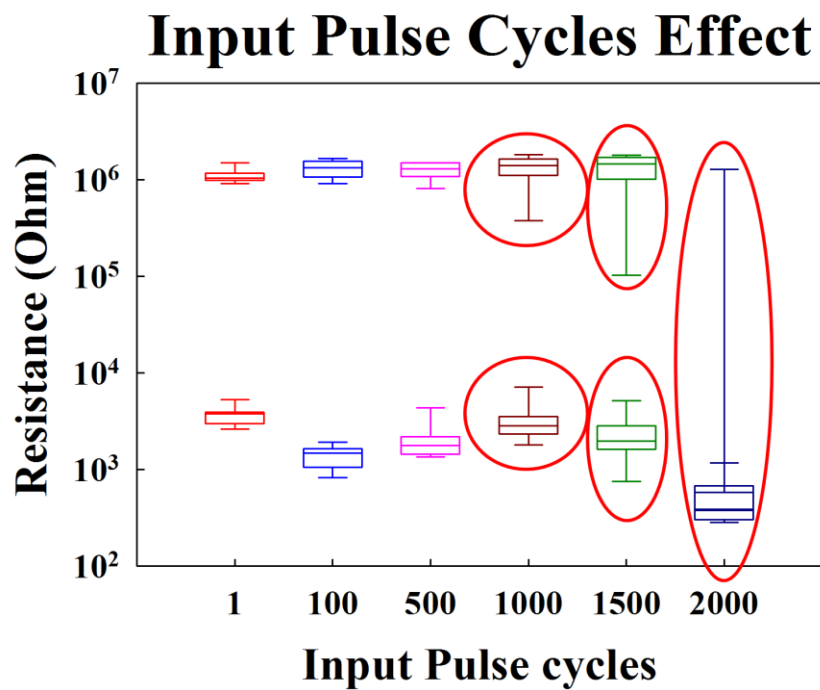


Fig-4.2-3 indicates the statistics of different pulse cycles effect.

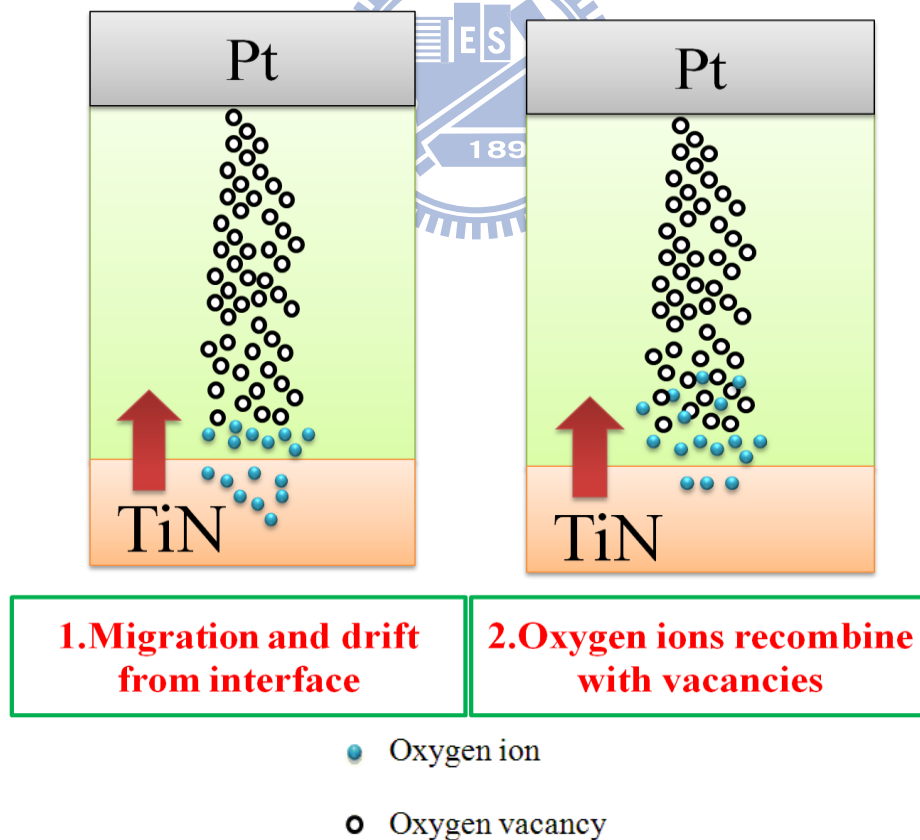


Fig-4.2-4 shows the oxygen ions have to undergo two steps, first is the oxygen ions migrate to bulk from TiN and second is the oxygen ions recombine with oxygen vacancies in the bulk.

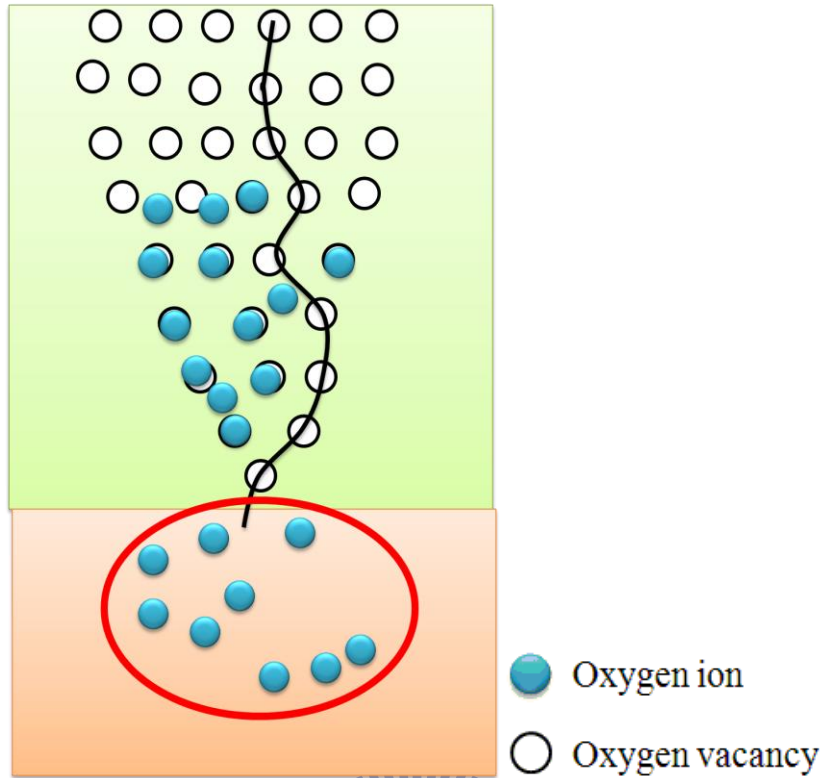


Fig-4.2-5 depicts the oxygen vacancies still exist in the bulk and then form a conduction path.

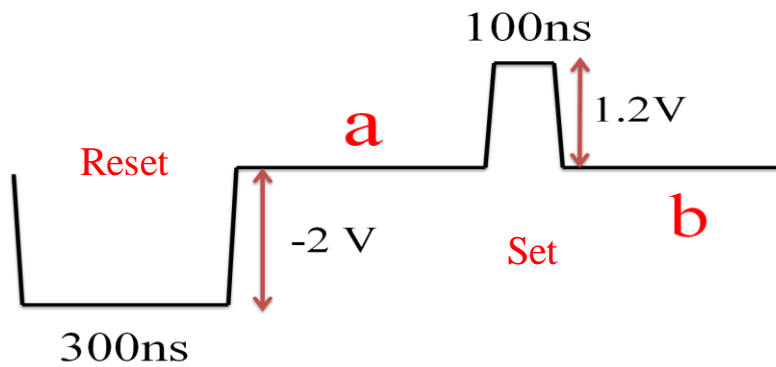


Fig-4.2-6 shows the width between reset and set is called “a” and the width between set and “next reset” is called “b”.

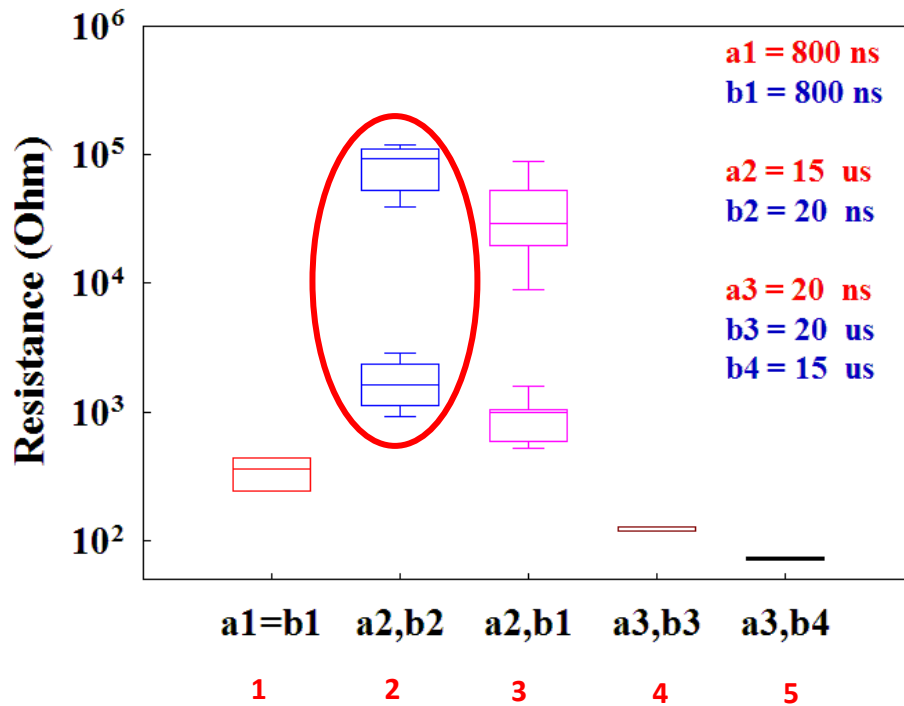


Fig-4.2-7 shows each pair of parameters possesses some different effects and the optimization condition is the second pair of parameters (i.e. a2 and b2). This condition possesses lower leakage and larger on/off ratio so the condition is applied to the further experiment.

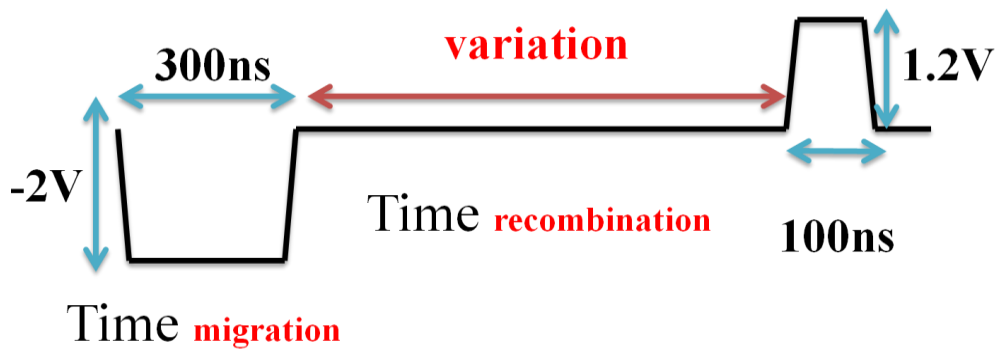


Fig-4.2-8 depicts the width between reset and set is extended.

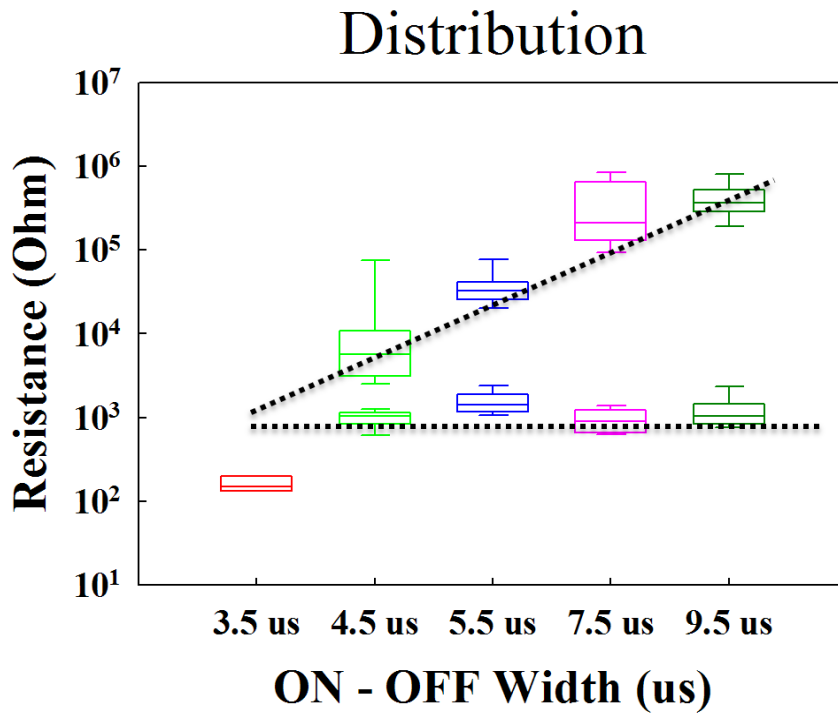


Fig-4.2-9 indicates a special phenomenon which the on/off ratio is enlarged with the a-region lengthening gradually.

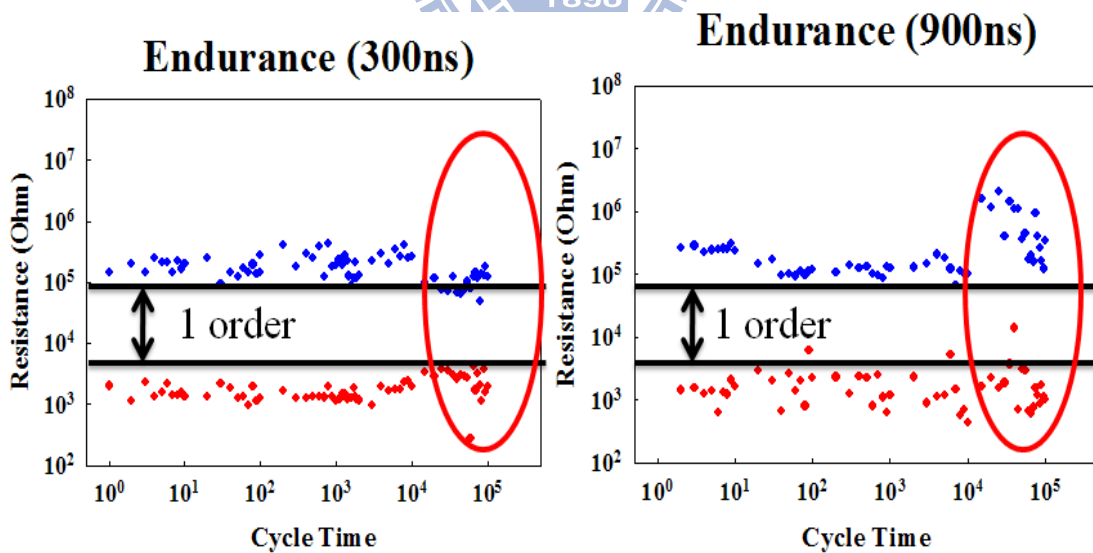


Fig-4.3-1 depicts the endurance of different reset width. And the 300ns and 900ns effects possess some different phenomenon which is the 900ns possesses higher instable than the 300ns.

Pulse I-V (-1.4V)

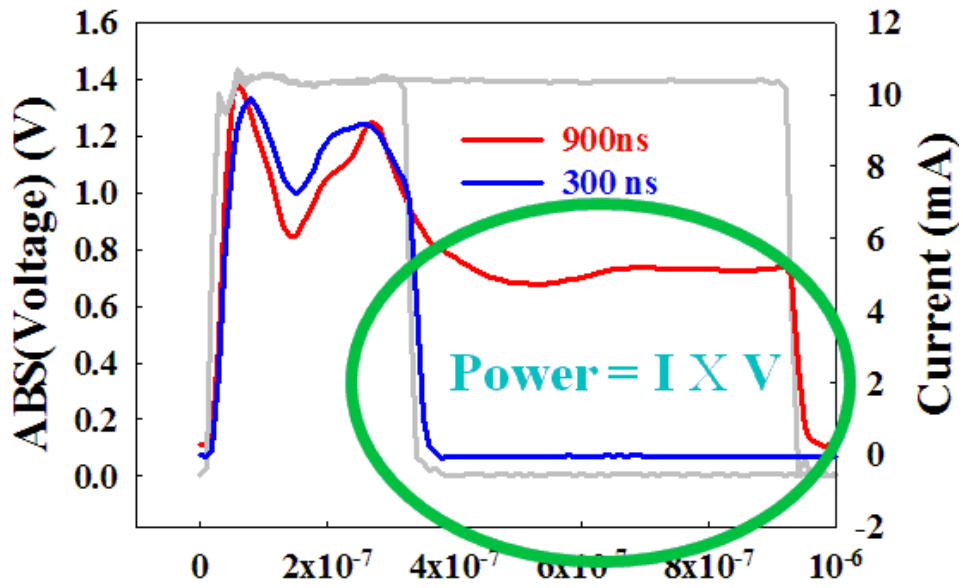


Fig-4.3-2 depicts the different width phenomenon affects the state of device because the unnecessary energy can influence the stability of device.

Endurance

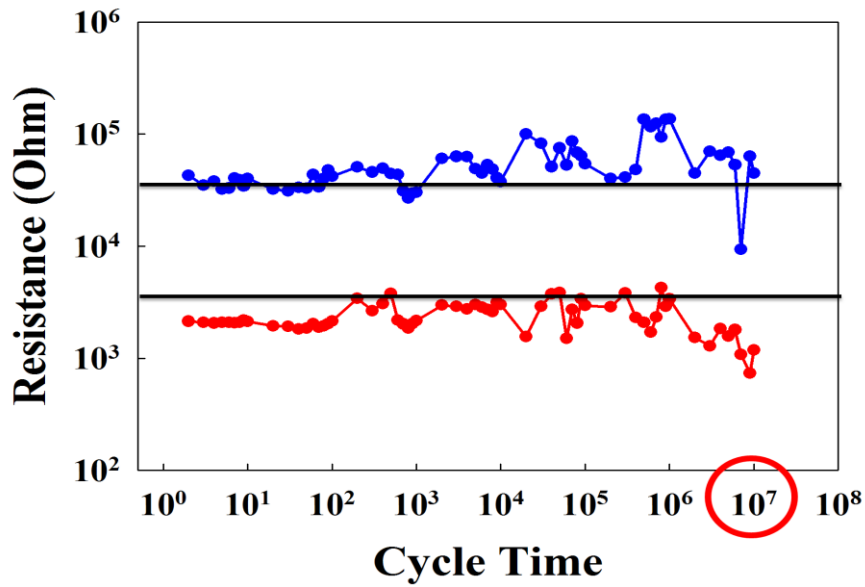


Fig-4.4-1 indicates the STD device can achieve 10^7 times operating times and the on/off ratio can keep one order and stable.

Chapter 5

Conclusion

In this section, we will conclude three chapters in the thesis. In Chapter2, we can observe the structure of Pt/DMO/TiN possesses resistive switching behavior. Our device has some oxygen vacancies through the analysis of XPS in the DMO film. And the thickness of DMO film is 12nm by TEM cross-section. The device is taken to test the reliability of device. Therefore, we can also observe the endurance and retention of the STD device. The retention of device maintains 10^4 second at 85°C high temperature so it means the device on or off state can store ten years without power. We can also see the AC and DC endurance test are good characteristic and it means the on/off ratio can maintain one-order at 10^5 and 100 times of operating, respectively and.

In chapter3, the NDR phenomenon is discovered at the current-voltage of DMO device. First, the IV curve is analyzed before forming process and temperature, constant voltage sampling and the film thickness effect influence the NDR voltage changing. The reason is that the oxygen ions accumulate near the interface and form an oxygen-rich region causes the NDR phenomenon. In other words, the NDR is interface effect. Second, the IV curve is analyzed after forming. In the same polarization, the NDR phenomenon is also discovered but the characteristic imply a sub-RRAM switching behavior. In fact, the oxygen ions affect the device and cause the NDR phenomenon is after forming process. Therefore, we think the phenomenon that the oxygen ions accumulate near interface has existed in DMO film. And the sub-RRAM and original-RRAM represent interface switching mechanism and filament switching mechanism, respectively. However, we cannot see a forming-free

switching behavior because the thickness of STD device is too thin to avoid breakdown. Subsequently, we can see the forming-free switching behavior when the film thickness is thick. The thick device verifies the oxygen ion model and our conjecture and the switching characteristic is interface switching mechanism. There is still the other evidence to verify the oxygen ion model in the double layer device (i.e. the DMON device) because the nitrogen attract to the oxygen ions. We can observe the huge NDR phenomenon exist in DMON device.

In chapter4, first, the reset time is changed with temperature by pulse IV. On the other hand, the reset speed is increased with increasing temperature due to the oxygen ions effect. Second, the endurance test is changed by inputting the amount of pulse cycles per time. In order to solve the problem, we change the pulse condition and then see the state of STD device. Therefore, we think the phenomenon cause from the time of recombination and heating effect. Finally, we test an optimized condition and then the condition can make the endurance test of device achieves 10^7 times and on/off ratio can maintain stable state.

Reference

- [1] D. Kahng and S. M. Sze, A floating-gate and its application to memory devices, *the Bell System Technical Journal*, **46**, #4 (1967), pp. 1288–1295.
- [2] Dudley A. Buck, "Ferroelectrics for Digital Information Storage and Switching." Report R-212, MIT, June 1952.
- [3] D.Takashima et.al., ISSCC, 787-792,May 1998
- [4] Iwao Kunishima et.al.
- [5] I. G Baek, M.S.L., S. Seo, M. J. Lee, D. H. Seo, D. S. Suh, J. C. Park, IEDM Tech. Dig., 2005: p. 587-590
- [6] Memory Devices Using Bistable Resistivity in Amorphous As-Te-Ge Films" C. H. Sie, PhD dissertation, Iowa State University, Proquest/UMI publication #69-20670, January 1969
- [7] C.H. Sie, A.V. Pohm, P. Uttecht, A. Kao and R. Agrawal, IEEE, MAG-6, 592, September 1970
- [8] Stefan Lai and Tyler Lowrey, IEDM Tech. Dig., pp. 803-806 (2001)
- [9] Moodera J S, Kinder L R, Wong T M and Meservey R, *Phys. Rev. Lett.* **74**, 3273, 1995.
- [10] Moodera J S and Mathon G, *J. Magn. Magn. Mater.* **200**, 248, 1999.
- [11] B. J. Choi, JOURNAL OF APPLIED PHYSICS **98**, 033715, 2005
- [12] H. Y. Lee et al, [IEEE Electron Device Lett.](#) **31**, 44 _2010_.

- [13] W. C. Chien et al, [IEEE Electron Device Lett.](#) **31**, 126 _2010_.
- [14] Y. S. Chen et al, Int. Electron Device Meet. 2009, 105.
- [15] H. Y. Lee et al, Int. Electron Device Meet. 2010, 460.
- [16] S. Q. Liu, N. J. Wu, and A. Lgnatiev, *Appl. Phys. Lett.* 76. 2749 (2000)
- [17] A. Sawa et al, *Appl. Phys. Lett.* 85, 4073 (2004)
- [18] A. Beck et al, *Appl. Phys. Lett.* 77, 139 (2000)
- [19] Meijer, G. I. et al, *Phys. Rev. B*72, 155102 (2005)
- [20] S. Seo, M. J. Lee et al, *Applied Physics Letters*, 85(23), 2004
- [21] D. Lee, D.-J. Seong, H. J. Choi, I. Jo, R. Dong, W. Xiang, S. Oh, M. Pyun, S. Seo, S. Heo, M. Jo, D.-K. Hwang, H. K. Park, M. Chang, and M. Hasan, *Tech. Dig. - Int. Electron Devices Meet.* **2006**, 796.
- [22] D. S. Jeong, H. Schroeder, and R. Waser, [Appl. Phys. Lett.](#) **89**, 082909 _2006_.
- [23] B. J. Choi, D. S. Jeong, S. K. Kim, C. Rohde, S. Choi, J. H. Oh, H. J. Kim, C. S. Hwang, K. Szot, R. Waser, B. Reichenberg, and S. Tiedke, [J. Appl. Phys.](#) **98**, 033715 _2005_.
- [24] J. B. Yun, S. Kim, S. Seo et al, *Phys. Status Solidi (RRL)* 2007, 1, 280
- [25] Rainer Waser, Masakazu Aono, VOL 6, November 2007, *Nature Materials*
- [26] S. Seo, M. J. Lee et al., Reproducible resistance switching in polycrystalline NiO films, *Applied Physics Letters*, 85(23), 2004
- [27] U. Russo et al., *IEEE IEDM*, 2007, 775.
- [28] Ugo Russo, Carlo Cagli, and Andrea L. Lacaita *IEEE Transactions on Electron Devices*, VOL. 56, NO. 2, February 2009.
- [29] Watanabe, T et al. *Appl. Phys. Lett.* 78, 3738-3740 (2001)
- [30] M. Fujimoto, H. Koyama et al., *Applied Physics Letters*, 89, 223509, 2006

- [31] C. Yoshida, K. Tsunoda et al., *Applied Physics Letters*, 91, 2235110, 2007
- [32] B. Gao, S. Yu, N. Xu, L.F. Liu, B. Sun, X.Y. Liu, R.Q. Han, J.F. Kang, B. Yu, Y.Y. Wang, *IEDM Tech. Dig.*, (2008).
- [33] June Sik Kwak et al, *Applied Physics Letters*, 96, 223502, 2010
- [34] Akihito Sawa, *material today*, JUNE 2008 | VOLUME 11 | NUMBER 6
- [35] Beck, A., *et al.*, *Appl. Phys. Lett.* (2000) **77**, 139
- [36] Fujii, T., *et al.*, *Appl. Phys. Lett.* (2005) **86**, 139, 012107
- [37] Sawa, A., *et al.*, *et al.*, *Appl. Phys. Lett.* (2005) **86**, 139, 012107
- [38] *Physics of Semiconductor Devices, 3rd Ed.*, S. M. Sze and K. K. Ng, 815 pages, Wiley Interscience, Hoboken, 2007.
- [39] Uwamino Y., Ishizuka Y., Yamatera H., *J. Electron Spectrosc. Relat. Phenom.* **34**, 69 (1984).
- [40] Wagner C.D., Zlatko D.A., Raymond R.H. *Anal. Chem.* **52**, 1445 (1980).
- [41] George V. Chertihin and Lester AndrewsJ, *Phys. Chem. A* **1997**, **101**, **8547-8553**
- [42] *Chinese Chemical Letters* **2002**
- [43] Gao, B.; Chang, W.Y.; Sun, B.; Zhang, H.W.; Liu, L.F.; Liu, X.Y.; Han, R.Q.; Wu, T.B.; Kang, J.F.; *VLSI Technology Systems and Applications (VLSI-TSA), 2010 International Symposium on, 2010* , Page(s): 144 - 145
- [44] K. M. Kim et al., *Appl. Phys. Lett. Vol. 90*, no 24, p.242906 (2007)
- [45] Rainer Waser et al., *Adv. Mater.* 2009, 21, 2632-2663

- [46] J. J. Yang et al., *Nat. Nanotechnol.* 3, 429 (2008)
- [47] M. Durlam, Y. Chung, M. DeHerrera, B. N. Engel, G. Grynkewich, B. Martino, B. Nguyen, J. Salter, P. Shah, and J. M. Slaughter, *Proc. IEEE International Conference on Integrated Circuit Design and Technology*, (2007)
- [48] K. Miura, T. Kawahara, R. Takemura, J. Hayakawa, S. Ikeda, R. Sasaki, H. Takahashi, H. Matsuoka, and H. Ohno, *Proc. of the IEEE Symposium on VLSI Technology*, Kyoto, Japan, pp. 234–235 (2007).
- [49] B. Gao et al., “Oxide-Based RRAM Switching Mechanism: A New Ion-Transport-Recombination Model” [IEDM 2008](#)
- [50] B. Gao et al., *Appl. Phys. Lett.* Vol. **98**, p.232108 (2011)



Resume

姓名：黃偉立 (Wei-Li Huang)

出生日期：民國七十五年九月十八日

住址：300 屏東市前進里清進巷 139-9 號

學歷：

國立屏東教育大學 應用物理學系 學士

(2005.09~2009.01)

國立交通大學 電子研究所 碩士

(2009.09~2011.06)

論文題目：

新穎材料 DyMn_2O_5 在電阻式記憶體上的機制研究與應用

The Researching Mechanism and Application of the Novel Material
 DyMn_2O_5 (DMO) in Resistive Random Access Memory